

1. Report No. FHWA/TX-13/0-6607-2		2. Government Accession No.		3. Recipient's Catalog No.	
4. Title and Subtitle THE OVERLAY TESTER (OT): COMPARISON WITH OTHER CRACK TEST METHODS AND RECOMMENDATIONS FOR SURROGATE CRACK TESTS				5. Report Date October 2012 Published: August 2013	
				6. Performing Organization Code	
7. Author(s) Lubinda F. Walubita, Abu N. Faruk, Yasser Koochi, Rong Luo, Tom Scullion, and Robert L. Lytton				8. Performing Organization Report No. Report 0-6607-2	
9. Performing Organization Name and Address Texas A&M Transportation Institute College Station, Texas 77843-3135				10. Work Unit No. (TRAIS)	
				11. Contract or Grant No. Project 0-6607	
12. Sponsoring Agency Name and Address Texas Department of Transportation Research and Technology Implementation Office P. O. Box 5080 Austin, Texas 78763-5080				13. Type of Report and Period Covered Technical Report: September 2010–September 2012	
				14. Sponsoring Agency Code	
15. Supplementary Notes Project performed in cooperation with the Texas Department of Transportation and the Federal Highway Administration. Project Title: Search for a Test for Fracture Potential of Asphalt Mixes URL: http://tti.tamu.edu/documents/0-6607-2.pdf					
16. Abstract Presently, one of the principal performance concerns of hot-mix asphalt (HMA) pavements is premature cracking, particularly of HMA surfacing mixes. Regrettably, however, while many USA transportation agencies have implemented design-level tests to measure the rutting potential of HMA mixes; there is hardly any standardized national design-level test for measuring and characterizing the HMA cracking resistance potential. Currently, the Texas Department of Transportation (TxDOT) uses the Overlay Tester (OT) to routinely evaluate the cracking susceptibility of HMA mixes in the laboratory. While the OT effectively simulates the reflective cracking mechanism of opening and closing of joints and/or cracks, repeatability and variability in the test results have been major areas of concern. As an effort towards addressing these repeatability/variability issues, this laboratory study was undertaken, namely to: 1) conduct a comprehensive sensitivity evaluation of the OT test procedure so as to improve its repeatability and minimize variability in the OT test results; 2) recommend updates and modifications to the Tex-248-F specification including development of OT calibration and service maintenance manuals; 3) explore other alternative OT data analysis methods; 4) comparatively evaluate and explore other crack test methods (both in monotonic and dynamic loading modes) that could serve as supplementary and/or surrogate tests to the OT test method; and 5) develop new crack test procedures, specifications, and technical implementation recommendations. As documented in this report, the scope of work to accomplish these objectives included evaluating the following crack test methods: 1) the standard repeated (OT _R , Tex-248-F) and monotonic loading OT test (OT _M); 2) the monotonic (IDT) and repeated loading indirect-tension (R-IDT) test; 3) the monotonic (SCB) and repeated loading semi-circular bending (R-SCB) test; 4) the disk-shaped compaction tension test (DSCTT); and 5) the monotonic (DT) and repeated loading direct-tension (R-DT) tests.					
17. Key Words HMA, Cracking, Repeatability, Variability, Coefficient of Variation, Overlay Tester (OT _R), Monotonic OT (OT _M), Indirect Tension (IDT, R-IDT), Semi-Circular Bending (SCB, R-SCB), Disk-Shaped Compaction Tension Test (DSCTT), Fracture Energy (FE), FE Index, Cycle Index			18. Distribution Statement No restrictions. This document is available to the public through NTIS: National Technical Information Service Alexandria, Virginia 22312 http://www.ntis.gov		
19. Security Classif. (of this report) Unclassified		20. Security Classif. (of this page) Unclassified		21. No. of Pages 180	22. Price

THE OVERLAY TESTER (OT): COMPARISON WITH OTHER CRACK TEST METHODS AND RECOMMENDATIONS FOR SURROGATE CRACK TESTS

by

Lubinda F. Walubita
Research Scientist
Texas A&M Transportation Institute

Rong Luo
Associate Research Engineer
Texas A&M Transportation Institute

Abu N. Faruk
Research Associate
Texas A&M Transportation Institute

Tom Scullion
Senior Research Engineer
Texas A&M Transportation Institute

Yasser Koochi
Graduate Research Assistant
Texas A&M Transportation Institute

Robert L. Lytton
Research Engineer
Texas A&M Transportation Institute

Report 0-6607-2

Project 0-6607

Project Title: Search for a Test for Fracture Potential of Asphalt Mixes

Performed in cooperation with the
Texas Department of Transportation
and the
Federal Highway Administration

October 2012

Published: August 2013

TEXAS A&M TRANSPORTATION INSTITUTE
College Station, Texas 77843-3135

DISCLAIMER

The contents of this report reflect the views of the authors, who are responsible for the facts and the accuracy of the data presented herein. The contents do not necessarily reflect the official view or policies of the Federal Highway Administration (FHWA) or the Texas Department of Transportation (TxDOT). This report does not constitute a standard, specification, or regulation, nor is it intended for construction, bidding, or permit purposes. The United States Government and the State of Texas do not endorse products or manufacturers. Trade or manufacturers' names appear herein solely because they are considered essential to the object of this report. The engineer in charge was Tom Scullion, P.E. #62683.

ACKNOWLEDGMENTS

This project was conducted for TxDOT, and the authors thank TxDOT and FHWA for their support in funding this research project. In particular, the guidance and technical assistance of the project director, Richard Izzo, P.E., of TxDOT, proved invaluable. The following project advisors also provided valuable input throughout the course of the project: Karl Bednarz, Miles Garrison, Ronald Hatcher, Feng Hong, Martin Kalinowski, and Stephen Smith.

The authors extend their special appreciation to Gautam Das, Hossain Tanvir, Jason Huddleston, Guillermo Ramos, Jacob Hoeffner, Carlos Flores, Lee Gustavus, and Tony Barbosa from the Texas A&M Transportation Institute (TTI) for their help with laboratory and field work. Likewise, thanks to Brett Haggerty and Thomas Smith of TxDOT-CST for their assistance with laboratory testing at the TxDOT-CST lab.

The following TxDOT lab personnel are also acknowledged for their assistance with the round-robin testing: Ronald Hatcher (Childress), Hop-Ming Tang (Houston), and Josiah Yuen (Houston). The following TxDOT individuals and institutions are gratefully thanked for supplying both the plant-mix and raw materials for lab testing: Ramon Rodriquez (Laredo), Chico TxDOT District Lab, Miles Garrison (Atlanta), Bryan District Office, Waco, Odessa, and Fort Worth.

TABLE OF CONTENTS

List of Figures	ix
List of Tables	x
List of Notations and Symbols	xiii
Chapter 1: Introduction	1-1
Research Objectives and Scope of Work	1-2
Research Methodology and Work Plans	1-2
Report Contents and Organizational Layout	1-3
Summary.....	1-4
Chapter 2: Experimental Design Plan and HMA Mixes	2-1
Materials and HMA Mix-Designs	2-1
HMA Specimen Fabrication.....	2-3
Summary.....	2-55
Chapter 3: The TEX-248-F Specification and OT Test Procedure	3-1
OT Sensitivity Evaluation and TEX-248-F Updates	3-1
OT Round-Robin Testing and Operator Effect	3-9
OT Software, Calibration, and Maintenance	3-13
Summary.....	3-18
Chapter 4: The OT Test Method – Dynamic and Monotonic Loading Modes	4-1
Test Setup	4-1
Test Response Curves and Data Analysis	4-4
The OT _M and OT _R Test Results.....	4-7
Comparison of the OT _M and OT _R Test Methods.....	4-14
Summary.....	4-15
Chapter 5: The IDT and R-IDT Test Methods	5-1
TEST SETUP	5-1
Test Response Curves and Data Analysis Models	5-4
IDT and R-IDT Test Results	5-7
Comparison of the IDT and R-IDT Test Methods	5-15
Summary.....	5-15
Chapter 6: The SCB and R-SCB Test Methods	6-1
Test Setup	6-1
Test Response Curves and Data Analysis Models	6-3
SCB and R-SCB Test Results.....	6-6
Comparison of the SCB and R-SCB Test Methods.....	6-13
Summary.....	6-14
Chapter 7: The DSCTT Test Method	7-1
The DSCTT Test Procedure	7-1
The DSCTT Data Analysis Models.....	7-2
DSCTT Test Results.....	7-4
Other Data Analysis and Test Methods Evaluated.....	7-5
Summary.....	7-6

Chapter 8: Comparison of the Crack Test Methods	8-1
HMA Crack Tests Evaluated.....	8-1
Test Loading Parameters and Output Data.....	8-1
Loading Configuration and Specimen Failure Modes.....	8-3
Test Repeatability and Load-Displacement Response Curves	8-5
Potential to Differentiate and Screen Mixes.....	8-7
Sensitivity to HMA Mix-Design Variables.....	8-8
Case Studies and Field Correlations.....	8-11
Comparative Evaluation and Ranking of the Test Methods.....	8-13
Summary.....	8-14
Chapter 9: Summary, Conclusions, and Recommendations	9-1
OT Sensitivity Evaluation	9-1
Supplementary and Surrogate Crack Tests.....	9-2
References	R-1
Appendix A: OT Machine Check, Calibration, and Verification prior to Round- Robin Testing	A-1
Appendix B: OT Parallel Testing with TxDOT-CST (Austin).....	B-1
Appendix C: Load-Displacement Response Curves for Monotonic Loading Crack Tests.....	C-1
Appendix D: Advanced OT Data Analysis Methods Using Energy Concept and Numerical Modeling	D-1
Appendix E: The DT and R-DT Test Methods	E-1

LIST OF FIGURES

Figure 3-1. Effects of Displacement Variations at Constant Frequency – 10 Sec/Cycle.	3-4
Figure 3-2. Loading Frequency Variations at Constant Displacement – 0.025 Inches.	3-5
Figure 3-3. Effects of Sample Notching on the OT Results.	3-6
Figure 3-4. Single and Multiple Cracking in Some OT Samples.	3-7
Figure 3-5. The New OT Calibration Kit and Examples of Linear Graphical Screen Plots.....	3-15
Figure 3-6. Typical Load-Voltage Response Curve – Well-Calibrated OT Load Cell.	3-16
Figure 3-7. OT Verification of the Raw Data Files.	3-17
Figure 4-1. Overlay Tester (OT) Setup.....	4-2
Figure 4-2. Load-Displacement Response Curve: OT _M Testing.	4-4
Figure 4-3. OT _R Output Data and Interpretation of Results.	4-6
Figure 4-4. Comparison of HMA Mixes Based on OT _M and OT _R Test Results.....	4-8
Figure 4-5. Relationship between the OT _R Cycles and OT _M FE Index.	4-9
Figure 4-6. OT _M and OT _R Test Parameter Sensitivity to AC Variation.	4-12
Figure 5-1. IDT Horizontal Displacement Calculation from Vertical (Ram) Displacements.	5-3
Figure 5-2. Load-Displacement Response Curve: IDT Testing.	5-5
Figure 5-3. R-IDT Load (Input) – Displacement (Output) Curve.	5-6
Figure 5-4. Evolution of Peak Displacement with the Number of Load Cycles.	5-7
Figure 5-5. IDT Test Outputs: Load-Displacement Response Curves.	5-8
Figure 5-6. Summary of IDT Test Results.....	5-9
Figure 5-7. IDT and R-IDT Test Parameter Sensitivity to AC Variation.....	5-13
Figure 6-1. Load-Displacement Response Curve: SCB Testing.	6-4
Figure 6-2. R-SCB Load (Input) – Displacement (Output) Curve.	6-5
Figure 6-3. Evolution of Peak Displacement with the Number of Load Cycles.	6-6
Figure 6-4. SCB Test Outputs: Load-Displacement Response Curves.	6-7
Figure 6-5. Summary of SCB Test Results.....	6-8
Figure 6-6. SCB and R-SCB Test Parameter Sensitivity to AC Variation.....	6-12
Figure 6-7. SCB and R-SCB Testing at High AC Levels: Multiple Crack Failure Modes.	6-13
Figure 7-1. DSCTT Testing Setup and Specimen Dimensions.	7-1
Figure 7-2. Load-Displacement Response Curve: DSCTT Testing.	7-3
Figure 7-3. DSCTT Load-Displacement Response Curve: Type D (5.5% AC).....	7-4
Figure 8-1. Multiple Cracking in OT _R , SCB, and R-SCB Tests.....	8-5
Figure 8-2. Comparison of Test Repeatability (Load-Displacement Response Curves).....	8-7

LIST OF TABLES

Table 2-1. Materials and Mix-Design Characteristics.....	2-2
Table 2-2. HMA Mixing and Compaction Temperatures.....	2-4
Table 3-1. OT Sensitivity Evaluation and Recommendations for Tex-248-F Updates.....	3-2
Table 3-2. OT Sample Thickness Variation Results.....	3-3
Table 3-3. Alternative OT Data Analysis Methods (Walubita et al., 2012).....	3-9
Table 3-4. OT Round-Robin Results – Laredo Type C Mix.....	3-10
Table 3-5. OT Round-Robin Results – Four Different HMA Mixes.....	3-10
Table 3-6. OT Operator Effect.....	3-11
Table 3-7. Trained Operator Effect.....	3-11
Table 3-8. Trained Operator and Equipment Effect.....	3-12
Table 3-9. OT Results – New (Version 1.9.0) versus Old Software.....	3-14
Table 4-1. OT _M and OT _R Test Parameters.....	4-1
Table 4-2. OT Results Summary.....	4-7
Table 4-3. Screening of HMA Mixes Based on Discriminatory Ratios.....	4-10
Table 4-4. Screening of HMA Mixes Based on ANOVA and Tukey’s HSD Analysis.....	4-11
Table 4-5. Sensitivity to AC Variations.....	4-12
Table 4-6. Sensitivity to AC: Discriminatory Ratios and Statistical Analysis.....	4-13
Table 4-7. AC Sensitivity: Type D Mix.....	4-14
Table 4-8. Temperature Sensitivity of the OT _M and the OT _R Tests.....	4-14
Table 4-9. Comparison of OT _M and OT _R Test Methods.....	4-15
Table 5-1. IDT and R-IDT Test Parameters.....	5-1
Table 5-2. Summary of IDT Test Results.....	5-9
Table 5-3. Summary of R-IDT Test Results.....	5-10
Table 5-4. Screening of HMA Mixes Based on Discriminatory Ratios.....	5-11
Table 5-5. Screening of HMA Mixes Based on ANOVA and Tukey’s HSD Analysis.....	5-12
Table 5-6. Sensitivity to AC Variations.....	5-12
Table 5-7. Sensitivity to AC: Discriminatory Ratios and Statistical Analysis.....	5-14
Table 5-8. Comparison of IDT and R-IDT Test Methods.....	5-15
Table 6-1. SCB and R-SCB Test Parameters.....	6-1
Table 6-2. Summary of SCB Test Results.....	6-7
Table 6-3. Summary of R-SCB Test Results.....	6-9
Table 6-4. Screening of HMA Mixes Based on Discriminatory Ratios.....	6-10
Table 6-5. Screening of HMA Mixes Based on ANOVA and Tukey’s HSD Analysis.....	6-11
Table 6-6. Sensitivity to AC Variations.....	6-11
Table 6-7. Comparison of SCB and R-SCB Test Methods.....	6-13
Table 7-1. DSCTT Loading Parameters.....	7-2
Table 7-2. DSCTT Results Summary: Type D Mix.....	7-5
Table 8-1. Summary of HMA Cracking Tests Evaluated: Loading Parameters and Output Data.....	8-2
Table 8-2. Crack Test Loading Configuration and Failure Modes.....	8-4
Table 8-3. Comparison of Test Repeatability.....	8-6
Table 8-4. Differentiating of HMA Mixes: Discriminatory Ratios.....	8-7
Table 8-5. Differentiating of HMA Mixes: Statistical Analysis.....	8-8
Table 8-6. Sensitivity to AC Variations.....	8-9

Table 8-7. Sensitivity to AC Change: Discriminatory Ratios.....	8-9
Table 8-8. Sensitivity to AC Change: Comparison of the OT _M and OT _R Tests.	8-10
Table 8-9. Sensitivity to Temperature Change: Comparison of the OT _M and OT _R Tests.	8-10
Table 8-10. Field Correlation: OT _R Test.....	8-12
Table 8-11. Field Correlation: APT Testing.	8-12
Table 8-12. Comparative Evaluation of the Crack Test Methods.	8-13
Table 8-13. Crack Test Ranking, Practicality, and Implementation.....	8-14

LIST OF NOTATIONS AND SYMBOLS

AC	Asphalt-binder content
ADT	Average daily traffic
ALF	Accelerated Loading Facility
APT	Accelerated pavement testing
AR	Asphalt-rubber
ASTM	American Society for Testing and Materials
AV	Air voids
Avg	Average
BMD	Balanced mix-design method
CAM	Crack attenuating mixtures
COV	Coefficient of variation
CS	College Station
DOT	Department of Transportation
DSCTT	Disc-Shaped Compact Tension Test
DSR	Dynamic Shear Rheometer
DT	Direct-Tension test (monotonic loading)
FE Index	Fracture energy index
HMA	Hot mix asphalt
IDT	Indirect Tension Test (monotonic loading)
LA	Louisiana
LTRC	Louisiana Transportation Research Center
LVDT	Linear variable displacement transducer
MTS	Material testing system
NMAS	Nominal maximum aggregate size
OAC	Optimum AC
OGFC	Open graded friction course
OT	Overlay Tester
OT _R	Repeated load OT test or OT testing conducted in repeated loading mode
OT _M	Monotonic OT test or OT testing conducted in monotonic loading mode
PG	Performance grade

RAP	Reclaimed asphalt pavement
PM	Plant-mix
RAS	Recycled asphalt shingles
R-DT	Repeated loading DT test
R-IDT	Repeated loading IDT test
R-SCB	Repeated loading SCB test
SCB	Semi-circular bending test (monotonic loading)
SGC	Superpave gyratory compactor
SMA	Stone mastic asphalt
TTI	Texas A&M Transportation Institute
TxDOT	Texas Department of Transportation
WMA	Warm mix asphalt
G_f	Specific fracture energy
σ_t	HMA tensile strength
ε_t	Tensile strain at peak failure load (ductility potential)
E_t	HMA tensile modulus (stiffness)
ΔK	Stress Intensity Factor (SIF)

CHAPTER 1: INTRODUCTION

Over the past decade, TxDOT attempted to help mitigate rutting in the early life of HMA pavements through using stiffer mixes. Unfortunately, this has come at the expense of reflective cracking. One of the contributing factors to this issue is the complexity of the current mix designs since HMA is now predominately produced with recycled materials such as RAP and RAS. The adaptation of the Hamburg rutting test ([Tex-242-F, 2009](#)) and stiffer asphalt binders, while almost eliminating rutting distresses, has not helped to reduce resistance to cracking. Consequently, there still remains a great need for a simple and practical performance-related cracking test that can be performed routinely during the laboratory mix design process and production to ensure that HMA is not susceptible to premature cracking.

Reflective cracking is one of the predominant types of cracking in flexible pavements of new HMA overlays placed on HMA pavements that have experienced cracking caused by fatigue, aging, and/or thermal stresses. The opening and closing of joints and/or cracks induced by daily temperature variations and vehicle loading contributes to the rapid propagation of the subsurface defects through the overlay to the surface. This mechanism is simulated in the laboratory using a specially modified Overlay Tester (OT) device, which TxDOT currently uses to evaluate the cracking susceptibility of HMA mixes ([Tex-248-F, 2009](#)).

Since its adaption through Specification Tex-248-F, application of the OT as a reliable cracking susceptibility lab test has been a challenge due to repeatability and variability issues, particularly with the coarse and dense-graded mixes. While the test is fairly satisfactory with SMA and CAM, variability has been an issue with most conventional TxDOT dense-graded mixes such as Type C and D mixes; that constitute approximately 75 percent of all HMA produced for TxDOT.

A laboratory mix test to characterize the cracking susceptibility of HMA is thus greatly needed for all the Texas HMA mix types. As a minimum, such a test protocol must have the following characteristic features:

- Applicable for routine HMA mix-design and screening (not necessarily performance prediction such as fatigue life).
- Practical and easy implementation by TxDOT.
- Easy sample preparation with potential to test both lab-prepared and field cores.
- Reasonable test duration of no more than a day.

- Acceptable level of variation and test reliability.
- Potential to simulate and/or correlate with the field conditions.

RESEARCH OBJECTIVES AND SCOPE OF WORK

As part of the efforts to address the OT variability issues as well as explore new supplementary and/or surrogate crack tests, this two-year study was initiated with the following technical objectives:

- Evaluate the current OT procedure and make it more repeatable and robust. Perform a comprehensive sensitivity evaluation of all key steps in the OT protocol ([Tex-248-F, 2009](#)) and data analysis procedure.
- Recommend updates and modifications to the Tex-248-F specification including development of the OT calibration and maintenance manuals.
- Evaluate the repeatability between laboratories for the OT test in a production environment by running duplicate tests in both the TTI and TxDOT labs on plant mixes from in-service and/or ongoing TxDOT projects.
- Evaluate the potential for having alternative and/or surrogate tests to identify crack-susceptible mixes. Identify and evaluate other cracking tests that must:
 - Be performance related.
 - Be sensitive to critical mix-design parameters such as asphalt content, mix type, etc.
 - Provide improved repeatability.
- Develop new test procedures, specifications, and technical implementation recommendations.

RESEARCH METHODOLOGY AND WORK PLANS

To achieve the technical objectives of the study, the research methodology incorporated extensive laboratory testing of actual HMA mixes being placed on Texas highways using the OT and various other potential supplementary/surrogate crack tests. Additionally, the research team compared the field performance of some selected HMA mixes with the laboratory test results to provide TxDOT designers and engineers with defensible data to justify and validate the need for

implementing the new test procedures recommended from this study. Overall, the work plans and scope of work incorporated the following eight major tasks:

- Task 1: Data search and literature review.
- Task 2: Comprehensive OT sensitivity evaluation and improvements to the Tex-248-F test procedure.
- Task 3: Parallel and Round-robin testing of split OT samples from TxDOT projects.
- Task 4: Development of test procedures for alternative cracking tests.
- Task 5: Comprehensive laboratory evaluations of potential supplementary and/or surrogate fracture tests.
- Task 6: Correlation of lab test results with field test data.
- Task 7: Recommendation of test procedures and specifications.
- Task 8: Case study: demonstration of how to improve the HMA mix-design using the recommended crack test procedures.

While this report is tailored to provide a complete documentation of all the work accomplished during the whole two-year study period, focus is on Tasks 4 through 8. Tasks 1 through 3 were extensively covered in the previous Year 1 Technical Report 0-6607-1 ([Walubita et al., 2012](#)). However, a summary documentation of the key findings and other relevant aspects of Tasks 1 through 3 are incorporated in this report including the proposed OT calibration and maintenance procedures.

REPORT CONTENTS AND ORGANIZATIONAL LAYOUT

This report consists of 10 chapters including this one ([Chapter 1](#)) that provides the background, research objectives, methodology, and scope of work. [Chapter 2](#) follows, presenting the experimental design plan and the HMA mixes that were evaluated. [Chapters 3](#) through [9](#) are the main backbone of this report that includes the OT test and other alternative crack test methods evaluated (both in monotonic and repeated loading modes). These chapters cover the following key aspects, respectively:

- Chapter 3** The Tex-248-F Specification and OT Test Procedure– this includes the modified sample fabrication procedure, the modified Tex-248-F specification with a video demo, and the Round-robin OT test results.
- Chapter 4** The OT test method–comparing the dynamic and the monotonic loading modes.
- Chapter 5** The IDT and R-IDT test methods.
- Chapter 6** The SCB and R-SCB test methods.
- Chapter 7** The DSCTT test method.
- Chapter 8** Statistical and sensitivity comparison of all the crack test methods including correlation with field data and demonstration case studies.

Chapter 9 is primarily a summation of the report with a list of the major findings and recommendations. Some appendices of important data are also included at the end of the report. A CD/DVD video demo of the revised Tex-248-F test procedure and sample fabrication process is included as an integral part of this report. The CD video also includes a demo of the other crack test methods that were evaluated by these researchers. Reference should also be made to Report 0-660701 ([Walubita et al., 2012](#)) that has a comprehensive documentation of the OT sensitivity evaluation.

SUMMARY

In this introductory chapter, the background and the research objectives of this project were discussed. The research methodology and scope of work were then described, followed by a summary of the project work plan. The chapter ended with a description of the report contents and the organizational layout.

CHAPTER 2: EXPERIMENTAL DESIGN PLAN AND HMA MIXES

Four HMA mix types (Type B, C, CAM, and D) with over 10 different mix designs were evaluated and are discussed in this chapter. The experimental design including the test plan, HMA specimen fabrication, and air void (AV) measurements are also discussed in this chapter. To wrap up the chapter, researchers summarized the key points.

MATERIALS AND HMA MIX-DESIGNS

Various aspects in terms of the materials and HMA mix-design were considered in developing the experimental design plan. As a minimum, the following important aspects were considered:

- Evaluate at least two commonly used Texas dense-graded mixes, with known poor and good field cracking performance, respectively, preferably a Type C (typically poor crack-resistant) and CAM (good crack-resistant) mix.
- Evaluate at least two asphalt-binder contents: optimum and optimum ± 0.5 percent.
- Evaluate at least two asphalt-binder types, with a PG 76-22 included in the matrix.
- Evaluate at least two commonly used Texas aggregate types, typically limestone (relatively poor quality) and crushed gravel or quartzite (good quality).

HMA Mix Types

On the basis of the above experimental design plan, four commonly used Texas HMA mixes (Type B, C, CAM, and D) with over 10 different mix designs were utilized and are discussed in this chapter. [Table 2-1](#) lists these mixes and includes the material type, material sources, and asphalt-binder content (AC). Where applicable, names of highways where the mix had recently been used are also indicated in the table. In terms of usage, the selected mixes cover a reasonable geographical and climatic span of Texas, which includes the central, northern, and southwestern regions; see [Figure 2-1](#). HMA samples of these mixes were molded from both plant-mix and raw materials in the laboratory.

Table 2-1. Materials and Mix-Design Characteristics.

#	Mix Type	District Source	Hwy Used	Binder	Aggregate	AC (%)
1	CAM	Paris	SH 121	PG 64-22 (PG 76-22)	Igneous/limestone	7.0
2	CAM	Bryan	FM 158	PG 76-22	Limestone + 1% Lime	6.7
3	Type D	Chico	-	PG 70-22	Limestone	4.5, 5.0, & 5.5
4	Type D	Atlanta	US 59	PG 64-22	Quartzite + 20% RAP	5.0, 5.2, 5.4, 5.5, 5.6, 5.8, & 6.2
5	Type B	Waco	IH 35	PG 64-22	Limestone + 30% RAP	4.6
6	Type C	Laredo	US 59, Spur 400, Loop 20	PG 64-22	Crushed Gravel + 20% RAP	5.0
7	Type D	Childress	US 287	PG 58-28	Granite + 20% RAP	4.9
8	Type C	Fort Worth	-	PG 70-22	Granite + 15% RAP	4.6
9	Type C	Odessa	-	PG 70-22	Limestone	5.8
10	Type C	Waco	SH 31	PG 64-22	Gravel/Limestone/Dolomite + 16% RAP + 3% RAS + 1% Lime	5.0
11	Type C	Corpus Christi	SH 358	PG 70-22	Limestone + 20% RAP	4.9
12	Type C	LTRC (LA)	APT (ALF)	PG 76-22	Limestone	4.3
13	Type D	Amarillo	US 54	PG 58-28, PG 64-28, PG 70-28	Limestone/Dolomite + 1% Lime + 15.2% RAP + 4.2% RAS	4.5 – 6.5

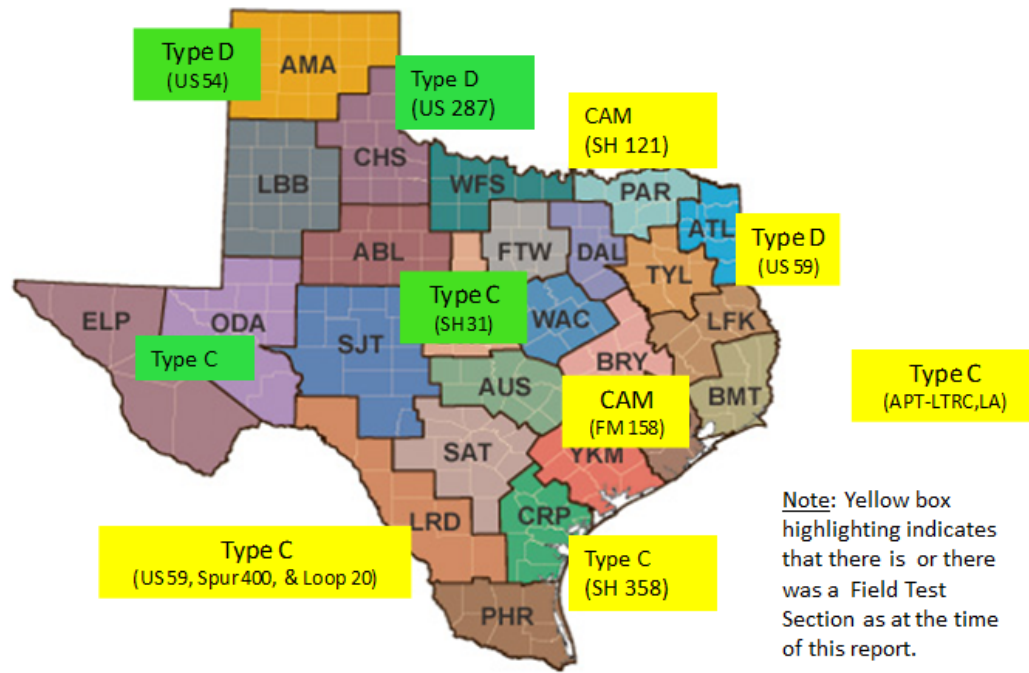


Figure 2-1. Geographical Location of Some of the HMA Mixes Used in This Study.

Aggregate Sieve Analysis

Aggregate sieve analysis was also performed where HMA samples were molded directly from the raw materials in the laboratory. To accurately reflect the specified aggregate gradation for each mix type and account for the dust particles, adjustments were made to the original aggregate gradation based on the results of a wet sieve analysis. Wet sieve analysis is necessary when adjusting the aggregate gradation because quite often, dust particles and the aggregate fractions passing the number 200 sieve size tend to cling to the surfaces of the particles that are larger than the number 200 sieve size. This phenomenon is often not well accounted for in a given gradation specification.

Wet sieve analysis is basically an iterative process of aggregate sieving, wetting/washing, and drying, followed by subsequent gradation adjustments based on the aggregate mass loss or gain on the individual sieve sizes. For this study, researchers accomplished the analysis based on the TxDOT standard specification Tex-200-F ([TxDOT, 2004](#)). On average, three to four iterations were required prior to achieving the final adjustment.

After gradation adjustment, new maximum theoretical specific gravities were accordingly determined using the ASTM standard D2041. A wet sieve adjustment does not change the fundamental properties of the gradation but instead gives a more accurate representation of the specified gradation.

HMA SPECIMEN FABRICATION

For the lab-molded samples directly from raw materials, the HMA specimen preparation procedure was consistent with the TxDOT standard specifications Tex-205-F and Tex-241-F ([TxDOT, 2009](#)). The basic procedure involved the following steps: aggregate batching, wet sieve analysis, asphalt-aggregate mixing, short-term oven aging, compaction, cutting, and, finally, volumetric analysis to determine the AV. [Table 2-2](#) summarizes the HMA mixing and compaction temperatures.

Table 2-2. HMA Mixing and Compaction Temperatures.

#	Asphalt Binder Performance Grade (PG)	Mixing Temperature	Compaction Temperature
1	PG 76-22	325°F (163°C)	300°F (149°C)
2	PG 70-22	300°F (149°C)	275°F (135°C)
3	PG 64-22	290°F (143°C)	250°F (121°C)

Aggregate Batching

For fabricating the lab-molded samples directly from raw materials, the aggregates (including recycled materials, when applicable) were batched according to the mix-design sheets (Tex-204-F) based on the Tex-205-F test procedure (TxDOT, 2011). The procedure was carefully followed so that it was consistent with the TxDOT standard specification Tex-205-F. Calculated amounts of dry aggregates for each sieve size were added to the pan along with mineral filler and hydrated lime where applicable, then mixed thoroughly. The mixed aggregates were left in the oven at an appropriate mixing temperature.

Mixing and Sample Molding

Once the aggregates reached the required mixing temperature in the case where raw materials were used, they were removed and placed in the mixing bowl along with the heated recycled material (RAP). Required amounts of asphalt binder were added and were thoroughly mixed using a mechanical mixer. The mixture was placed into the oven at an appropriate compaction temperature for short-term aging.

HMA short-term oven aging for both lab-molded samples and plant mixes lasted for two hours at the compaction temperature consistent with the American Association of State Highway and Transportation Officials (AASHTO) PP2 aging procedure for Superpave mix performance testing. Short-term oven aging simulates the time between HMA mixing, transportation, and placement up to the time of in situ compaction in the field.

All the HMA specimens (both from plant-mix materials and raw materials) were gyratory compacted and molded using the standard SGC according to Tex-241-F (TxDOT, 2009). All the HMA specimens were compacted to a target AV content of 7 ± 1 percent. Based on the

recommendations from Technical Report 0-6607-1 (Walubita et al. 2012), all the HMA samples were compacted to a height of 5.0 inches in a 6.0-inch diameter mold.

Cutting of Specimens and AV Measurements

Based on the test specimen geometries and the required OT specimen dimensions, typically two OT specimens were obtainable from a 5.0-inch long molded sample using a double-blade saw following the recommendations from Technical Report 0-6607-2 (Walubita et al. 2012). After the specimens were cut and cored, volumetric analyses based on fundamental water displacement principles as specified in ASTM D2726 were completed to determine the exact AV content of each test specimen. HMA specimens that failed to meet AV specification (i.e., 7 ± 1 percent) were discarded. The good specimens meeting the target AV were stored at ambient temperature on flat shelves in a temperature-controlled facility prior to gluing and testing.

SUMMARY

This chapter provided a presentation of the materials and mix designs used in this study. In total, four common Texas mix types (Type B, C, D, and CAM) with over 10 different mix designs were evaluated. The experimental design including the HMA specimen fabrication, short-term oven aging, and specimen cutting were also discussed.

CHAPTER 3: THE TEX-248-F SPECIFICATION AND OT TEST PROCEDURE

In an attempt to optimize the OT repeatability and minimize variability in the test results, a comprehensive sensitivity evaluation of the critical steps of the OT test procedure was conducted. As documented in this chapter, this laboratory study of a step-by-step evaluation of the current Tex-248-F OT test procedure included the following key aspects:

- OT sensitivity evaluation of the influencing variables and their effects on the variability in the test results.
- Recommend modifications and updates to the Tex-248-F specification.
- OT Round-robin testing between TTI and TxDOT labs.
- OT software updates, calibration, and service maintenance.

In addition, the chapter also includes a discussion of an accompanying OT Video Demo that demonstrates the updated Tex-248-F test procedure, calibration, and maintenance processes. A summary of the key findings and recommendations is then presented to conclude the chapter.

OT SENSITIVITY EVALUATION AND TEX-248-F UPDATES

One of the primary goals for initiating this two-year study was to search for ways to improve repeatability and minimize variability in the OT test results. Toward this goal, these researchers identified and studied over 15 different variables in the OT testing procedure to determine how they could be improved so as to enhance the OT repeatability and minimize variability in the test results. [Table 3-1](#) summarizes these variables together with the key findings and proposed recommendations to the Tex-248-F specification. The proposed updates to the Tex-28-F specification are included in the accompanying CD.

Detailed results and corresponding analysis of the [Table 3-1](#) sensitivity evaluation are documented in Report 0-6607-1 ([Walubita et al., 2012](#)). However, variables such as sample thickness variation, load variations, sample notching, operator effect, etc., which were not included in Report 0-6607-1 ([Walubita et al., 2012](#)) are discussed in the subsequent text. The statistical threshold for all the analyses in this report is a COV of 30 percent ([Walubita et al., 2012](#)). To exclude the aging effects and ensure usage of the same batch, a different sets of samples were molded and tested each time the factors/variables were changed.

Table 3-1. OT Sensitivity Evaluation and Recommendations for Tex-248-F Updates.

#	Factor	Variables Investigated	Key Finding	Tex-248-F Spec Item	Tex-248-F Spec Recommendation
1	Operator effect	2 → Untrained & trained	More consistent results with Trained Operators	----	- Start certification program - Train at least 2 Techs per lab
2	Sample replicates	3 → 3, 4, & 5	Testing 5 or 4 & picking best 3 gives good results – discard outliers	5.1.1 & 6.2	Test 5 & pick best 3 based on lowest COV (<i>testing 5 is better</i>)
3	Drying method after cutting samples	3 → Air (room), Oven (104°F), → & Core dryer (room)	Oven @ 104°F best followed by core dryer	5.2.3	Use Oven drying at 104°F (40°C); ≥ 12 hrs to constant weight
4	Sample molding size	4 → 5.0" (cut 2), 4.5" (cut 1), → 4.5" (cut 2), & 2.5" (cut 1)	- Use 5" (cut 2) or 2.5" (cut 1) - 4.5" (cut 1) is too wasteful	4.1 & 5.1.1	Mold 5" tall & cut 2 specimens from the middle
5	Sample sitting time from day of molding	7 → 3, 5, 7, 9, 11, 15, & 20 days	Testing within 5 days → more consistent results; record if > 5 days	4.1 & 5.7.2	Test within 5 days
6	Glue type	3 → (1) Plastic steel putty, (2) High strength epoxy, & (3) 2-ton epoxy; all Devcon two-part	Devcon 2-ton 2-part epoxy → reasonable price, workability, & better results	5.3.3	Use 2500 psi strength epoxy or gluing compound with ≤ 8 hrs curing time to full strength
7	Glue quantity (Devcon 2 ton 2-part epoxy)	4 → 12, 14, 16, & 18 grams	- Old plates = 15±1 grams - New plates = 13±1 grams	5.3.3	Use 14±2 grams (12 – 16 mils)
8	Plate/sample gap width	2 → ¼" (tape & metal bar spacer)	- New base/plates better - Easy to align & efficient	3.3	Use new base/plates, but be cautious with metal space bar (Lubrication & 5-10 min waiting time)
9	Sample AV uniformity	5 → 5%, 6%, 7%, 8%, & 9% (±0.5, ±1, ±1.5%, ±2.0%)	7±0.5% → more consistent results	4.1.1	- Use 7±1% for practicality - Target 7±0.5% if possible
10	Test temperature differential	5 → 73, 75, 77, 79, & 81°F (±2, ±4, ±6%, ±8%)	High variability for > 2°F temperature differential	5.7.1	- Use ≤ ±2°F tolerance @ 77°F - TTI OT ≤ ±0.5°F
11	Wait time prior to test commencement after tying the sample to the machine	5 → 5, 10, 20, & 30 minutes	Better consistency for ≥ 10 minutes wait time	5.7.1	Use ≥ 10 minutes wait time
12	Test loading parameters - displacement	5 → 0.0125, 0.015, 0.017, 0.020, & 0.025 inches	- Significant effect on cycles - No definite trend on variability	2.1 & 5.7	Continue using 0.025 inches
13	Test loading parameters - frequency	3 → 5, 10, & 20 sec/cycle	- Has some effect on cycles - No definite trend on variability	2.1 & 5.7	Stick with the current standard = 10 sec/cycle
14	Sample batching & molding	2 → 1 batch (multiple samples) & 1 batch (1 sample)	Single → slight improvement in consistency	4.1	Small batches better, but more work & time
15	Sample thickness	4 → 1.0, 1.5, 2.0, & 2.5 inches	- Significant effect on cycles - No definite trend on variability	5.2.1.3	Stick with the current spec
16	Sample notching	2 → 0.0" & ¼" notch depth	- ¼" notch → No definite trend, but reduction in COV for Type B mix - No major impact on cycles	4.1, 5.1.1.1 & 5.1.3	Stick to the current spec (however, consider notching as an option for samples from coarse-graded mixes such as Type B)

Effects of OT Sample Thickness Variation

Three HMA mixes were evaluated and the sample thickness was varied from 1.0 to 2.5 inches. The standard OT test parameters were utilized, namely 0.025 inches displacement at a loading frequency of 10 sec/cycle and a test temperature of 77°F. For each mix and sample thickness, the research team molded and tested five replicate samples. [Table 3-2](#) shows the average results based on the best three (lowest COV).

Table 3-2. OT Sample Thickness Variation Results.

Thickness (Inches)	Avg OT Cycles (Best 3 of 5)		
	Type B with Limestone	Type C with Limestone RAP + RAS	Type D with Quartzite + RAP
1.0	-	-	67
1.5	28	9	304
2.0	237	347	1,000+
2.5	1,000+	970	-
Thickness (Inches)	Statistical Variability (COV ≤ 30%)		
1.0	-	-	23%
1.5	22%	12%	11%
2.0	19%	18%	-
2.5	-	16%	-

In [Table 3-2](#), the NMAAS (refer to [Table 2-1](#)) and the marginal OT performance at 1.5 inch sample thickness did not warrant the need to evaluate the 1.0-inch thickness for the Type B and C mixes. Therefore, only the Type D mix was evaluated at 1.0-inch thickness. From the results in [Table 3-2](#), the following two key points are evident:

- As theoretically expected, the laboratory OT cracking performance of the mixes significantly improved with increasing sample thickness, i.e., the number of OT cycles to failure rose almost exponentially with an increase in the sample thickness.
- There is no consistency or definitive trend in terms of the impact of the sample thickness on variability as measured in terms of the COV. Therefore, varying the sample thickness, while obviously improving the laboratory cracking performance (i.e., number of cycles to failure), may not necessarily reduce variability in the test results.

Effects of OT Load Variations – Displacement and Frequency

For this task, both the loading displacement and frequency were varied (minimum three levels each) while the sample thickness was maintained at 1.5 inches. The displacement was varied from 0.0125 to 0.025 inches, all applied at a loading frequency of 10 sec/cycle and a test temperature of 77°F. Note that 0.025 inches is the currently specified OT loading displacement based on the Tex-248-F test procedure (TxDOT, 2011); see Appendix A for comparisons with some field data.

In the second part of the task, the loading frequency was varied from 5 to 20 sec/cycle while maintaining the displacement and test temperature at 0.025 inches and 77°F, respectively. Samples from the same batch for each mix type were specifically molded and tested for this task. Figures 3-1 and 3-2 show these results (for up three HMA mixes).

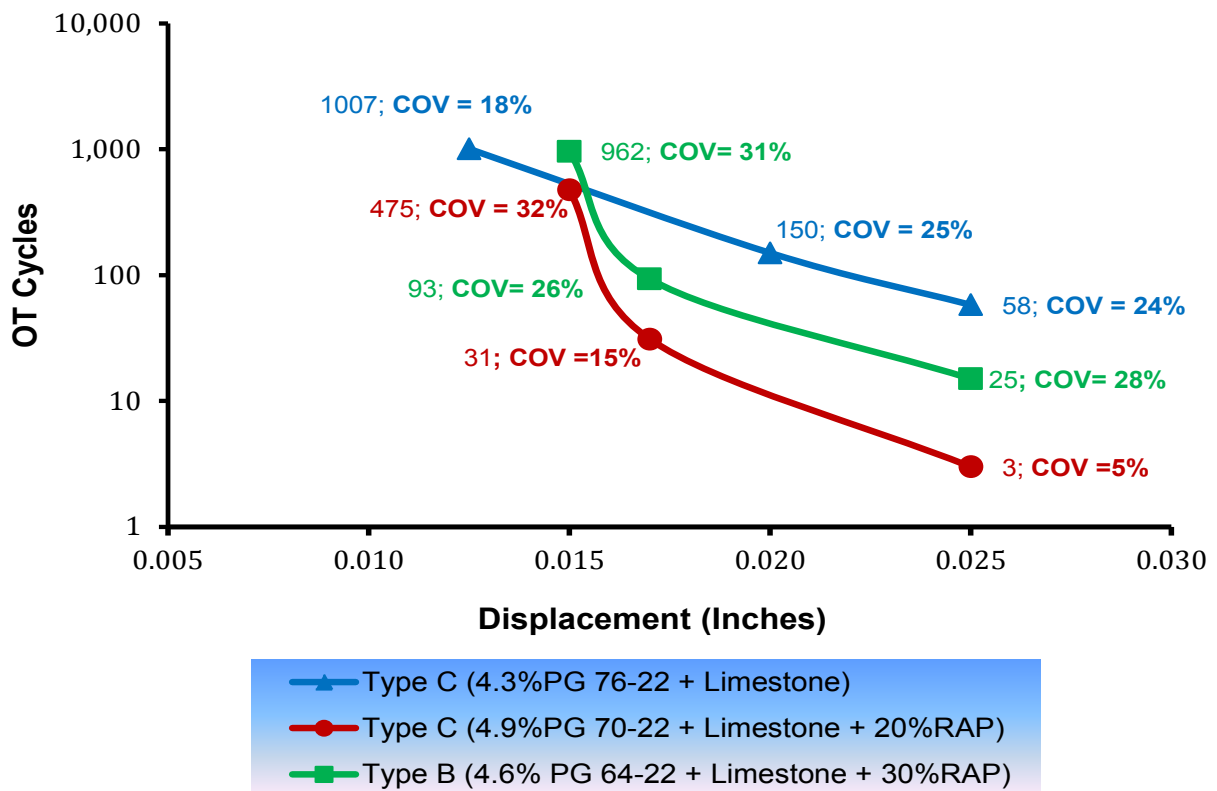


Figure 3-1. Effects of Displacement Variations at Constant Frequency – 10 Sec/Cycle.

Since this task entailed reducing the displacement as well as varying the loading frequency, only marginally performing mixes at 0.025 inches were selected for evaluation, namely the Type B and C mixes. For the three HMA mixes evaluated, it is clear from [Figure 3-1](#) that the following inferences can be made:

- There is a significant impact on the OT cycles with decreasing displacement, i.e., the OT cycles are increasing as the displacement magnitude is decreased.
- There is no definitive trend or consistent effect on variability in terms of the COV. This means that reducing the displacement while obviously increasing the number of OT cycles may not necessarily reduce variability in the test results.
- As shown in [Figure 3-2](#), changing the loading frequency at 0.025 inches constant displacement, while having some effects on the number of OT cycles, offers little benefit in terms of optimizing repeatability and minimizing variability in the test results. Therefore, the current Tex-248-F specification of 0.025 inches and 10 sec/cycle should be maintained.

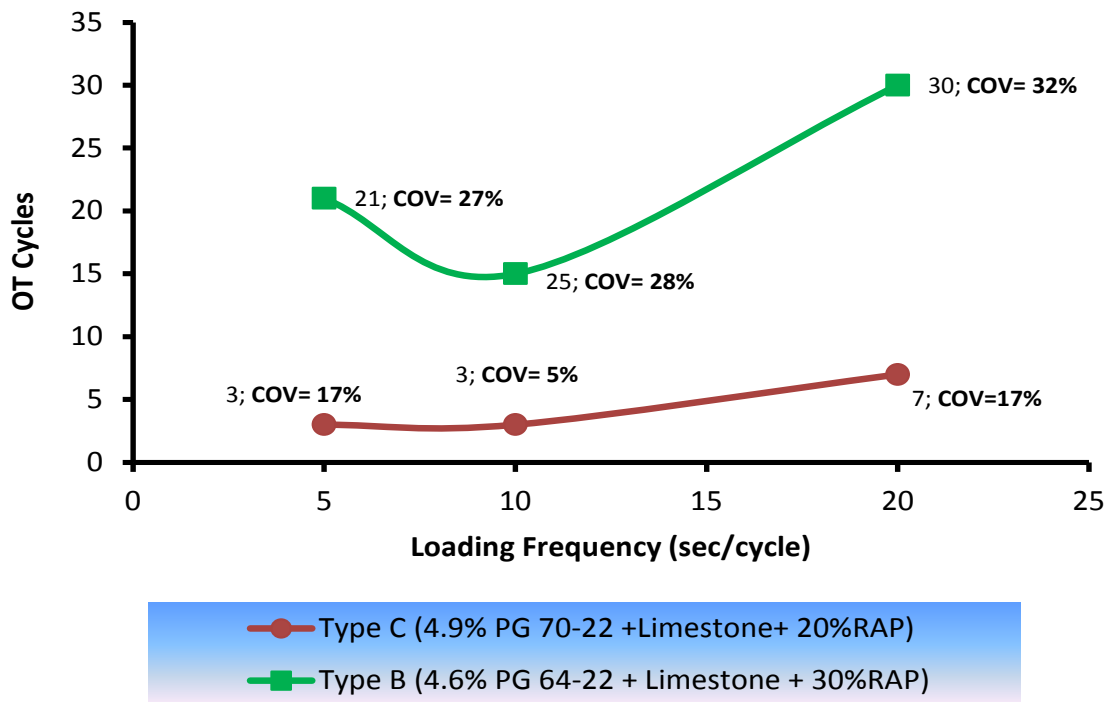


Figure 3-2. Loading Frequency Variations at Constant Displacement – 0.025 Inches.

Effects of Sample Notching

Three mixes were evaluated for this task; with ¼-inch notching (by ⅛-inch width) versus zero notching. The standard Tex-248-F sample thickness of 1.5 inches was utilized. The notching process took at least 45 minutes additional time. Different from the preceding tasks, different samples, but coming from the same batch per mix type, were specifically molded and tested for this particular task. Figure 3-3 shows the results of this sensitivity task based on the best three replicate samples out of a total of five.

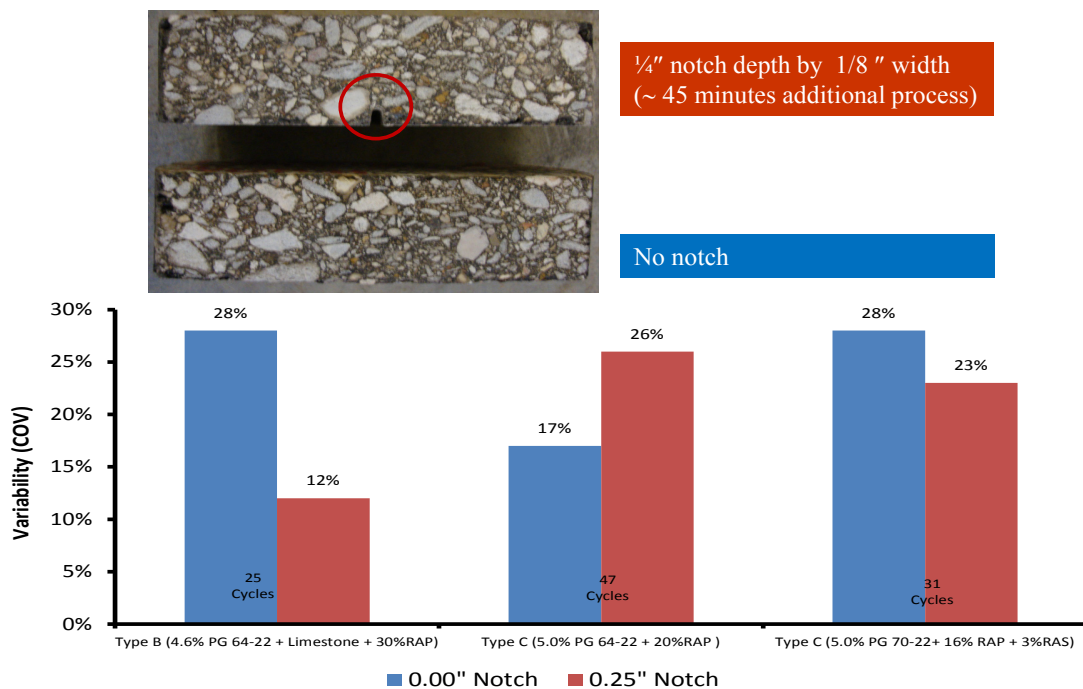


Figure 3-3. Effects of Sample Notching on the OT Results.

As shown in Figure 3-3, the sample notching measuring ¼-inch (depth) by ⅛-inch (width) had the following effects on the three mixes that were evaluated:

- There is no significant impact on the number of OT cycles to failure, i.e., the number of OT cycles were insignificantly different when comparing the notched to the un-notched sample results.
- There is no definitive trend or significant impact on variability in terms of the COV for the dense-graded Type C mixes. Although not shown in Figure 3-3, a similar trend was also observed for the fine-graded mixes.

- However, a significant decrease in the COV was noted for the coarse-graded Type B mix. While the average number of OT cycles were hardly different, the COV for the notched samples was over half that of the un-notched samples, i.e., 12 percent (notched) versus 28 percent.

Therefore, recommendations are to stick to the current practice of not notching the 1.5-inch thick samples. However, notching should be considered an option for samples from coarse-graded mixes such as Type B to improve consistency.

OT Crack Failure Mode

Theoretically, single cracking is the desired failure mode for HMA samples subjected to OT testing. In practice however, this is not often the case. Multiple cracking will often (but not always) occur in some samples, particularly for the coarse-graded mixes. Examples of both single and multiple cracking are shown in [Figure 3-4](#).

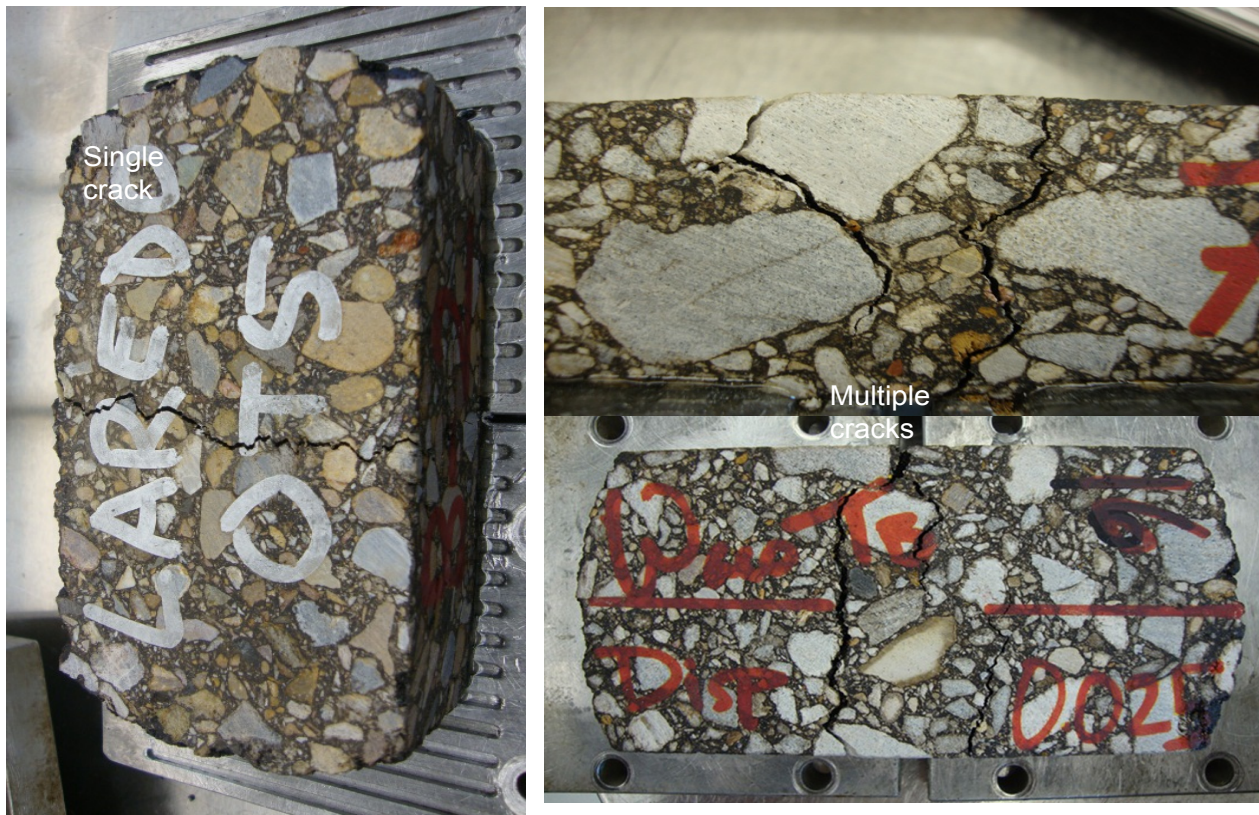


Figure 3-4. Single and Multiple Cracking in Some OT Samples.

As can be noted in [Figure 3-4](#), aggregate size and orientation are the predominant factors contributing to the occurrence of multiple cracking, with the coarse-graded mixes being more vulnerable. Multiple cracking particularly occurs when a big rock is in the direction of the crack and the crack (s) has to go around the rock. When multiple cracking occurs, the samples will typically sustain higher number of OT cycles than its counterpart samples with single cracks. In addition to an increase in the OT cycles, there will also be high variability in the overall test results.

Based on the aforementioned observations in [Figure 3-4](#) and for the mixes evaluated in this study, the following can be concluded:

- Multiple cracking will often (but not always) occur, particularly in coarse-graded mixes – predominantly when a big rock is in the direction of the crack.
- Compared to fine- or dense-graded mixes, coarse-graded mixes because of their aggregate size and orientation are more prone to multiple cracking under OT testing. Therefore, the occurrence of high variability in the coarse-grade mixes such as Type B should also not be unexpected when testing these coarse-graded mixes in the OT.
- As per part of the Tex-248-F modification recommendations, the number of cracks occurring on OT test specimens should be recorded and reported as part of the OT test results.
- However, where there is an opportunity to re-mold more samples or the best three results ($COV \leq 30\%$) can be obtained from the tested pool of 5 sample replicates, then it is recommended to simply discard all the samples with multiple cracks.

Alternative OT Data Analysis Methods

As a supplement to just reporting the number of OT cycles to failure, various alternative approaches to analyzing the OT test data were investigated. [Table 3-3](#) summarizes the results of these investigations. Report 0-6607-1 ([Walubita et al., 2012](#)) documents the detailed discussions of these methods along with the analyses.

Table 3-3. Alternative OT Data Analysis Methods (Walubita et al., 2012).

#	Method	Variables Investigated	Key Findings and Recommendations
1	Load reduction criterion	50, 75, 85, & 93% load drop	<ul style="list-style-type: none"> - 50 & 75% – Not viable, sharp drop in load with small & hardly differentiable OT cycles - 85% load drop gives reasonable COV with interpretable OT cycles, but still requires validation & correlation with field data
2	Rate of load decrease	Slope change in the load-cycle response curve	Unsatisfactory results. The inflexion point could not be determined beyond 50% load drop.
3	Pseudo fracture energy (Pseudo-FE)	Area under the load-cycle response curve	No improvement in variability with the use of Pseudo-FE
4	OT monotonic testing and fracture parameters	Tensile strength (σ_t), failure strain (ϵ_f), fracture energy (FE), and FE Index	The FE Index exhibited promising potential and is discussed in details in Chapter 4.

Of the four approaches evaluated in [Table 3-3](#), only the FE Index measured and computed from the OT monotonic testing exhibited promising potential. Note that as opposed to the classical tensile strength, failure strain, and fracture energy (FE), the FE Index is a new HMA fracture parameter derived in the course of this study. [Chapter 4](#) discusses this FE Index in greater detail.

OT ROUND-ROBIN TESTING AND OPERATOR EFFECT

Following the Tex-248-F specification recommendations in [Table 3-1](#), the research team conducted parallel and round-robin testing between TTI and three TxDOT laboratories. Prior to starting these tests, the team checked and calibrated all the OT machines in each laboratory; see examples in [Appendices A](#) and [B](#).

As a minimum, each laboratory was tasked to test the same three mixes with five replicate samples per HMA mix type per variable evaluated. [Table 3-4](#) through [3-8](#) shows the results based on an average of the best three replicates (out of a total of five replicates) considering the lowest COV. Note that a statistical Excel® macro was developed and is available to automatically pick the best three results out of a total of four or five replicates. As indicated in [Table 3-1](#), outliers should be discarded—only the best three results with the lowest COV should be reported.

Table 3-4. OT Round-Robin Results – Laredo Type C Mix.

Laredo Type C Mix = 5% PG 64-22 + Gravel + 1% Lime + 20% RAP					
Sample ID#	TxDOT Lab (Austin)	TxDOT Lab (Childress)	TxDOT Lab (Houston)	TTI Lab (Lubinda)	TTI Lab (Hossain)
OT1	54	41	72	43	46
OT2	38	53	73	36	41
OT3	52	37	52	32	71
Avg	48	44	66	37	55
COV ($\leq 30\%$)	18%	19%	18%	15%	26%
Results considering all 5 OT replicate samples					
Avg	60	51	50	43	79
COV	29%	59%	47%	29%	54%

Table 3-5. OT Round-Robin Results – Four Different HMA Mixes.

HMA Mix	TxDOT Lab (Austin)	TxDOT Lab (Childress)	TxDOT Lab (Houston)	TTI Lab (CS)
Chico Type D (4.5% AC)	-	119	-	118
Laredo Type C (+ 20% RAP)	48	44	66	46
Waco Type C (+16% RAP & 3% RAS)	-	25	37	38
Atlanta Type D (+20% RAP)	389	410	354	304
Statistical Variability (COV $\leq 30\%$)				
Chico Type D (4.5% AC)	-	9%	-	12%
Laredo Type C (+20% RAP)	18%	19%	18%	27%
Waco Type C (+16%RAP & 3% RAS)	-	34%	10%	30%
Atlanta Type D (+20% RAP)	29%	12%	31%	11%

Table 3-6. OT Operator Effect.

Sample ID#	TTI – Hossain (Trained)	TTI – Unnamed (Untrained)	TTI – Lubinda (Self-Trained)
OT1	150	180	250
OT2	242	458	186
OT3	239	143	196
Avg	210	260	211
COV ($\leq 30\%$)	25%	66%	16%
Results considering all 5 OT replicate samples			
Avg	175	348	247
COV	39%	108%	31%

Table 3-7. Trained Operator Effect.

Type D = 5.0% PG 70-22 + Limestone					
Operator	Year of Testing	Location	Avg OT Cycles	COV	Comment
Lubinda	2009 Round-robin	TTI, TxDOT labs, & PaveTex	258	23%	28 replicate samples in total were molded & tested; 1 sample cut from 2.5"
Lubinda	2011 (June)	TxDOT-CST	213	17%	Best 3 out of 5; 2 samples cut from 5.0"
Hossain	2011 (June)	TTI	230	27%	Best 3 out of 5; 2 samples cut from 5.0"
Hossain	2011 (June)	TTI	210	25%	Best 3 out of 5; 1 sample cut from 4.5" (New base & plates)
Jason	2012 (July)	TTI	197	23%	Best 3 out of 5; 2 samples cut from 5.0"
Jacob	2012 (Aug)	TTI	211	16%	Best 3 out of 5; 2 samples cut from 5.0"

Table 3-8. Trained Operator and Equipment Effect.

Type D = 5.1% PG 64-22 + Quartzite + 20% RAP				
	AV (7±1%)		OT Cycles	
Operator	Hossain (Trained)	Lubinda (self-trained)	Hossain (Trained)	Lubinda (Self-trained)
OT equipment & location			TTI	TxDOT – Austin
OT1	6.8%	7.1%	309	294
OT2	6.1%	6.6%	121	241
OT3	6.4%	6.5%	334	197
OT4	6.3%	6.4%	269	257
OT5	6.6%	6.9%	240	306
Avg (all)	6.4%	6.7%	255	259
COV (all)	4.3%	4.4%	32.6%	17%
Results – Best 3 out of 5				
Avg (best 3)	6.4%	6.5%	304	286
COV (best 3) (≤ 30%)	2.4%	1.5%	11%	9%

In general, [Tables 3-4](#) through [3-8](#) show reasonable and acceptably promising results in terms of variability, with most of the COV values being less than 30 percent. As theoretically expected, variability was generally higher for the coarse-graded, RAP, and RAS mixes compared to the fine- and dense-graded mixes; but still within the COV tolerance limit. Therefore, high variability in these mixes (i.e., coarse-graded, RAP, RAS, etc.) should not be completely unexpected when subjected to the OT testing in repeated loading mode.

Overall, the results shown in [Table 3-4](#) through [3-8](#) suggest that the OT repeatability can be optimized and variability minimized if the following actions are considered:

- The Tex-248-F updates and modifications as suggested in [Table 3-1](#) should be adhered to. Based on these recommendations, TxDOT is strongly encouraged to implement these updates and modifications as itemized in [Table 3-1](#). A CD is also included to provide a step-by-step video demo of these new updates and suggested changes.

- The OT machines should be periodically checked and calibrated for both load and displacement measurements. This aspect is discussed in the subsequent sections of this chapter.
- All technicians and operators running the OT machines must be trained and certified. For starters, at least two technicians/operators must be trained per lab and a certification program initiated. This OT certification program can either be an online course along with video demos or following the format of the TxDOT standard certification training programs.

OT SOFTWARE, CALIBRATION, AND MAINTENANCE

As discussed in the subsequent text, an effort was also made to address the following OT machine operational aspects (in liaison with ShedWorks):

- Harmonization and upgrading of the OT software.
- Development of a new OT calibration kit/software.
- Development of OT calibration and service maintenance manuals; see the included CD.

OT Software Updates

To ensure software consistency, an OT software upgrade (Version 1.9.0) was installed on two TTI and TxDOT-Austin machines with the assistance of ShedWorks. Childress and Houston District labs are next in line. New features accompanying the OT Version 1.9.0 software include the following:

- The Start button is disabled when the machine pump is off.
- A time delay function has been installed. With this function, the operator can input the desired sample relaxation or temperature conditioning time prior to testing, i.e., prior to applying load to the sample.
- The software has been reprogrammed to terminate only and only if five load peaks in a consecutive row are below the specified threshold. This feature eliminates the occurrence of premature test termination due to sudden drops or spikes in the load, which was a problem with the previous software versions.

To verify the operational status of the new software (Version 1.9.0), verification testing was conducted on one TTI machine using HMA mixes of known OT results from the previous version of the software, on the same OT machine. Following the recommendations in [Table 3-1](#) and picking the best three replicate results out of a total of five, [Table 3-9](#) shows that there is a slight improvement in terms of optimizing repeatability and minimizing variability for the dense-graded Type C and D mixes that were tested. For the same OT machine, the COV values based on the new software (Version 1.9.0) are comparatively lower than those based on the older software version.

Table 3-9. OT Results – New (Version 1.9.0) versus Old Software.

HMA Mix		Old Software	New Software (Version 1.9.0)	Comment
Type D = 5.5% PG 64-22 + Limestone	AVG OT cycles =	822	769	Significant decrease in COV
	COV =	31.30%	1.03%	
Type C = 4.8% PG 70-22 + 20% RAP	AVG OT cycles =	9	8	About 37.5% decrease in COV
	COV =	12.29%	7.53%	
Type B with RAP (Coarse-graded)	AVG OT cycles =	25	39	COV insignificantly different & high – typical of coarse-graded mixes
	COV =	28.00%	31.20%	

OT Calibration – Load and Displacement

As part of the OT software upgrade, ShedWorks also developed and supplied a new calibration kit along with the associated software. [Figure 3-5](#) shows that the key feature of this new calibration kit is its ability to automatically measure and record both load and displacement data while simultaneously displaying linear graphical plots on the screen. The recorded data can then be used for later analyses as needed.



Figure 3-5. The New OT Calibration Kit and Examples of Linear Graphical Screen Plots.

Unlike the old kit that was not automated and did not record any data or directly measure displacements, this new calibration kit shows potential towards optimizing the operational accuracy of the OT machines. The OT calibration procedure and steps are documented in the OT Calibration Manual, which is included in the accompanying CD. A video demo of the calibration process is also included in the CD.

The key recommendations based on the calibrations that were conducted on the TTI OT machines include the following:

- If possible, the OT Calibration Manual should be an integral part of or be used in conjunction with the Tex-248-F specification.
- The calibrations should be performed semi-annually and whenever needed (i.e., when abnormalities are observed in the machine and/or results).
- Both the load and displacement tolerances should not exceed ± 5 percent when and after performing the calibrations. Otherwise, the OT Calibration Manual should be referenced to address this aspect.
- The typical load and displacement calibration curves should be linear; see the example in [Figure 3-6](#) for the load-voltage curve for a well-calibrated OT load cell.

- It is also recommended to verify both the calibrations and control tuning with dummy trial testing (minimum three samples) or using synthetic samples and thereafter, checking the raw data files as shown in [Figure 3-7](#). During verification of the raw data files, the initial load prior to start of testing should not exceed ± 10 lb while the displacement should be within the ± 5 percent tolerance limit; otherwise the OT machine should be recalibrated or checked for control tuning. Details of these aspects can be found in the OT Calibration Manual in the CD accompanying this report.

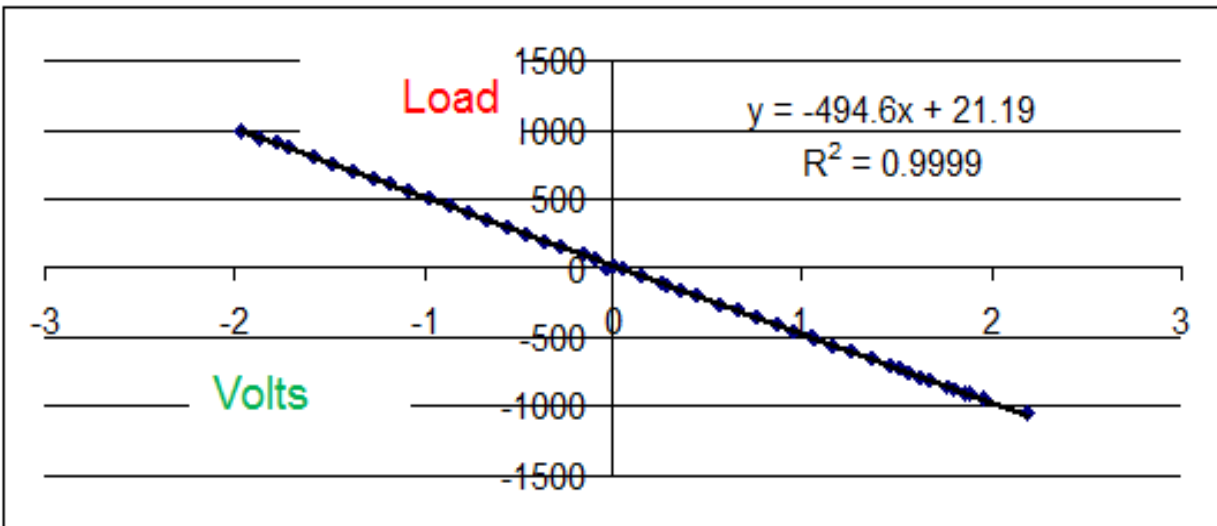
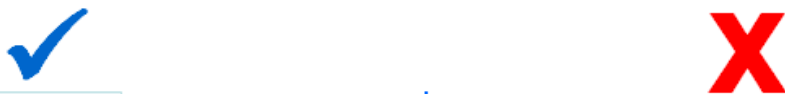


Figure 3-6. Typical Load-Voltage Response Curve – Well-Calibrated OT Load Cell.



8	Actuator	Load Cell	Temperature	Time
9	0.00000	2.0000000	0.0000000	sec
10	[NEW]	0	-0.00909	-0.00909
11	0.0062	0.781075	77	0.0992
12	0.0062	1.989551	77	0.1992
13	0.0062	1.225648	77	0.2992
14	0.0062	0.839712	77	0.3992
15	0.0062	1.381991	77	0.4992
16	0.0062	1.159615	77	0.5992
17	0.0062	0.992045	77	0.6992
18	0.0062	1.167257	77	0.7992
19	0.0062	1.362975	77	0.8992
20	0.0062	1.298954	77	0.9992
21	[NEW]	5	0.853242	0.853242
22	0.0063	5.834171	77	1.04
23	0.0063	22.981428	77	1.08
24	0.0065	57.926501	77	1.12
25	0.0066	87.78095	77	1.16

8	Actuator	Load Cell	Temperature	Time
9	0.0000000	0.0000000	0.0000000	00 sec
10	[NEW]	0	0	0
11	0.011462	43.3545	77	0.0992
12	0.011351	-114.957	77	0.1992
13	0.012871	54.37211	77	0.2992
14	0.012102	-135.66	77	0.3992
15	0.01164	-191.406	77	0.4992
16	0.01188	-215.238	77	0.5992
17	0.012097	-215.079	77	0.6992
18	0.012358	-208.004	77	0.7992
19	0.012505	-200.577	77	0.8992
20	0.012627	-197.345	77	0.9992
21	[NEW]	5	0.853242	0.853242
22	0.012308	-34.2653	77	1.04
23	0.013363	18.02818	77	1.08
24	0.013202	-11.7464	77	1.12
25	0.012989	-7.93757	77	1.16

Figure 3-7. OT Verification of the Raw Data Files.

OT Service Maintenance

Routinely checking and servicing the OT machine is one way to optimize its operational accuracy and longevity. As part of this study, the researchers developed the OT Service Maintenance Manual, a draft copy of which is included in the accompanying CD of this report. Based on the observations of this study and as detailed in the OT Service Maintenance Manual, the key aspects associated with the OT service maintenance should include the following:

- If possible, the OT Service Maintenance Manual should be an integral part of or be used in conjunction with the Tex-248-F specification.
- Perform routine service maintenance on a yearly basis and whenever needed, i.e., when abnormalities are observed in the machine and/or results.
- Check the hydraulic, mechanical, and electrical components.
- Check for oil leaks, dust, etc.

SUMMARY

While taking due cognizance of the fact that repeated loading crack tests are by their nature inherently associated with high variability (particularly for coarse-graded, RAP, and RAS mixes) and that the OT is no exception, the work presented in this chapter shows promise to optimize the OT repeatability and minimize variability in the test results. With this in mind, the key findings and recommendations derived from this chapter are summarized as follows:

- The recommended Tex-248-F updates and modifications should be implemented.
- A training and certification program should be initiated for all the technicians and operators that will be running the OT machines. As a minimum, two technicians/operators should be trained and certified per laboratory.
- For consistency and software harmonization, the new updated OT software (Version 1.9.0) should be installed on all the TTI and TxDOT OT machines.
- OT calibrations and service maintenance should be routinely performed semi-annually and yearly, respectively; and whenever needed, i.e., when abnormalities are observed in the machine and/or test results.
- If OT calibration and control tuning verification are needed, dummy samples (minimum three) or synthetic samples should be used for this purpose.
- The calibration and service manuals along with the video demo should accompany the modified Tex-248-F specification.
- A Round-robin must be conducted once the new software (Version 1.9.0) has been installed on all the OT machines and they have all been calibrated using the new calibration kit.
- Since ShedWorks is going out of business, the team recommends that TxDOT and/or TTI consider purchasing and evaluating one of the OT machines that other suppliers are currently manufacturing.



CHAPTER 4: THE OT TEST METHOD – DYNAMIC AND MONOTONIC LOADING MODES

In an attempt to identify a surrogate crack test to be routinely used to evaluate HMA cracking resistance potential in the laboratory, the researchers explored the Overlay Tester (OT) test in a monotonic loading mode in addition to the more commonly used repeated (dynamic) loading mode. For easy identification, the following abbreviations, “OT_R” and “OT_M” are used to denote the “Repeated (dynamic)” and “Monotonic” loading OT tests, respectively. This chapter discusses and compares the test setups and test results for both of these tests.

TEST SETUP

The same test setup is used for both the monotonic loading and repeated loading OT tests. In the repeated loading test, the ram moves back and forth horizontally to apply the loading cycles (Tex-248-F); for the monotonic loading OT, the ram movement is unidirectional. [Figure 4-1](#) presents the overlay test setup and the loading configurations. [Table 4-1](#) lists and compares the key aspects of the two test methods; subsequent sections discuss these aspects in further details.

Table 4-1. OT_M and OT_R Test Parameters.

	OT _M	OT _R (Tex-248-F)
Test configuration		
Sample dimensions	6" L × 3" W × 1.5" T	6" L × 3" W × 1.5" T
Loading mode	Monotonic tension displacement controlled	Repeated tension displacement controlled
Test parameters	Loading rate = 0.125 inch/min Temperature = 77°F	Frequency = 10 sec/cycle (or 0.1 Hz) (5 sec loading + 5 sec unloading) Loading rate = 0.025 inches displacement Temperature = 77°F
Output data	Strength (σ_t), Strain (ϵ_t), Stiffness (E_t), FE (G_f), & FE Index	Number of load repetitions (cycles) to failure & peak load
Test time per specimen	≤ 10 minutes	≤ 180 minutes

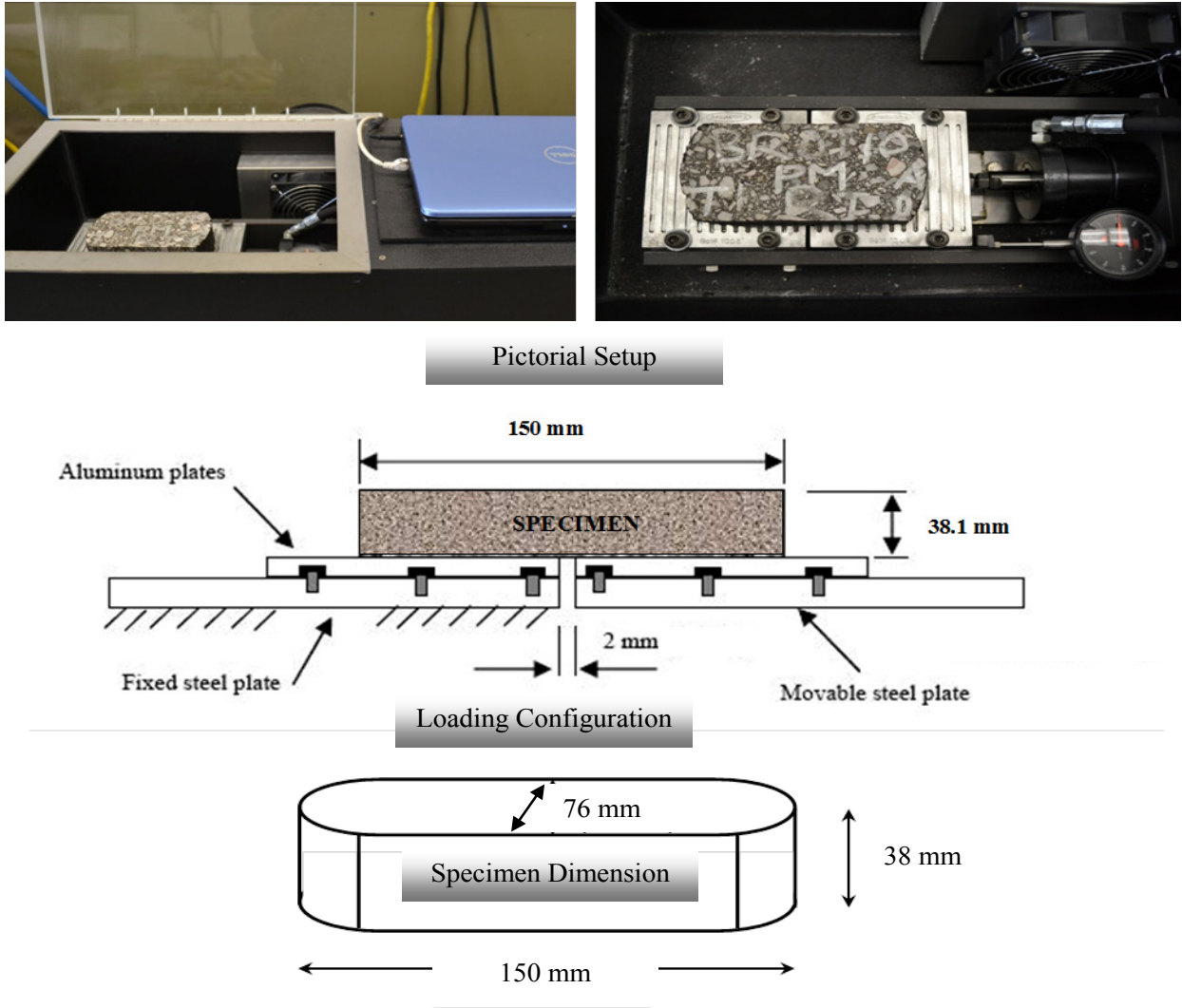


Figure 4-1. Overlay Tester (OT) Setup.

The Monotonic OT (OT_M) Test Method

The OT is a simple performance test traditionally used for characterizing the reflective cracking resistance potential of HMA mixes in the laboratory under repeated loading (tension) mode (Zhou et al., 2007). It is an electro-hydraulic system that applies direct tension load to specimens.

The key components of the OT device, as shown schematically in Figure 4-2, consist of two steel plates, one fixed and the other able to move horizontally to simulate the opening and closing of joints or cracks in the old pavements beneath an overlay. The specimen is spanned across the opening and epoxied to the horizontal surface platens with half of the length of the

specimen resting on each platen. The OT test specimens are 6 inches long, 3 inches wide and 1.5 inches thick (Figure 4-1); which can either be laboratory molded, cut from field cores, or fabricated from field sawn slabs (Walubita et al., 2011). Based on the Texas standards, the laboratory molded test specimens for most conventional Texas HMA mixes are typically fabricated to a total final air voids (AV) content of 7 ± 1 percent (Zhou and Scullion, 2005).

As demonstrated in this study, the OT test setup was also run in monotonic loading mode to supplement the standard repeated loading OT test (Tex-248-F) (Walubita et al., 2012). That is the specimen was tested within the OT test setup in a controlled displacement mode where the monotonic loading rate and test temperature can be suitably selected or changed as desired. For this study, the monotonic loading rate was 0.125 inch/min and the test temperature was 77°F, with a minimum pre-conditioning time of two hours (Walubita et al., 2011). This temperature was monitored via a thermocouple probe attached inside a dummy HMA specimen also placed in the same OT temperature chamber as the test specimens. At 0.125 inch/min loading rate, the total test time was no more than 10 minutes. With temperature pre-conditioning of the test specimens conducted in a separate chamber, over 20 HMA specimens can easily be tested within a day.

The Repeated OT (OT_R) Test Method

The overall test setup is the same for a repeated loading and a monotonic loading OT test with the ram direction and loading rates being the only significant difference. For the OT_R test, the setup is programmed to move the ram back and forth horizontally at a much faster loading rate than its monotonic counterpart. Each loading cycle lasts for 10 seconds with 5 seconds loading and 5 seconds unloading with a maximum horizontal displacement of 0.025 inches until crack failure occurs. The specimen dimensions for the standard OT_R test are the same as those for the OT_M test. Details of the OT test procedure can be found in the TxDOT test specification Tex-248-F (TxDOT, 2011).

TEST RESPONSE CURVES AND DATA ANALYSIS

This section discusses the output data from the two test methods and their subsequent data analysis models.

The OT_M Data Analysis Models

During OT monotonic loading testing, the measurable parameters include the applied load, the horizontal tensile displacement rate, time, and the test temperature. The primary output of the OT monotonic loading test is the stress-strain response curve of the HMA mix. Figure 4-2 illustrates a typical OT monotonic loading test output data.

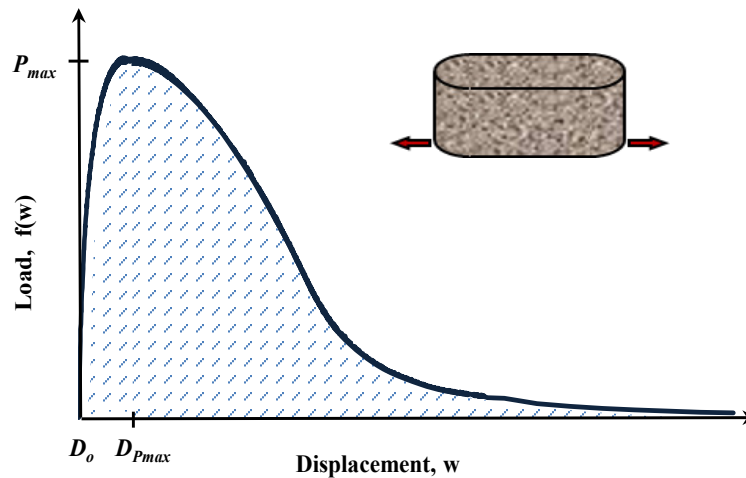


Figure 4-2. Load-Displacement Response Curve: OT_M Testing.

The fracture parameters measured from the OT_M tests in this study include the HMA tensile strength (σ_t), HMA tensile strain at peak failure load or ductility potential (ε_t), HMA tensile modulus or stiffness in tension (E_t), HMA fracture energy or FE (G_f), and the fracture energy index or FE Index. The tensile strength is determined according to the standard models of mechanics as the ratio of the peak failure load and the specimen x-sectional area as follows:

$$\sigma_t = \frac{P_{\max}}{tb} \quad 4-1$$

where t and b are the thickness and the width of the specimen respectively, and P_{\max} is the axial peak load (see Figure 4-2). The tensile strain at peak load or the ductility potential is measured as:

$$\varepsilon_t = \frac{\text{Disp. @ pick load}}{\text{Initial disp. @ zero load}} = \frac{D_{P_{\max}} - D_o}{D_o} \quad 4-2$$

where $D_{P_{\max}}$ and D_o are the displacement at peak load and initial displacements, respectively (Figure 4-2). The ratio of the tensile strength and the tensile strain is denoted as the tensile modulus or the stiffness in tension.

$$E_t = \frac{\text{HMA tensile strength}}{\text{Tensile strain}} = \frac{\sigma_t}{\varepsilon_t} \quad 4-3$$

The fracture energy is defined as the work required to produce a crack of unit surface area, measured in J/m^2 . The work required to fracture the sample is represented by the area under the load versus displacement curve (see Figure 6-2). Therefore, a general expression for Fracture Energy can be written as:

$$G_f = \frac{\text{Work}}{\text{Area of cracked section}} = \frac{1}{A} \int f(x) dx \quad 4-4$$

Finally, the fracture energy index is defined as a parametric ratio of the fracture energy to the HMA tensile strength and tensile strain at peak failure load per unit crack length.

$$\text{FE Index} = 1 \times 10^3 \frac{G_f}{l_{cr} \sigma_t} \varepsilon_t \quad 4-5$$

where l_{cr} is the length traversed by the crack (the specimen thickness t , in case of the OT_M test).

Note that the parameters σ_t , ε_t , E_t , and FE (G_f) [i.e., Equations 4-1 through 4-4] are the traditional HMA fracture parameters typically measured and computed from most monotonic crack tests. The FE Index, on the other hand, is a new HMA fracture parameter derived in the course of this study.

The OT_R Outputs and Data Interpretation

Compared to its monotonic counterpart, the data analysis for the OT_R is simpler. Whereas the measurable parameters remain the same, the parameters of interest from an OT_R test are the number of load cycles to failure and peak load. Both these parameters are automatically recorded on a computer connected to the OT machine and can be extracted without performing any post-processing analysis. The specimen is determined as failed when the cycle peak load drops by 93 percent with respect to the first peak loading cycle or a preset value of cycles (e.g., 1000) is reached. However, occasionally, researchers might want to analyze the complete loading history of the specimen and extract the output data for a tested sample. Figure 4-3 illustrates the output data from a typical OT_R test. For clear illustration, a specimen with fewer OT_R cycles to failure is chosen for this example.

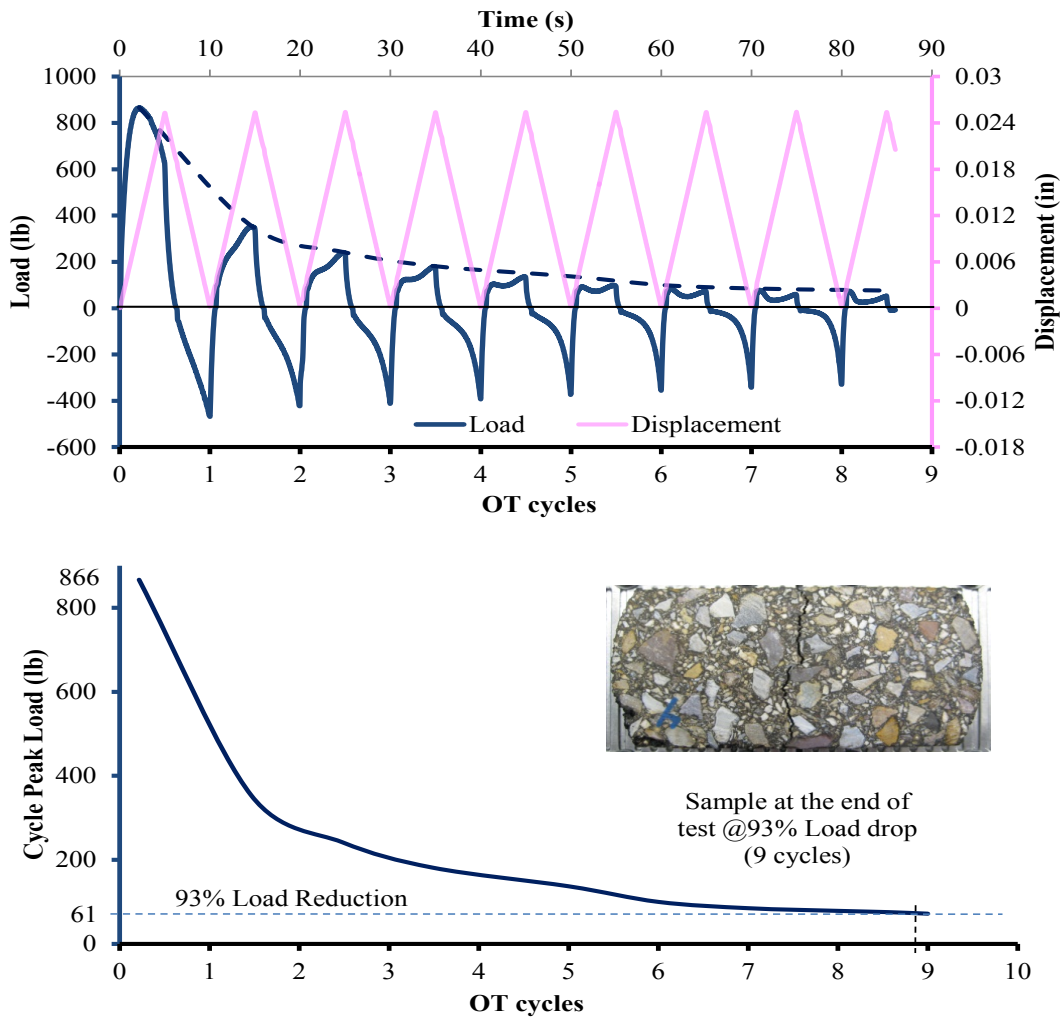


Figure 4-3. OT_R Output Data and Interpretation of Results.

In the example shown in [Figure 4-3](#), the tested sample failed after only nine cycles. From the curve, it is observed that the peak load keeps decreasing in each cycle as the crack steadily propagates to the top surface through the 1.5 inches thickness. When the cycle peak load reaches 7 percent of that of the first peak cycle, the sample is considered to have failed, at which time cracking would have propagated throughout the specimen thickness.

THE OT_M AND OT_R TEST RESULTS

The laboratory test results are presented and analyzed in this section. A number of different HMA mixes were tested side by side in both OT_M and OT_R test setups, and the resulting HMA fracture parameters were comparatively analyzed using the procedures described in the preceding sections ([Equations 4-1](#) through [4-4](#)). The obtained fracture parameters (OT_M) and OT_R cycles to failure are presented in [Table 4-2](#) and [Figure 4-4](#).

Table 4-2. OT Results Summary.

Mix Type	Highway	OT _M				OT _R Cycles
		G _f (J/m ²)	σ _t (psi)	ε _t (in/in)	FE Index	
Type F (7.4% AC)	US 271	1151 <i>(13%)</i>	105 <i>0.3%</i>	0.263 <i>15%</i>	11.13 <i>26%</i>	1000+ -
CAM (7.0% AC)	SH 121	786 <i>14%</i>	58 <i>7.4%</i>	0.300 <i>31%</i>	15.32 <i>34%</i>	1000+ -
CAM (6.7% AC)	-	1504 <i>3.6%</i>	124 <i>4.6%</i>	0.261 <i>2.0%</i>	12.05 <i>5.4%</i>	961 <i>25%</i>
CAM (6.7% AC)	FM 158	1479 <i>13%</i>	131 <i>3.1%</i>	0.221 <i>19%</i>	9.5 <i>18%</i>	796 <i>27%</i>
Type D (5.5% AC)	US 59	1620 <i>4.6%</i>	169 <i>3.0%</i>	0.187 <i>4.2%</i>	6.83 <i>1%</i>	506 <i>34%</i>
Type D (5.2% AC)	US 59	1475 <i>15%</i>	193 <i>7.9%</i>	0.151 <i>27%</i>	5.44 <i>17%</i>	269 <i>24%</i>
Type D (5.0% AC)	-	734 <i>13%</i>	91 <i>3.3%</i>	0.172 <i>5.2%</i>	5.28 <i>4.2%</i>	210 <i>25%</i>
Type C (5.0% AC)	Loop 20	1152 <i>29%</i>	130 <i>10%</i>	0.128 <i>24%</i>	4.62 <i>26%</i>	24 <i>30%</i>
Type C (5.8% AC)	-	1150 <i>3.1%</i>	170 <i>3.3%</i>	0.152 <i>3.6%</i>	3.94 <i>9.3%</i>	126 <i>29%</i>
Type B (4.6% AC)	IH 35	640 <i>31%</i>	99 <i>8.7%</i>	0.142 <i>29%</i>	3.68 <i>49%</i>	47 <i>22%</i>

Values in parenthesis are Coefficient of Variation (COV)

The mixes in [Table 4-2](#) are arranged in a descending order of the mixes' overall perceived crack resistance performance, i.e., the best performing mixes on top followed by mixes

with relatively poor performances, for easy comparison. This perception of the mix cracking performance is based on their historical field and laboratory performance. The primary assessment of the results presented in Table 4-2 suggests that among the four fracture parameters calculated from the OT_M test, only the FE Index values correlates to the perceived performance of their corresponding mixes and the OT_R cycles, whereas the fracture energy, tensile strength, and tensile strain parameters show no justifiable trend. On the other hand and as shown in Figure 4-4, the repeated OT cycles to failure very closely follow the order of mixes, which is further evidence to the well-established correlation of the OT_R with the field performances of the HMA mixes.

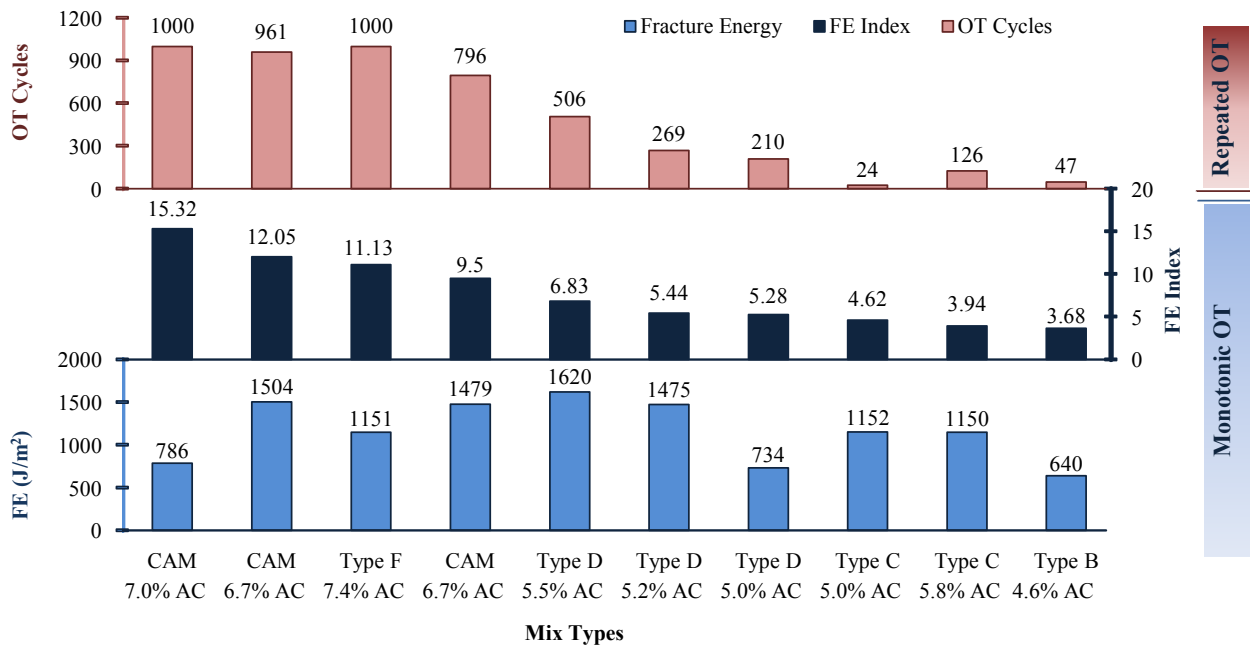


Figure 4-4. Comparison of HMA Mixes Based on OT_M and OT_R Test Results.

However, the failure of the OT_M fracture parameters, other than the FE Index, to reflect the mixes' perceived performances is not completely unexpected. The tensile strength (function of the peak load) and the strain (function of displacement at the peak load) only takes the load increment portion of the load-displacement response curve into account (Figure 4-2). On the other hand, the fracture energy (function of the area under the load-displacement curve), while considering the complete loading history of the specimen, fails to effectively capture the mixes' behavior due to the compensating effects of increasing and decreasing areas under the response

curves (Figure 4-2) (Walubita et al., 2012). The FE Index effectively combines these three fracture parameters to capture the complete loading history of the specimen so that it can show a better reflection of the expected cracking performance of the mix. This is also clearly presented in Figure 4-4, where the FE Index exhibits a clear trend from the best performing CAM mix to the least crack-resistant Type B mix. Consequently, the FE Index parameter has a clear correlation with the OT_R cycles to failure. To further investigate this correlation, the OT_R cycles to failure for the tested mixes were plotted against their corresponding FE Index values from OT_M test and are presented in Figure 4-5.

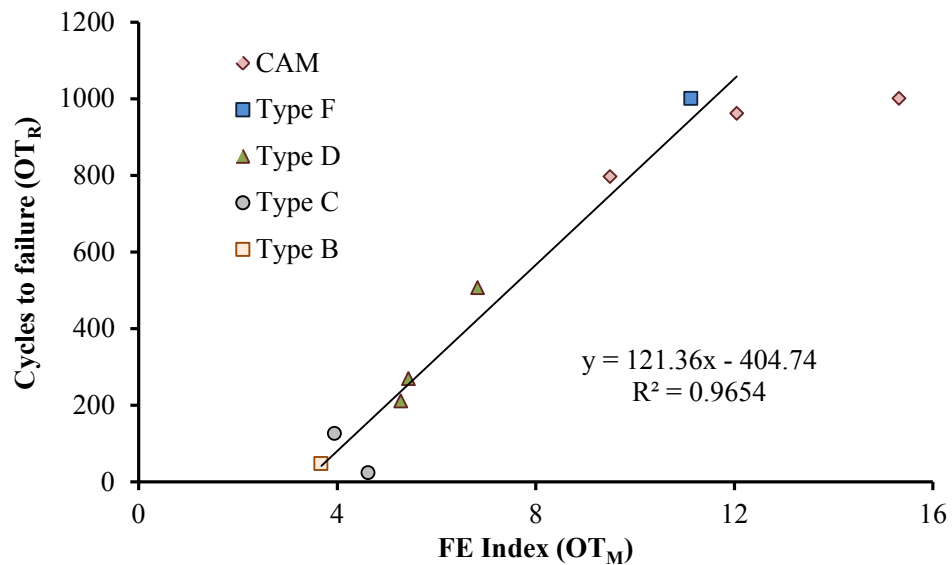


Figure 4-5. Relationship between the OT_R Cycles and OT_M FE Index.

Data shown in Figure 4-5 provide evidence of a linear relationship between the values of OT cycles (from repeated loading OT test) and FE Index (from monotonic loading OT test), with a coefficient of correlation (R^2) of 96.5 percent. Inevitably, Figure 4-5 suggests that there is promising potential in using the FE Index as a surrogate and/or supplementary screening parameter to the OT cycles. In addition, this analysis provided a correlation model to estimate the OT cycles to failure based on its FE Index measured from the monotonic loading OT test. The general form of this correlation equation is:

$$OT\ Cycles = A \times (FE\ Index) - B \quad 4-6$$

where the parameters A and B are determined using simple linear curve fitting of the data in Figure 4-5. Theoretically, this correlation would imply that the number of OT cycles can be

estimated based on the FE Index computed from the much simpler and shorter monotonic loading OT test. Note that by comparison, the monotonic loading OT test is a practically much shorter test to run than the repeated loading OT test—an average of 5 to 10 minutes test time (monotonic loading OT) versus a test time range of 30 minutes to as much as over 3 hours (repeated loading OT), depending on the HMA mix type. However, results from more HMA mixes need to be considered and analyzed to calibrate this regression function (Equation 4-6), before it can be reliably used as a means to correlate the two parameters.

Screening of HMA Mixes: Discriminatory Ratios and Statistical Analysis

One important aspect to consider for the HMA cracking tests is their ability to perform as HMA mix screeners, which is crucial in the HMA mix-design process. Already based on the results presented in Table 4-2 and Figure 4-4, an assessment of the potential of the evaluated fracture parameters to differentiate the crack resistance potential of the mixes is obtained. To further investigate the ability of the fracture parameters to screen mixes, two approaches were used: the discriminatory ratio (DR) concept and Tukey’s HSD statistical analysis.

The discriminatory ratio (DR) is an arithmetic ratio of two corresponding parametric values (e.g., G_f , σ_t , FE Index, and OT_R Cycles) comparing a good mix with a relatively poor mix. The larger the DR in magnitude, the greater the difference between the mixes and the more effective the fracture parameter is in discriminating and differentiating the mixes. To compare the DR-based mix screening ability of the fracture parameters, researchers intuitively chose three mixes, namely the CAM (7.0 percent AC) designated as ‘very good’ (VG) mix, the Type D (5.2 percent AC) as a ‘good’ (G) mix, and the Type B (4.6 percent AC) as a ‘poor’ (P) mix. Table 4-3 presents the resulting DR values.

Table 4-3. Screening of HMA Mixes Based on Discriminatory Ratios.

Mix Type	<u>OT_M</u>				<u>OT_R</u>
	G_f	σ_t	ϵ_t	FE Index	Cycles
CAM/Type B	1.23	0.59	2.11	4.16	21.28
CAM/Type D	0.53	0.30	1.99	2.82	3.72
Type D/Type B	2.30	1.95	1.06	1.48	5.72

Based on the DR values computed in Table 4-3, it is evident that the OT_R cycles to failure provides a significantly superior degree of discrimination between any pair of mixes than the

fracture parameters from OT_M test. Among the OT_M fracture parameters, only the FE Index shows acceptable discrimination between the mixes, though not nearly as prominent as the OT_R cycles.

Analysis of variance (ANOVA) and Tukey’s Honestly Significant Differences (HSD) multiple comparison procedure at a 95 percent confidence level were also used to statistically investigate the potential of the test parameters’ ability to differentiate the crack resistance potential of the HMA mixes. The interpretation of the ANOVA results in Table 4-4 is as follows: for a particular test method; the mixes having parametric values that are statistically not significantly different are listed in the same group (e.g., A, B, or C). A mix categorized in Group A has higher numerical values than a mix listed in Group B for the same parameter and the difference in their numeric values are statistically significant. For example in the last column of Table 4-4, the Type F and the CAM mixes has the highest OT_R cycles and hence, are categorized in Group A, whereas the Type B and Type C mixes fall in the same group (Group C), which indicates that the difference in their OT_R cycles is statistically insignificant. The OT_R cycles for Type D mixes fall in between these two groups and are categorized in the same group (Group B), which also signifies that their respective values are not significantly different from each other.

Table 4-4. Screening of HMA Mixes Based on ANOVA and Tukey’s HSD Analysis.

Mix Type	Highway	OT _M			FE Index	OT _R Cycles
		G _f (J/m ²)	σ _t (psi)	ε _t (in/in)		
Type F (7.4% AC)	US 271	A	B	A	A	A
CAM (7.0% AC)	SH 121	B	C	A	A	A
CAM (6.7% AC)	-	A	B	A	A	A
CAM (6.7% AC)	FM 158	A	B	A	A	A
Type D (5.5% AC)	US 59	A	A	B	B	B
Type D (5.2% AC)	US 59	A	A	B	B	B
Type D (5.0% AC)	-	B	B	B	B	B
Type C (5.0% AC)	Loop 20	A	B	B	B	C
Type C (5.8% AC)	-	A	A	B	B	C
Type B (4.6% AC)	IH 35	B	B	B	B	C

Before discussing the significance of the results presented in Table 4-4, it is important to note that, while comparing two mixes based on a certain parametric value, the Tukey’s HSD method of statistical analysis takes their respective result variability into account. Therefore, any fracture parameter that has a high degree of result variability (high COV) is less likely to show any statistical discrimination among mixes. Therefore, despite showing good discrimination

among mixes based on the DR values (Table 4-2), in the statistical analysis, the FE Index parameter, due to relatively high results variability, does not show effectiveness in categorizing mixes. As expected, the fracture energy and the tensile strength parameters categorized the mixes in a totally random fashion. However, the mix categorization based on the tensile strain and that based on the FE Index are identical.

Sensitivity to Change in Mix Design Parameters

A Type D mix (PG 70-22 + Limestone) with three different AC levels (4.5, 5.0, and 5.5 percent) was utilized to assess the sensitivity of the two test methods to HMA mix-design variables such as AC variations. Table 4-5 and Figure 4-6 present the computed failure parameters.

Table 4-5. Sensitivity to AC Variations.

AC	<u>OT_M</u>				<u>OT_R</u>
	G_f (J/m ²)	σ_t (psi)	ϵ_t (mm/mm)	FE Index	Cycles
4.5%	728 (3.0%)	107 (8.2%)	0.132 (13%)	3.4 (3.4%)	165 (6.6%)
5.0%	734 (13%)	91 (3.3%)	0.172 (5.2%)	5.28 (4.2%)	210 (25%)
5.5%	826 (7.8%)	72 (4.6%)	0.264 (12%)	11.51 (10%)	822 (31%)

Values in parenthesis are Coefficient of Variation (COV)

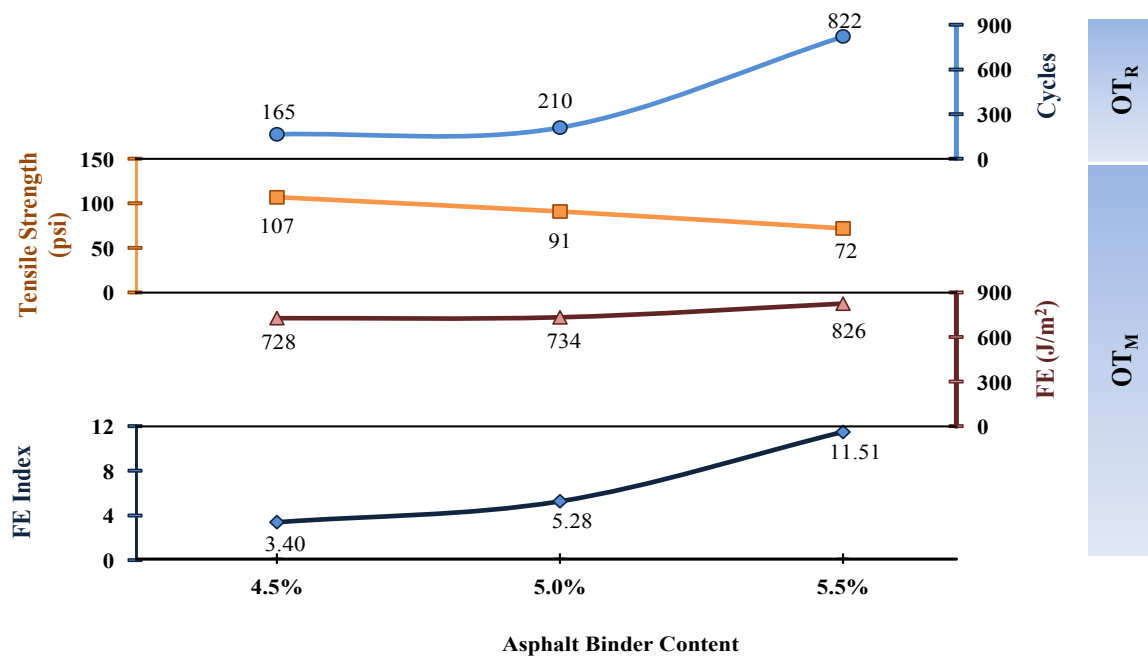


Figure 4-6. OT_M and OT_R Test Parameter Sensitivity to AC Variation.

The results in [Table 4-5](#) and [Figure 4-6](#) show that among the OT_M fracture parameters assessed, the FE Index is the most sensitive to AC change. Theoretically, cracking resistance potential of mixes should show an increasing trend with increasing asphalt binder content since, at higher binder contents, mixes become softer and more ductile. This is reflected in the increasing trend that the FE Index and OT_R cycles show. Also, decreasing tensile strength with increasing asphalt content is an expected trend, since at higher binder contents the mix gets softer and fails at a lower peak load. The fracture energy values, on the other hand, did not show any significant differences for 4.5 percent and 5.0 percent AC levels.

To further investigate the sensitivity of the OT_M fracture parameters to asphalt binder content change, discriminatory ratios were evaluated and are presented in [Table 6-8](#) along with the results from the ANOVA and Tukey's HSD statistical analysis.

Table 4-6. Sensitivity to AC: Discriminatory Ratios and Statistical Analysis.

Analysis Type	AC	OT_M				OT_R
		G_f	σ_t	ϵ_t	FE Index	Cycles
Discriminatory Ratio (DR)	5.5%/4.5%	1.13	0.79	1.53	3.39	4.98
	5.5%/5.0%	1.13	0.67	2.00	2.18	3.91
	5.0%/4.5%	0.99	1.18	0.77	1.55	1.27
Statistical (ANOVA & Tukey's HSD)	4.5%	A	A	B	C	B
	5.0%	A	B	B	B	B
	5.5%	A	C	A	A	A

From the results in [Table 4-6](#), the sensitivity of the fracture parameters of the two test methods are clearly evident. Both the FE Index and the OT_R cycles parameters show satisfactory sensitivity when DR values are considered. However, it is more evident in case of the statistical analysis, particularly the FE Index that discriminates the three AC levels in the theoretically expected order, i.e., 5.5 percent AC categorized in the group A followed by 5.0 percent AC in group B and finally 4.5 percent AC in group C. However, the OT_R cycles are not as efficient in categorizing the different AC levels in appropriate groups primarily due to their high variability in the test results.

To further investigate the sensitivity of the OT (both monotonic and repeated loading), another Type D mix (PG 64-22 + Quartzite +20 percent RAP) was tested by varying the asphalt binder content between 5.2 percent and 6.2 percent; [Table 4-7](#) presents the results.

Table 4-7. AC Sensitivity: Type D Mix.

Mix	Parameter	5.2% AC	5.6% AC	6.2% AC
Atlanta Type D: PG 64-22 + Quartzite + 20% RAP	OT _M FE Index (Monotonic)	5.44	6.28	7.13
	OT cycles (Repeated)	269	469	655

[Table 4-7](#) bears further evidence that both the monotonic loading and the repeated loading OT tests are sensitive to asphalt binder content change. Often it is important for a test procedure to be able to differentiate among specimens tested at different temperatures. Therefore, a Type C mix was tested in the OT_M and the OT_R test setups to evaluate the sensitivity to temperature variations. The results are presented in [Table 4-8](#).

Table 4-8. Temperature Sensitivity of the OT_M and the OT_R Tests.

Mix	Parameter	50°F	59°F	77°F
Laredo Type C: PG 64-22 + Crushed Gravel + 20% RAP + 1% Lime	OT _M FE Index (Monotonic)	0.66	0.70	1.93
	OT _R cycles (Repeated)	2	3	25

From the above table, it is evident that both the OT_R and the OT_M tests are sensitive to temperature variation with the repeated loading mode showing significantly higher sensitivity. However, at low temperatures, the mixes get much more brittle resulting in lower crack resistance and Type C being a relatively poor crack-resistant mix somewhat magnifies this effect for specimens tested at lower temperatures.

COMPARISON OF THE OT_M AND OT_R TEST METHODS

Based on the results presented in the preceding sections and the subsequent discussions, [Table 4-9](#) compares the characteristic attributes of the two test methods.

Table 4-9. Comparison of OT_M and OT_R Test Methods.

Category	OT _M	OT _R
Sample preparation	Easy	Easy
Potential to test field cores	Yes	Yes
Overall test simplicity	Very simple	Very simple
Test time per specimen	≤ 10 minutes	≤ 180 minutes
Test variability at 77°F (COV ≤ 30%)	Repeatable	Reasonable if the recommendations in Chapter 3 are adhered to!
Mix screening ability	Good	Very Good
Sensitivity to AC variations	Good	Very good
Correlation to field data	Needs validation	Yes
Practicality of implementation	Yes	Yes

From the overall comparison of the two test methods, it is observed that both tests have promising potential to be routinely used as HMA fracture tests. The repeated OT ranks above the monotonic OT when correlation to field data and mix screening capabilities are considered; on the other hand, the OT_M is a faster, cost-effective test with better repeatability. However, the potential correlation between these two test methods based on the FE Index (OT_M) and number of cycles (OT_R) is a promising avenue for further studies that can lead to the establishment of a more complete HMA routine crack test.

SUMMARY

This chapter provided a comparative exploration of two of the prospective routine HMA crack test methods, namely the monotonic loading overlay tester (OT_M) test and the repeated loading overlay tester (OT_R) test using the same OT equipment setup. From the overall findings of this study, these researchers recommend both tests as having promising potential as HMA routine crack tests using the same equipment setup, with the OT_R ranking ahead of the OT_M. Therefore, the OT_M can serve as a supplement and/or surrogate to the current OT_R Tex-248-F, which is easily implementable since the two test methods use the same equipment setup.

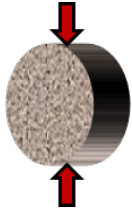
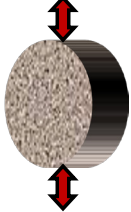
CHAPTER 5: THE IDT AND R-IDT TEST METHODS

In view of developing test procedures for surrogate HMA cracking tests, the indirect tension test was explored in repeated loading mode (R-IDT) as well as the more traditional monotonic loading mode (IDT). This chapter presents the testing setups and obtained results.

TEST SETUP

Table 5-1 lists and compares the key aspects of the two test methods, which are discussed in further detail in the subsequent sections of this chapter.

Table 5-1. IDT and R-IDT Test Parameters.

	IDT	R-IDT
Test configuration		
Sample dimensions	$6''\phi \times 2.5'' T$	$6''\phi \times 2.5'' T$
Loading mode	Monotonic compressive	Repeated compressive (load/stress controlled)
Test parameters	Loading rate = 2.0 inch/min Temperature = 77°F	Frequency = 1 Hz (0.5 sec loading + 0.5 sec rest) Input load = 25% of the averaged IDT peak loads of all mixes evaluated in study (630 lb for all mixes) Contact load = 5% of input load for all mixes Temperature = 77°F
Output data	Strength (σ_t), Strain (ϵ_t), Stiffness (E_t), FE (G_f), & FE Index	Number of load repetitions (cycles) to failure & cycle index
Test time per specimen	≤ 10 minutes	≤ 180 minutes

Legend: L = length; W = width; T = thickness, H = height; ϕ = diameter

The Indirect Tension (IDT) Test

Indirect-tension testing is more of more traditional monotonic crack test used to characterize the fracture properties of HMA mixes in the laboratory (TxDOT, 2004, Walubita et al., 2002). The typical IDT setup requires a servo-hydraulic closed-loop testing machine capable of axial compression (Huang et al., 2005). Several publications recommend using a loading rate of 2 inches/min; most notably are the standard procedures in Tex-226-F (TxDOT, 2004) and ASTM D6931 (ASTM, 2005). Typical IDT specimens are 6 inches in diameter and 2.5 inches thick (TxDOT, 2004).

The specimen is typically loaded diametrically in compression and this indirectly induces horizontal tensile stresses in the middle zone of the specimen that ultimately causes cracking. For the evaluation of the tensile properties of HMA, the permanent deformation under the loading strip is undesirable (Huang et al., 2005). Therefore, the compressive load is distributed using loading strips, which are curved at the interface to fit the radius of curvature of the specimen.

The strain at the center of the specimen is determined from the horizontal displacements measured using Linear Variable Displacement Transducers (LVDTs) with 2-inch gauge length. However, one issue that may be problematic with the IDT set-up is the gauge length of the LVDTs. The existence of large aggregates, particularly for coarse-graded mixes, in the middle of the specimen can affect the displacement measurements between gauge points if the length is too short. So, caution must be exercised to watch out for such potential problems and account for them in the subsequent data analyses and interpretation of the results.

However, to address the complications associated with the measurement of horizontal displacement using LVDTs, particularly in the case of test practicality and industry applications, these researchers have established correlation models to predict the horizontal displacement from the vertical RAM displacement for different mixes. Three specimens were tested for each mix type, namely Type D, Type B, Type C, and CAM, and the horizontal displacements recorded from the LVDTs were plotted against the vertical RAM displacement (Figure 5-1). Curve fitting techniques were then applied to generate correlation models for each mix types; as shown in Figure 5-1. Corresponding Excel macros were also developed to automatically calculate the horizontal displacements from the vertical RAM displacements so the operators would not have to worry about LVDTs.

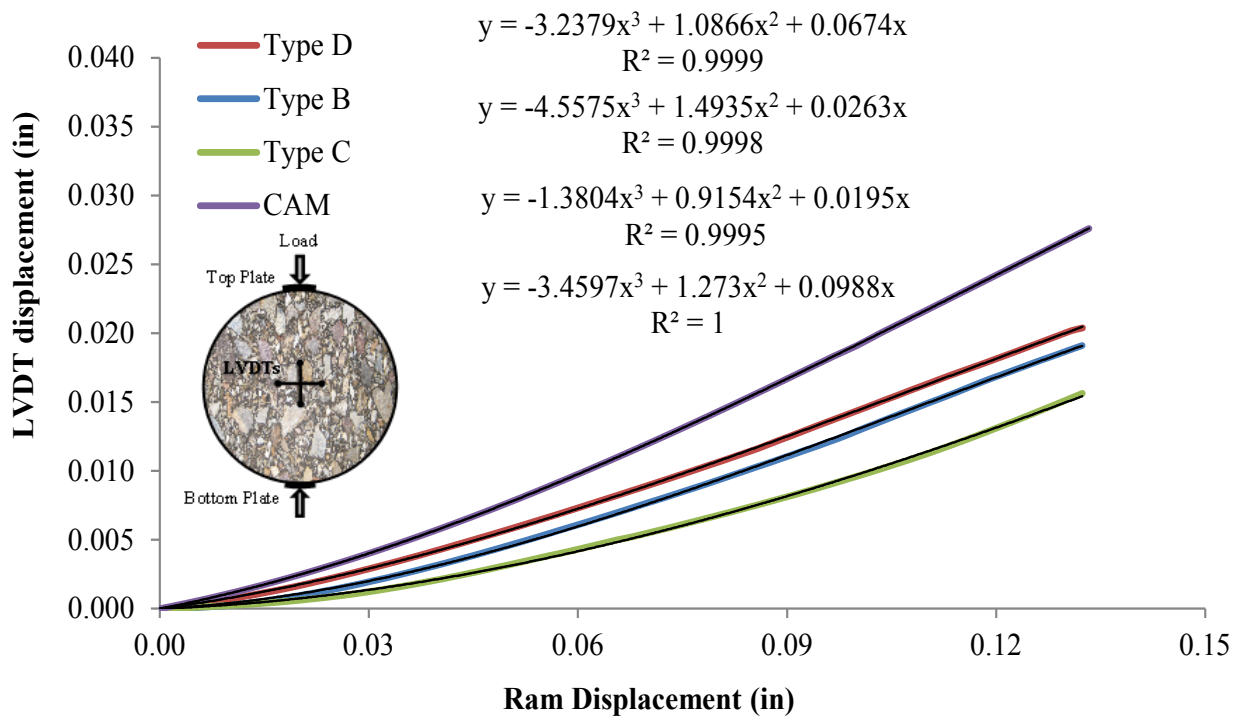


Figure 5-1. IDT Horizontal Displacement Calculation from Vertical (Ram) Displacements.

For consistency with the OT tests, the specimens were tested at 77°F. The data captured during IDT testing include time, applied load, and horizontal and vertical specimen deformation.

The Repeated Loading Indirect Tension (R-IDT) Test

Preliminary repeated IDT loading tests were also conducted to investigate their R-IDT suitability and practicality for characterizing the HMA mix cracking resistance potential in the lab. With the R-IDT test method, the cracking resistance potential of a mix is characterized by the number of IDT load repetitions to crack failure. While the IDT test is a fairly established HMA testing procedure, its use as a repeated loading test is a novel approach. Therefore, no standard specification was found for this test method. The only literature reference was found in [Walubita et al. \(2010\)](#) and was used as the primary basis towards establishing the testing procedures. A tentative test loading parameter set was established after several trial testing sessions and is summarized in this section.

The same specimen dimension as the regular IDT test (6 inches diameter × 2.5 inches thick) is used for its repeated R-IDT counterpart. The test is a two-point loading setup in a

load-controlled mode, which is the primary difference of the R-IDT with the repeated OT test that is a displacement controlled test. The reason for running this test in a load-controlled mode instead of a displacement controlled mode is that the sample configuration and loading setup to run these tests in displacement-controlled mode is very complex. The repeated loading mode is established by loading the specimen at a frequency of 1 Hz with 0.5 seconds of loading followed by 0.5 seconds of rest. Twenty-five percent of the average IDT peak load of all the mixes in this study was selected as the R-IDT input load (i.e., 630 lb in this study for all mixes) and 5 percent of the input load was selected as the contact load (i.e., rounded off to 30 lb for all mixes in this study) (Walubita et al., 2010). Consistent with the OT and IDT tests, the R-IDT tests were also conducted at room temperature (77°F). In summary, the test conditions, test parameters, and input loads were the same for all the mixes evaluated under the R-IDT test in this study.

Permanent deformation at the points of loading in both the IDT and R-IDT tests may undesirably occur at test temperatures such as 77°F or higher, leading to a possible combination of both compressive and tensile failure modes in the specimen with multiple cracks (Molenaar et al., 2002). This was not accounted for in this study. However, the temperature used for these tests (i.e., 77°F) was chosen for consistency of comparison with the OT tests, i.e., the OT_R based on the Tex-248-F specification (TxDOT, 2009) is required to be performed at 77°F. Therefore, all other tests were performed at the same temperature. This temperature also facilitates use in industry procedures, since 77°F is considered room temperature.

TEST RESPONSE CURVES AND DATA ANALYSIS MODELS

The output data from the two tests and their subsequent data analysis models are discussed in this section.

The IDT Data Analysis Models

Typically the result of interest from an IDT test is the axial peak load, which is analyzed using established models to calculate the HMA tensile strength. However, the full potential of the IDT as a HMA cracking test is utilized when the complete loading history of a sample is taken into consideration by analyzing the full load-displacement response. Figure 5-2 shows a typical load-displacement response from an IDT test. Several fracture parameters in addition to the HMA tensile strength are calculated from this output response curve.

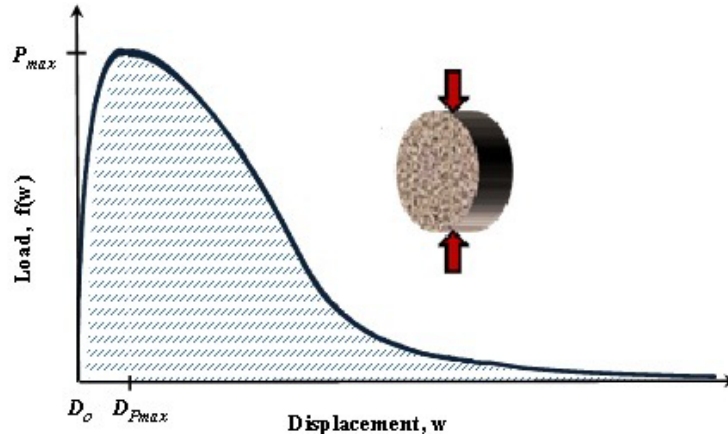


Figure 5-2. Load-Displacement Response Curve: IDT Testing.

The typical fracture parameters measured from the IDT tests in this study include the HMA tensile strength (σ_t), HMA tensile strain at peak failure load or ductility potential (ε_t), HMA tensile modulus or stiffness in tension (E_t), and HMA fracture energy or FE (G_f). There are several models for calculating the tensile strength available in the literature. For this study, the model that [Huang et al. \(2005\)](#) proposed was used assuming plane stress conditions:

$$\sigma_t = \frac{2P_{\max}}{\pi t D} \quad 5-1$$

where t and D are the thickness and the diameter of the specimen respectively, and P_{\max} is the axial peak load, as indicated in [Figure 5-2](#). The tensile strain at peak load or the ductility potential is calculated as follows:

$$\varepsilon_t = \frac{\text{Disp. @ pick load}}{\text{Initial disp. @ zero load}} = \frac{D_{P_{\max}} - D_o}{D_o} \quad 5-2$$

where $D_{P_{\max}}$ and D_o are the displacement at peak load and initial displacements, respectively ([Figure 5-2](#)). The ratio of the tensile strength and the tensile strain is denoted as the tensile modulus or the stiffness in tension.

$$E_t = \frac{\text{HMA tensile strength}}{\text{Tensile strain}} = \frac{\sigma_t}{\varepsilon_t} \quad 5-3$$

The fracture energy is defined as the work required to produce a crack of unit surface area, measured in J/m^2 . The work required to fracture the sample is represented by the area under the load versus displacement curve, as shown in Figure 5-2. Therefore, a general expression for Fracture Energy can be written as:

$$G_f = \frac{\text{Work}}{\text{Area of cracked section}} = \frac{1}{A} \int f(x) dx \quad 5-4$$

Finally, the fracture energy index (FE Index), which is a new parameter derived in this study, is defined as a parametric ratio of the fracture energy to the HMA tensile strength and tensile strain at peak failure load per unit crack length. This FE Index was computed as follows:

$$FE\ Index = 1 \times 10^5 \frac{G_f}{l_{cr} \sigma_t} \varepsilon_t \quad 5-5$$

where l_{cr} is the length traversed by the crack.

The R-IDT Test Outputs and Data Analysis Models

The primary output response parameters from the R-IDT test are the displacement, cycles, and time count. Figure 5-3 shows a plot of the input load and the resulting displacement outputs for a typical R-IDT test. For clarity, only the first eight cycles were presented.

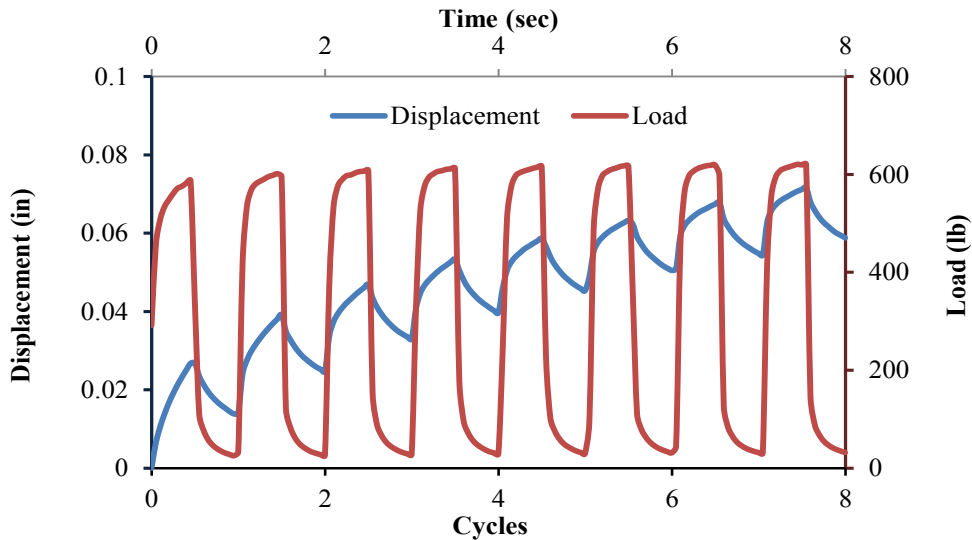


Figure 5-3. R-IDT Load (Input) – Displacement (Output) Curve.

Figure 5-4 presents cycle peak displacements plotted against R-IDT cycles to demonstrate the selection of failure cycles. The notations S#1, S#2, and S#3 refer to sample #1, sample #2, and sample #3, respectively.

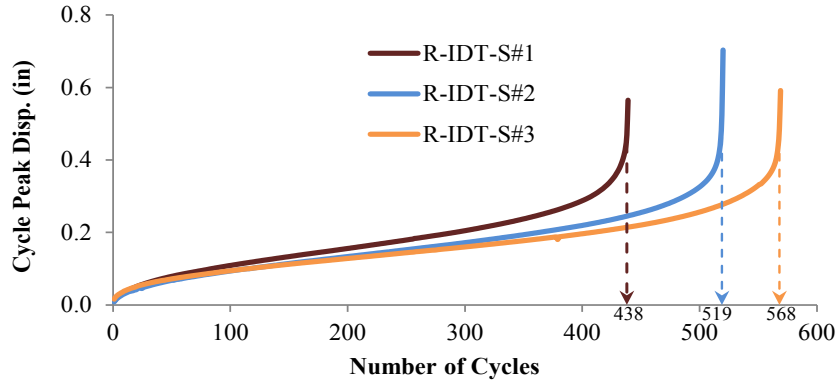


Figure 5-4. Evolution of Peak Displacement with the Number of Load Cycles.

In addition to the number of load cycles and to account for the load-controlled mode of the R-IDT test method, the data analysis from these tests included the Cycle Index concept (Equation 5-6). The Cycle Index was introduced to provide a baseline comparison with the OT_R results that are based on displacement controlled loading mode and was computed as follows:

$$Cycle\ Index = Cycles^{-1} \times \frac{Input\ Load}{Sitting\ Load} \quad 5-6$$

In the above equation, *Cycles* corresponds to the number of R-IDT load cycles to crack failure as illustrated in Figure 5-4. The input and sitting load were 630 lb and 30 lb, respectively for all mixe, as defined in the previous section and illustrated in Figure 5-3. Like the number of cycles in the OT_R test, the higher the Cycle Index in magnitude, the better the HMA mix in terms of crack resistance potential.

IDT AND R-IDT TEST RESULTS

The laboratory test results for the IDT and the R-IDT tests are presented and analyzed in this section, including test method comparisons and sensitivity to AC variations.

IDT Test Results: Comparison of HMA Mixes

Like in [Chapter 4](#) for the OT, the same three mixes were tested, namely a Type B mix from Waco District, a Type D mix from Atlanta District, and a CAM mix from Paris District. The details mix designs for each of these three mixes are discussed in [Chapter 2](#). [Figure 5-5](#) presents the IDT test results for the three mixes.

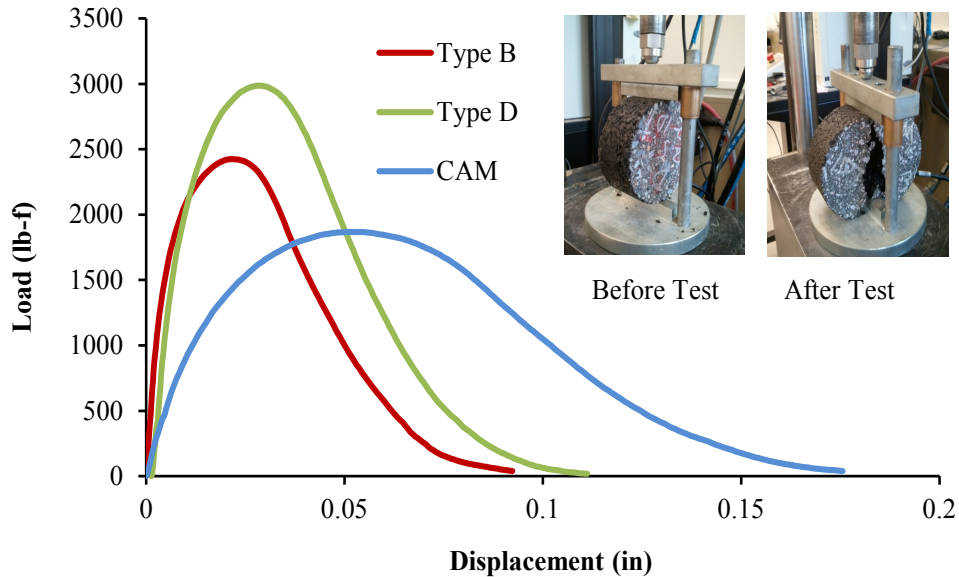


Figure 5-5. IDT Test Outputs: Load-Displacement Response Curves.

From the above figure, it is evident that the IDT test properly reflected the expected behavior of these three mixes. The CAM, usually known for being a softer and more crack-resistant mix, have the most ductile response curve with low peak load, whereas the Type B mix shows much more brittle response behavior. The Type D is clearly a better mix than Type B both in terms of higher peak load and ductility potential.

[Equations 5-1](#) through [5-5](#) were used on the generated load displacement response data to calculate the fracture parameters. [Table 5-2](#) and [Figure 5-6](#) present the results.

Table 5-2. Summary of IDT Test Results.

Mix Type	Fracture Energy, G_f		Tensile Strength, σ_t		Strain, ϵ_t	FE Index
	(J/m ²)	(lb-in/in ²)	(psi)	(MPa)	(mm/mm)	
Type B	136(2.3%)	0.779(2.3%)	103(3.8%)	0.710(3.8%)	0.0149(9.9%)	1.88(11.8%)
Type D	193(8.1%)	1.101(8.1%)	127(3.7%)	0.876(3.7%)	0.0190(19.4%)	2.76(24.4%)
CAM	226(5.2%)	1.290(5.2%)	79(2.0%)	0.547(2.0%)	0.0340(4.1%)	9.21(10.0%)

* Values in parenthesis are the Coefficient of Variance (COV).

Based on the COV values, the test seem to be very repeatable with all the COV values within the acceptable limit (≤ 30 percent). The computed parametric values also seem to be reasonable and are consistent with literature publications. For instance, the IDT tensile strength values are indifferent from the 85~200 psi Texas specification (TxDOT, 2004).

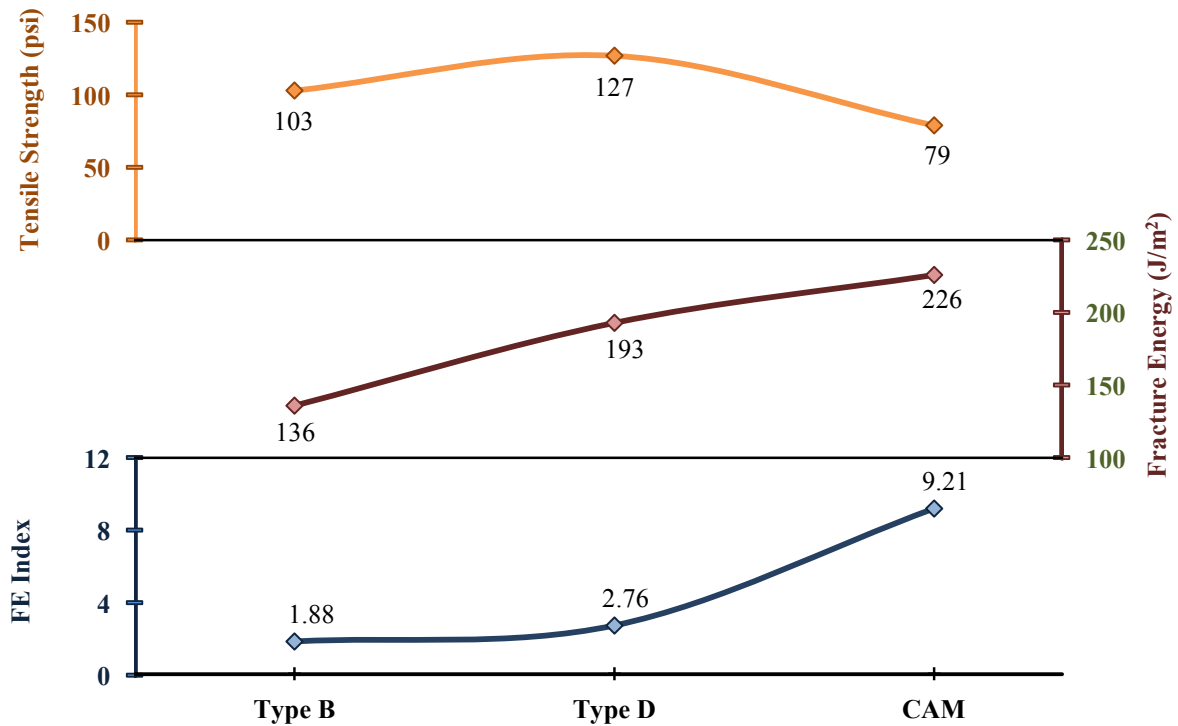


Figure 5-6. Summary of IDT Test Results.

From the computed fracture parameters in Table 5-2 and Figure 5-6, it is clear that the tensile and strain parameters are not very reflective of the mixes' perceived laboratory cracking resistance performance. The tensile strength (function of the peak load) and the strain (function

of displacement at the peak load) only take the load increment portion of the load-displacement response curve into account. On the other hand, the fracture energy (function of the area under the load-displacement curve) considers the complete loading history of the specimen, and the FE values for the three mixes are reflective of this. However, due to the compensating effects of increasing and decreasing areas under the response curves (Figure 5-5), the FE fails to effectively capture the mixes' behavior (Walubita et al., 2012). The FE Index effectively combines these three fracture parameters to capture the complete loading history of the specimen so that it can show a better reflection of the expected cracking performance of the mix. This is also clearly presented in Figure 5-6, where the FE Index exhibits a distinctive increasing trend from the poor Type B mix to the more crack-resistant CAM mix.

R-IDT Test Results: Comparison of HMA Mixes

The same three mixes that were tested in the IDT setup were tested in the repeated R-IDT loading mode and the results are listed in Table 5-3.

Table 5-3. Summary of R-IDT Test Results.

Mix Type	R-IDT Cycle Index	
	Mean	COV
Type B	26.02	65.8%
Type D	41.34	12.9%
CAM	57.85	49.7%

As expected, the Cycle Index values are in line with the mixes' expected behavior such that the CAM is the most crack-resistant mix, followed by the Type D and the Type B mix. However, the variability is very high marked by the high COV values, which is of course not unexpected from a repeated loading crack test (Cominsky et al., 1994).

Screening of HMA Mixes: Discriminatory Ratios and Statistical Analysis

One important aspect of these tests and the evaluated results is their ability to perform as HMA mix screeners, which is crucial in the HMA mix-design process. Figure 5-6 provided an assessment of the potential of the IDT fracture parameters to differentiate the crack resistance potential of the mixes in the lab. To further investigate the ability of the fracture parameters to

screen mixes, the researchers used two approaches: the discriminatory ratio (DR) concept and Tukey’s HSD statistical analysis.

The discriminatory ratio is an arithmetic ratio of two corresponding parametric values (e.g., G_f , σ_t , FE Index, and Cycle Index) comparing a good mix with a relatively poor mix. The larger the DR in magnitude, the greater the difference between the mixes and the more effective the fracture parameter is in discriminating mixes. Based on the DR values computed in [Table 5-4](#), it is evident that the IDT FE Index provides a superior degree of discrimination between good and poor lab crack-resistant mixes than the other fracture parameters. The R-IDT Cycle Index is also able to differentiate the mixes, but is not as pronounced when compared to the differentiating ability of the OT cycles of the OT_R test ([Table 4-3](#)).

Table 5-4. Screening of HMA Mixes Based on Discriminatory Ratios.

Mix Type	IDT			FE Index	R-IDT
	G_f	σ_t	ε_t		Cycle Index
CAM/Type B	1.66	0.77	2.28	4.90	2.22
CAM/Type D	1.17	0.62	1.79	3.34	1.40
Type D/Type B	1.42	1.23	1.28	1.47	1.59

Analysis of variance (ANOVA) and Tukey’s Honestly Significant Differences (HSD) multiple comparison procedure at a 95 percent confidence level were used to statistically investigate the potential of the test parameters’ ability to differentiate the crack resistance potential of the HMA mixes. The interpretation of the ANOVA results in [Table 5-5](#) is as follows: for a particular test method, the mixes having parametric values that are statistically not significantly different are listed in the same group (e.g., A or B). A mix categorized in Group A has higher numerical values than a mix listed in Group B for the same parameter and the difference in their numeric values are statistically significant. For example in the FE Index column of [Table 5-5](#), the CAM mix has the highest IDT FE Index value and hence is categorized in Group A. Type B and Type D fall in the same group (Group B), which indicates that the difference in their FE Index values is statistically insignificant.

Table 5-5. Screening of HMA Mixes Based on ANOVA and Tukey’s HSD Analysis.

Mix Type	<u>IDT</u>				<u>R-IDT</u>
	G_f (J/m ²)	σ_t (psi)	ϵ_t (mm/mm)	FE Index	Cycles Index
Type B	B	A	B	B	B
Type D	B	A	B	B	B
CAM	A	B	A	A	A

Following the results in [Table 5-5](#), it is clear that both the IDT and R-IDT tests yield similar categorization of the mixes based on the ANOVA and Tukey’s HSD statistical analysis. Likewise, this analysis mostly fails to show any clear discrimination among Type D and Type B mix types. However, one needs to consider that, while comparing two mixes based on a certain parametric value, the Tukey’s HSD method of statistical analysis takes their respective result variability into account. Therefore, any fracture parameter that has a high degree of result variability (high COV) is less likely to show any statistical discrimination among mixes. However, since only three mixes were evaluated, the research team recommends conducting additional testing with more mixes to substantiate these findings.

Sensitivity to Change in Asphalt Binder Content

Similar to the OT in Chapter 4, a Type D mix (PG 70-22 + Limestone) with three different AC levels (4.5, 5.0, and 5.5 percent) was utilized to assess the sensitivity of the tests to HMA mix-design variables such as AC variations. The computed fracture parameters are presented in [Table 5-6](#) and [Figure 5-7](#). Values in parenthesis in [Table 5-6](#) are Coefficient of Variation (COV).

Table 5-6. Sensitivity to AC Variations.

AC	<u>IDT</u>				<u>R-IDT</u>
	G_f (J/m ²)	σ_t (psi)	ϵ_t (mm/mm)	FE Index	Cycles Index
4.5%	114 (2.2%)	85 (3.1%)	0.0145 (1.4%)	1.84 (1.2%)	54.4 (28%)
5.0%	124 (4.7%)	75 (6.2%)	0.0179 (7.5%)	2.81 (4.6%)	59.8 (6.4%)
5.5%	203 (2.6%)	110 (3.9%)	0.0204 (6.9%)	3.59 (11%)	104.5 (18%)

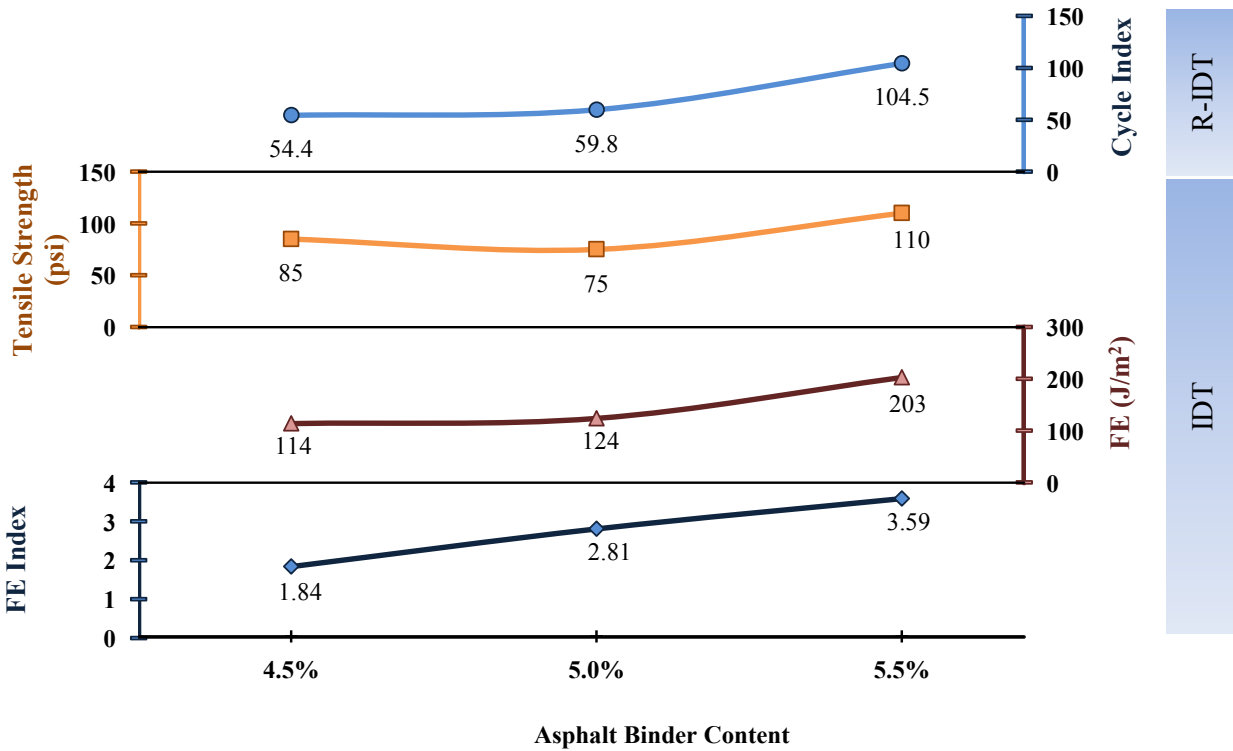


Figure 5-7. IDT and R-IDT Test Parameter Sensitivity to AC Variation.

The results in [Table 5-6](#) and [Figure 5-7](#) show that both the IDT and the R-IDT tests are capable of capturing the effect of AC variation. However, among the IDT fracture parameters, FE Index is the most sensitive to AC change. Theoretically, the cracking resistance potential of mixes should show an increasing trend with increasing asphalt binder content since, at higher binder contents, mixes become softer and more ductile. This is reflected in the increasing trend that the FE, FE Index, and Cycle Index parameters show. On the other hand, due to this increased softness, mixes should fail at lower peak loads, resulting in lower tensile strengths. However, the IDT tensile strength at 5.5 percent AC is higher than those at lower AC levels. The reason behind this behavior is that at higher binder contents, the IDT loading strips sink into the soft material at the contact surface, resulting in a failure mode that is both compressive and tensile. At some instances, multiple crack paths might also develop, requiring higher peak loads to failure. Therefore, caution must be exercised while applying the IDT and R-IDT test methods at higher AC levels and softer mixes, particularly at test temperatures of 77°F or higher.

To further investigate the sensitivity of the IDT and R-IDT fracture parameters to asphalt binder content change, discriminatory ratios are evaluated and presented in [Table 5-7](#) along with the results from the ANOVA and Tukey’s HSD statistical analysis.

Table 5-7. Sensitivity to AC: Discriminatory Ratios and Statistical Analysis.

Analysis Type	AC	IDT				Cycle Index
		G_f	σ_t	ε_t	FE Index	
Discriminatory Ratio (DR)	5.5%/4.5%	1.78	1.29	1.41	1.95	1.92
	5.5%/5.0%	1.64	1.47	1.14	1.28	1.75
	5.0%/4.5%	1.09	0.88	1.23	1.53	1.10
Statistical (ANOVA & Tukey’s HSD)	4.5%	B	B	B	C	B
	5.0%	B	C	A	B	B
	5.5%	A	A	A	A	A

From the results in [Table 5-7](#), the sensitivity of the fracture parameters of the two tests are clearly evident. Both the FE Index and the Cycle Index parameters show satisfactory sensitivity when DR values are considered. However, it is more evident in case of the statistical analysis. Specifically, the FE Index discriminates all three AC levels in the expected order, i.e., 5.5 percent AC categorized in group A, followed by 5.0 percent AC in group B, and finally 4.5 percent AC in group C. However, the R-IDT cycles are not as efficient in categorizing the different AC levels in the appropriate grouping due to their high result variability.

COMPARISON OF THE IDT AND R-IDT TEST METHODS

Based on the results presented in the preceding sections and the subsequent discussions, a comparison between the two test methods is presented in [Table 5-8](#).

Table 5-8. Comparison of IDT and R-IDT Test Methods.

Category	IDT	R-IDT
Sample preparation	Very Easy	Very Easy
Potential to test field cores	Yes	Yes
Overall test simplicity	Very simple	Fair
Test time per specimen	≤ 10 minutes	≤ 180 minutes
Test variability at 77°F (COV ≤ 30%)	Repeatable	Variable
Mix screening ability	Moderate	Moderate
Sensitivity to AC variations	good	Moderate
Correlation to field data	N e e d s v a l i d a t i o n	
Practicality of implementation	Yes	Possible

From the overall comparison of the two test methods, it is observed that both tests have promising potential to be routinely used as a HMA fracture test. However, due to its overall test simplicity, better repeatability, and slightly better mix screening ability, the IDT with shorter test time along with the use of the FE Index will rank ahead of its repeated loading counterpart (R-IDT) as a routine HMA crack test.

SUMMARY

This chapter provided a comparative exploration of two of the prospective surrogate crack test methods, namely the indirect tension test (IDT) and the repeated loading indirect tension test (R-IDT). From the overall findings of the study, the researchers recommend both tests to have promising potential as HMA routine crack tests with the IDT ranking ahead of the R-IDT test. However, caution and use of robust loading strips are strongly recommended, particularly for high AC mixes and/or high temperature testing where applying the IDT and R-IDT tests can be quite problematic.

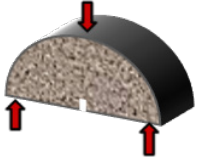
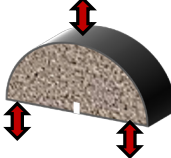
CHAPTER 6: THE SCB AND R-SCB TEST METHODS

As the continuation of the search for an alternative HMA cracking test, the semicircular bending test is evaluated in this chapter, both in the monotonic (SCB) and repeated (R-SCB) loading modes.

TEST SETUP

Table 6-1 lists and compares the key aspects of the two test methods, which are then discussed further in the subsequent sections of this chapter.

Table 6-1. SCB and R-SCB Test Parameters.

	IDT	R-SCB
Test configuration		
Sample dimensions	$6''\phi \times 3'' H \times 2.5'' T$ (0.25" notch)	$6''\phi \times 3'' H \times 2.5'' T$ (0.25" notch)
Loading mode	Monotonic compressive	Repeated compressive (load/stress controlled)
Test parameters	Loading rate = 0.05 inch/min Temperature = 77°F	Frequency = 1 Hz (0.5sec loading + 0.5 sec rest) Input load = ~50% of the averaged SCB peak load of all mixes studied (i.e., 175 lb for all mixes tested) Contact load = 5% of input load for all mixes Temperature = 77°F
Output data	Strength (σ_t), Strain (ε_t), Stiffness (E_t), FE (G_f), & FE Index	Number of load repetitions (cycles) to failure & cycle index
Test time per specimen	≤ 10 minutes	≤ 180 minutes

Legend: L = length; W = width; T = thickness, H = height; ϕ = diameter

The Semi-Circular Bending (SCB) Test

Development of SCB as a predictor of HMA cracking resistance potential in the lab has appeared relatively recent in the field of pavement engineering. The SCB specimen is a half disk, typically 6 inches in diameter that is loaded in compression using a three-point flexural apparatus. Different specimen thicknesses have been reported in the literature. However, to maintain consistency with the other considered tests, the research group tested 2.5-inch thick

samples in this study. The rate at which the specimen is loaded is also not very well-specified, but [Walubita et al. \(2002\)](#) have had success when using 0.05 in/min loading rate, and this was rate used in this study.

Specimen fabrication and preparation for the SCB test is somewhat complicated due to the notch in the base of the specimen. The notch ensures that the crack initiates at the center of the specimen base. Notch depths vary, depending on many factors such as specimen thickness, diameter, loading rate, test temperature, mix type, aggregate size, etc. Once again, the work of [Walubita et al. \(2002\)](#) was taken as reference while selecting the notch depth of 0.25 inch.

At first glance, the calculation of stiffness in the middle point of the lower specimen surface may seem difficult because affixing the strain gauges onto the specimen is time- and resource-consuming. In the case of the current study, however, HMA stiffness determination was an important parameter to explore. To accommodate this requirement, the research team calculated the horizontal strain based on the vertical RAM displacements following the procedures explained in [Chapter 5 \(Figure 5-1\)](#). Corresponding Excel macros were also developed to automatically calculate the horizontal displacements from the vertical RAM displacements so the operators would not have to worry about LVDTs.

For analysis purposes, the spacing between the supports is typically 0.8 times the specimen diameter. From the literature search, the typical test temperatures for the SCB test are between 50°F ([Huang et al., 2009](#)) and 77°F ([Molenaar et al., 2002](#)). To be consistent with the other crack tests repeated in the previous chapters, the researchers selected 77°F as the test temperature. The data captured during SCB testing include time, applied load, and horizontal and vertical specimen deformation.

The Repeated Loading Semi-Circular Bending (R-SCB) Test

The research team conducted preliminary repeated SCB loading tests to investigate the R-SCB suitability and practicality for characterizing the HMA mix cracking resistance. With the R-SCB test method, the cracking resistance potential of a mix is characterized by the number of SCB load repetitions to crack failure. Similar to the R-IDT test, the only literature reference was found in [Walubita et al. \(2010\)](#) and was used as the primary basis towards establishing the R-IDT testing procedures. A tentative test loading parameter set was established after several trial testing and is summarized in this section.

The same specimen dimensions as the regular SCB test (6 inches diameter × 3 inches tall × 2.5 inches thick) are used for its repeated R-SCB counterpart. The test involved a three-point dynamic compressive loading that induces tension at the bottom zone of the semicircular specimen. Similar to the R-IDT, the R-SCB is run in a load-controlled mode because the sample configuration and loading setup to run this test in displacement-controlled mode is very complex. The repeated loading mode is established by loading the specimen at a frequency of 1 Hz with 0.5 seconds of loading followed by 0.5 seconds of rest. Fifty percent of the average SCB peak loads of all the mixes evaluated in this study was selected as the R-SCB input load (i.e., 175 lb for all mixes) and the contact load (rounded off to 10 lbs) was set roughly at 5 percent of the input load for all the mixes tested (Walubita et al., 2010). Like the preceding tests, the R-SCB test were conducted at room temperature (77°F). In summary, the test conditions, test parameters, and input loads were the same for all the mixes evaluated under the R-SCB test in this study.

Although not accounted for in this study, it is necessary to note that permanent deformation at the points of loading in both the SCB and R-SCB tests may undesirably occur at test temperatures such as 77°F or higher; leading to a possible combination of both compressive and tensile failure modes in the specimen with multiple cracks (Molenaar et al., 2002). However, the temperature used for these tests (i.e., 77°F) was chosen for consistency of comparison, i.e., the OT_R based on the Tex-248-F specification (TxDOT, 2009) is required to be performed at 77°F. Therefore, all other tests were performed at the same temperature. This temperature also facilitates use in industry procedures, since 77°F is considered room temperature.

TEST RESPONSE CURVES AND DATA ANALYSIS MODELS

The output data from the two test methods and their subsequent data analysis models are discussed in this section.

The SCB Data Analysis Models

Typically, the result of interest from an SCB test is the axial peak load, which is analyzed using established models to calculate the HMA tensile strength. However, the full potential of the SCB as a HMA cracking test is utilized when the complete loading history of a sample is taken into consideration by analyzing the full load-displacement response. Figure 6-1 shows a

typical load-displacement response from an SCB test. Several fracture parameters in addition to the HMA tensile strength are calculated from this output response curve.

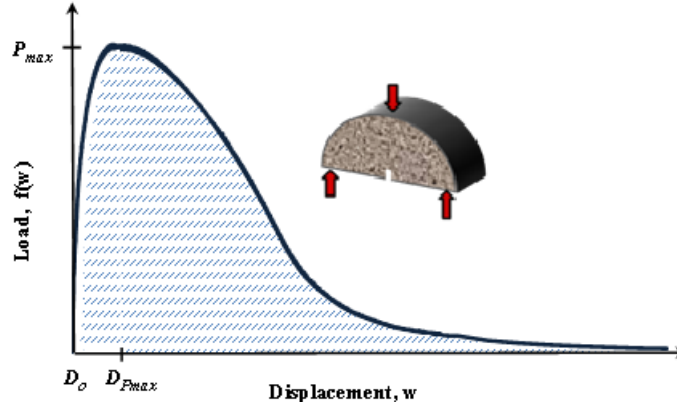


Figure 6-1. Load-Displacement Response Curve: SCB Testing.

The classical fracture parameters measured from the SCB tests in this study include (1) the HMA tensile strength (σ_t), (2) HMA tensile strain at peak failure load or ductility potential (ε_t), (3) HMA tensile modulus or stiffness in tension (E_t), and (4) HMA fracture energy or FE (G_f). There are several models for calculating the tensile strength available in the literature. For this study, the research group used the model that [Hofman et al. \(2003\)](#) proposed, assuming plane stress conditions:

$$\sigma_t = 4.263 \frac{P_{\max}}{tD} \quad 5-7$$

where t and D are the thickness and the diameter of the specimen, respectively, and P_{\max} is the axial peak load (see [Figure 6-1](#)). The tensile strain at peak load or the ductility potential is calculated as

$$\varepsilon_t = \frac{\text{Disp. @ pick load}}{\text{Initial disp. @ zero load}} = \frac{D_{P_{\max}} - D_o}{D_o} \quad 5-8$$

where $D_{P_{\max}}$ and D_o are the displacement at peak load and initial displacements, respectively (see [Figure 6-1](#)). The ratio of the tensile strength and the tensile strain is denoted as the tensile modulus or the stiffness in tension.

$$E_t = \frac{\text{HMA tensile strength}}{\text{Tensile strain}} = \frac{\sigma_t}{\varepsilon_t} \quad 5-9$$

The fracture energy is defined as the work required to produce a crack of unit surface area, measured in J/m^2 . The work required to fracture the sample is represented by the area under the load versus displacement curve (see Figure 6-1). Therefore, a general expression for Fracture Energy can be written as:

$$G_f = \frac{\text{Work}}{\text{Area of cracked section}} = \frac{1}{A} \int f(x) dx \quad 5-10$$

Finally, the fracture energy index (FE Index), which is a new parameter derived in this study, is defined as a parametric ratio of the fracture energy to the HMA tensile strength and tensile strain at peak failure load per unit crack length and is computed as follows:

$$FE\ Index = 1 \times 10^5 \frac{G_f}{l_{cr} \sigma_t} \varepsilon_t \quad 5-11$$

where l_{cr} is the length traversed by the crack.

The R-SCB Test Outputs and Data Analysis Models

The primary output response parameters from the R-SCB test are the displacement, cycles, and time count. Figure 6-2 shows a plot of the input loads and the resulting displacement outputs for a typical R-SCB test. For clarity, only the first eight cycles were presented.

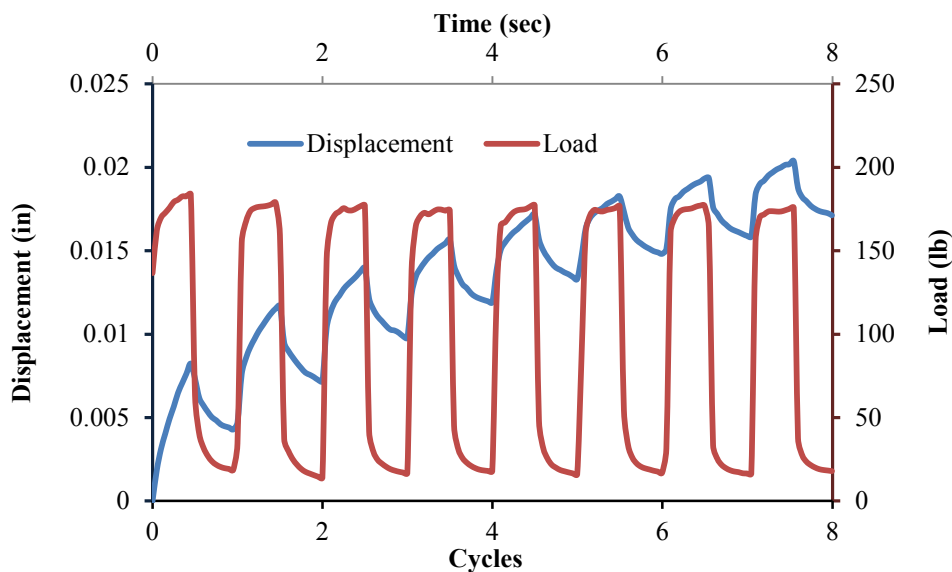


Figure 6-2. R-SCB Load (Input) – Displacement (Output) Curve.

Figure 6-3 presents cycle peak displacements plotted against R-SCB cycles to demonstrate the selection of failure cycles. The notations S#1, S#2, and S#3 refer to sample #1, sample #2, and sample #3, respectively.

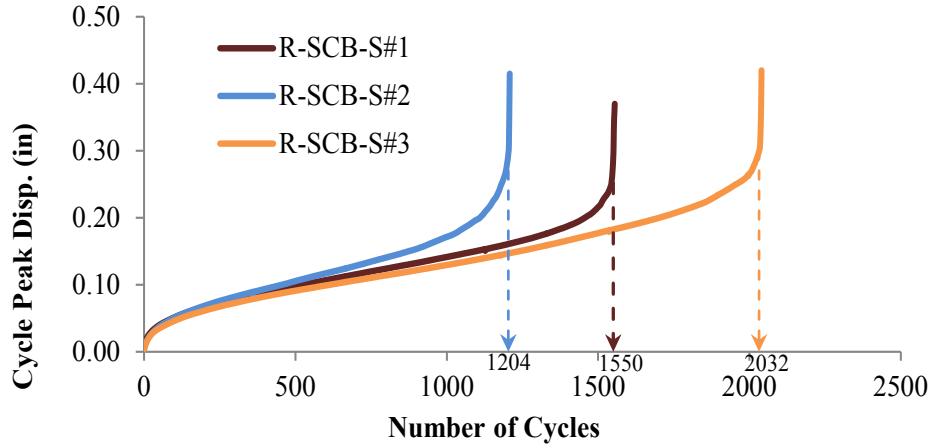


Figure 6-3. Evolution of Peak Displacement with the Number of Load Cycles.

In addition to the number of load cycles and to account for the load-controlled mode of the R-SCB test method, the data analysis from these tests included the Cycle Index concept (Equation 5-12). The Cycle Index was introduced to provide a baseline comparison with the OT_R results that are computed based on displacement-controlled testing and was computed as follows:

$$Cycle\ Index = Cycles^{-1} \times \frac{Input\ Load}{Sitting\ Load} \quad 5-12$$

In the above equation, *Cycles* corresponds to the number of R-SCB load cycles to crack failure (see Figure 6-3). The input and sitting load were 175 lb and 10 lb, respectively, as defined in the previous section and illustrated in Figure 6-2. Similar to the number of cycles in the OT_R test, and the Cycles Index in the R-IDT test, the higher the Cycle Index in magnitude, the better the HMA mix in terms of crack resistance potential.

SCB AND R-SCB TEST RESULTS

The laboratory test results for the SCB and the R-SCB tests are presented and analyzed in this section, including test method comparisons and sensitivity to AC variations.

SCB Test Results: Comparison of HMA Mixes

Similar to the preceding test methods, the same three mixes were tested, namely a Type B mix from Waco District, a Type D mix from Atlanta District, and a CAM mix from Paris District. Chapter 2 discusses the mix designs for each of these three mixes. Figure 6-4 presents the SCB test results for the three mixes.

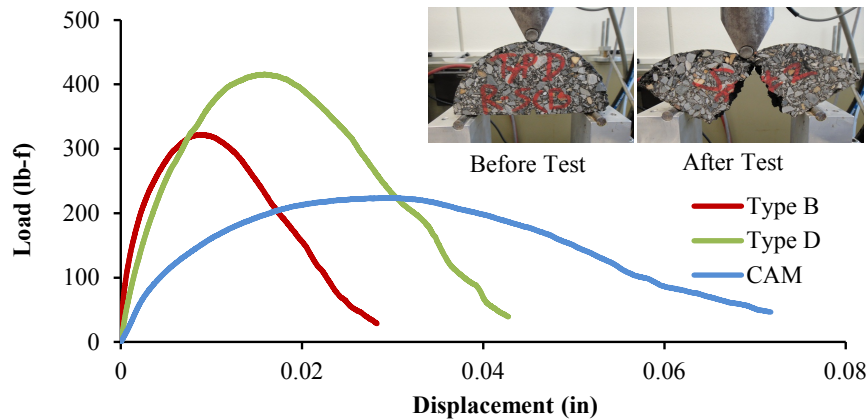


Figure 6-4. SCB Test Outputs: Load-Displacement Response Curves.

From the above figure, it is evident that the SCB test properly reflected the expected behavior of these three mixes. Just like the previous test method, the CAM, usually known for being a softer and more crack-resistant mix, has the most ductile response curve with low peak load, whereas the Type B mix shows much more brittle response behavior. Similar to the previous test results, Type D is clearly a better mix than Type B both in terms of higher peak load and ductility potential.

Equations 5-7 through 5-11 were used on the generated load displacement response data to compute the fracture parameters; the results are presented in Table 6-2 and Figure 6-5.

Table 6-2. Summary of SCB Test Results.

Mix Type	Fracture Energy, G_f		Tensile Strength, σ_t		Strain, ϵ_t	FE Index
	(J/m ²)	(lb-in/in ²)	(psi)	(MPa)	(mm/mm)	
Type B	145(26.4%)	0.828(26.4%)	203(18.6%)	1.400(18.6%)	0.0062(13.3%)	0.92(24.7%)
Type D	285(30.4%)	1.627(30.4%)	265(24.1%)	1.826(24.1%)	0.0108(23.9%)	2.46(40.9%)
CAM	280(7.7%)	1.601(7.7%)	147(4.4%)	1.013(4.4%)	0.0188(30.6%)	7.63(38.9%)

* Values in parenthesis are the Coefficient of Variance (COV).

The first observation from the results in [Table 6-2](#) is that the SCB is relatively a much less repeatable test when compared to the OT_M ([Table 4-2](#)) and the IDT ([Table 5-2](#)) tests, marked by the high COV results. Especially for the Type D and the CAM mixes, the FE Index COV is considerably higher than the threshold value of ≤ 30 percent. However, the computed parametric values seem to be reasonable and are consistent with literature publications. As [Huang et al. \(2005\)](#) and [Walubita et al. \(2010\)](#) reported, the SCB tensile strength values are about 1.5 to 2.0 times higher than the corresponding IDT values.

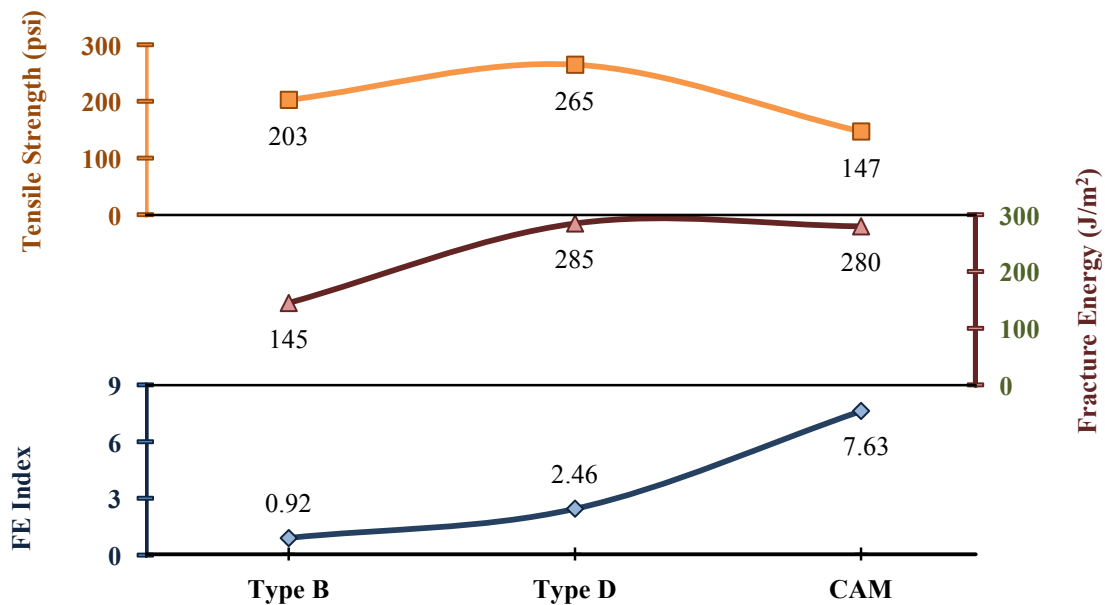


Figure 6-5. Summary of SCB Test Results.

From the computed fracture parameters in [Table 6-2](#) and [Figure 6-5](#), it is clear that the tensile strength and strain parameters are not very reflective of the mixes' perceived laboratory cracking resistance performance. The tensile strength (function of the peak load) and the strain (function of displacement at the peak load) only take the load increment portion of the load-displacement response curve into account. On the other hand, the fracture energy (function of the area under the load-displacement curve), while considering the complete loading history of the specimen, fails to effectively capture the mixes' behavior due to the compensating effects of increasing and decreasing areas under the response curves ([Walubita et al., 2012](#)). This is especially evident in case of the Type D and CAM mixes having very similar FE values (285 J/m²

and 280 J/m², respectively), whereas it is evident from [Figure 6-4](#) that their respective load-displacement responses are completely different. On the other hand, the FE Index effectively combines these three fracture parameters to capture the complete loading history of the specimen so that it can show a better reflection of the expected cracking performance of the mix. This is also clearly presented in [Figure 6-5](#), where the FE Index exhibits a distinctive increasing trend from the poor Type B mix to the more crack-resistant CAM mix.

R-SCB Test Results: Comparison of HMA Mixes

The same three mixes that were tested in the SCB setup were also tested in the repeated R-SCB loading mode and the results are listed in [Table 6-3](#). Values in parenthesis are in [Table 6-3](#) are Coefficient of Variation (COV).

Table 6-3. Summary of R-SCB Test Results.

Mix Type	R-SCB Cycle Index	
	Mean	COV
Type B	3.22	35.9%
Type D	5.49	26.1%
CAM	8.72	6.0%

As expected and consistent with the previous test results, the Cycle Index values are in line with the mixes' expected behavior such that the CAM is the most crack-resistant mix, followed by the Type D and the Type B mix. However, the variability is very high marked by the high COV values, which is of course not unexpected from a repeated loading crack test ([Cominsky et al., 1994](#)).

Screening of HMA Mixes: Discriminatory Ratios and Statistical Analysis

One important aspect of these tests and the evaluated results is their ability to perform as HMA mix screeners, which is crucial in the HMA mix-design process. [Figure 6-5](#) provided an assessment of the potential of the SCB fracture parameters to differentiate the crack resistance potential of the mixes. To further investigate the ability of the fracture parameters to screen mixes, two approaches were used: the discriminatory ratio (DR) concept and Tukey's HSD statistical analysis.

The discriminatory ratio (DR) is an arithmetic ratio of two corresponding parametric values (e.g., G_f , σ_t , FE Index, and Cycle Index) comparing a good mix with a relatively poor mix. The larger the DR in magnitude, the greater the difference between the mixes and the more effective the fracture parameter is in discriminating mixes. Based on the DR values computed in [Table 6-4](#), it is evident that the SCB FE Index provides a superior degree of discrimination between good and poor lab crack-resistant mixes than the other fracture parameters. The R-SCB Cycle Index is also able to differentiate the mixes, but is not as pronounced when compared to the differentiating ability of the OT cycles (see [Table 4-3](#)).

Table 6-4. Screening of HMA Mixes Based on Discriminatory Ratios.

Mix Type	SCB			FE Index	R-SCB
	G_f	σ_t	ε_t		Cycle Index
CAM/Type B	1.93	0.72	3.03	8.29	2.71
CAM/Type D	0.98	0.55	1.74	3.10	1.59
Type D/Type B	1.97	1.31	1.74	2.67	1.70

Analysis of variance (ANOVA) and Tukey's Honestly Significant Differences multiple comparison procedure at a 95 percent confidence level were used to statistically investigate the potential of the test parameters' ability to differentiate the crack resistance potential of the HMA mixes. The interpretation of the ANOVA results in [Table 6-5](#) is as follows: for a particular test method, the mixes having parametric values that are statistically not significantly different are listed in the same group (e.g., A or B). A mix categorized in Group A has higher numerical values than a mix listed in Group B for the same parameter and the difference in their numeric values are statistically significant. For example, the CAM mix has the highest SCB FE Index value in [Table 6-5](#) and hence, is categorized in Group A. Meanwhile, Type B and Type D fall in the same grouping (Group B), which indicates that the difference in their FE Index values is statistically insignificant

Table 6-5. Screening of HMA Mixes Based on ANOVA and Tukey’s HSD Analysis.

Mix Type	<u>SCB</u>				<u>R-SCB</u>
	G_f (J/m ²)	σ_t (psi)	ε_t (mm/mm)	FE Index	Cycle Index
Type B	A	A	B	B	B
Type D	A	A	B	B	A
CAM	A	B	A	A	A

Results in [Table 6-5](#) present inconclusive categorization of the mixes based on the ANOVA and Tukey’s HSD statistical analysis. For example, the SCB fracture energy parameter shows no discrimination among the three mixes, whereas other parameters fail to distinguish between at least two of the mixes. This is due to the high degree of variability in the SCB and R-SCB results ([Table 6-2](#) and [6-3](#)). This failure to discriminate different mixes makes it difficult for these researchers to use these two tests as routine HMA cracking test.

Sensitivity to Changes in Asphalt Binder Content

Like in the preceding chapters, the research team used a Type D mix (PG 70-22 + Limestone) with three different AC levels (4.5, 5.0, and 5.5 percent) to assess the sensitivity of the three tests to HMA mix-design variables such as AC variations. [Table 6-6](#) and [Figure 6-6](#) present the computed facture parameters. Values in parenthesis in [Table 6-6](#) are the COVs.

Table 6-6. Sensitivity to AC Variations.

AC	<u>SCB</u>				Cycle Index
	G_f (J/m ²)	σ_t (psi)	ε_t (mm/mm)	FE Index	
4.5%	175 (14%)	192 (6.1%)	0.0086 (17%)	1.63 (24%)	2.78 (25%)
5.0%	143 (11%)	140 (3.5%)	0.0090 (25%)	1.93 (34%)	8.01 (34%)
5.5%	225 (19%)	185 (15%)	0.0111 (23%)	2.90 (42%)	1.05 (43%)

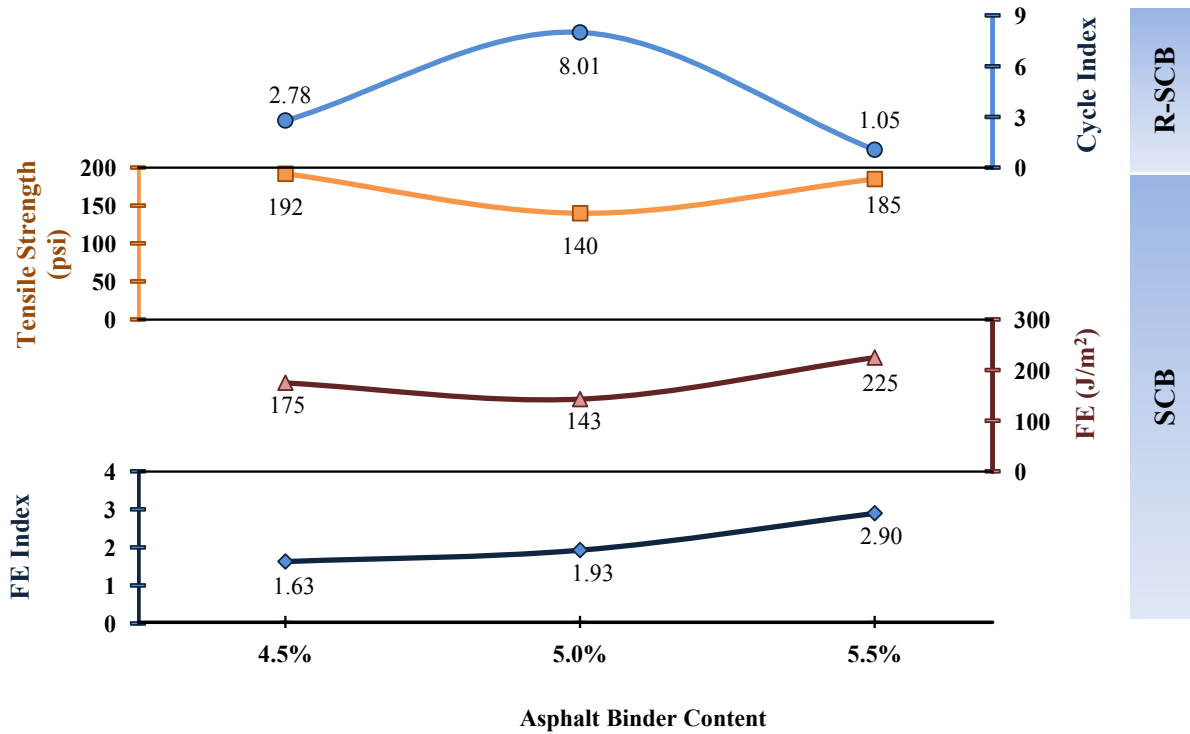


Figure 6-6. SCB and R-SCB Test Parameter Sensitivity to AC Variation.

The results in [Table 6-6](#) and [Figure 6-6](#) show the overall inability of the SCB and the R-SCB tests in capturing the effects of AC variability. Only the FE Index parameter follows an increasing trend that is expected with an increase in AC levels. All the other parameters fail to behave according to theoretical expectations. For example, the HMA tensile strength at 5.5 percent is higher than the strength at 5.0 percent, whereas ideally the strength should be decreasing with increasing binder content. Consequently, the fracture energy at 5.5 percent AC also defies the expected theoretical HMA behavior. All these results point to the challenges associated with running the SCB and R-SCB tests at high asphalt binder contents and 77°F when the mixes get relatively softer. The SCB and R-SCB test setups are such that, in the case of softer mixes (at higher asphalt binder contents and/or higher temperatures), the loading strips induce permanent deformations at the points of loading, resulting in a composition of both compressive and tensile failure modes in the specimen. This leads to formation of multiple crack paths, which yields irregular test results. [Figure 6-7](#) present examples of such failure modes. The left sample in [Figure 6-7](#) is a Type D sample with 5.5 percent AC tested in the R-SCB setup, while the right sample is the same mix tested in the SCB setup.

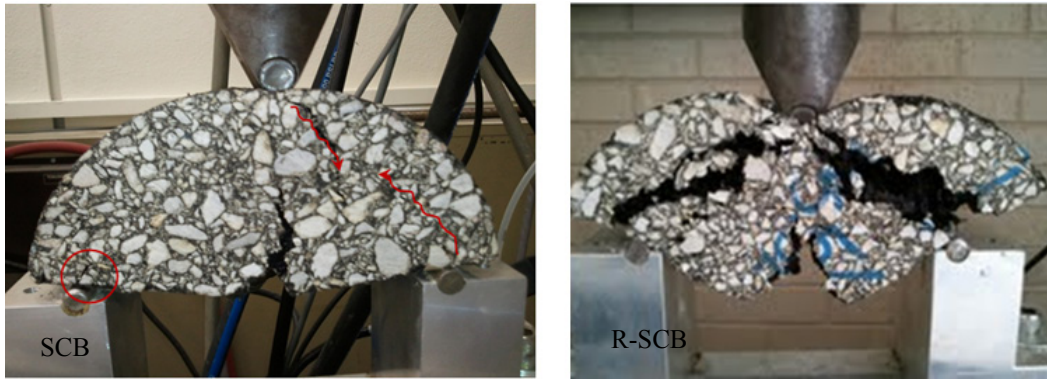


Figure 6-7. SCB and R-SCB Testing at High AC Levels: Multiple Crack Failure Modes.

COMPARISON OF THE SCB AND R-SCB TEST METHODS

Based on the results presented in the preceding sections and the subsequent discussions, a comparison between the two test methods is presented in [Table 6-7](#). From the overall comparison of the two test methods, researchers have observed that both tests have failed to show enough potential to be routinely used as a HMA fracture test at room temperature (i.e., 77°F).

Table 6-7. Comparison of SCB and R-SCB Test Methods.

Category	SCB	R-SCB
Sample preparation	Difficult (Notching required)	
Potential to test field cores	Yes	Yes
Overall test simplicity	Simple	Complex
Test time per specimen	≤ 10 minutes	≤ 180 minutes
Test variability at 77°F (COV ≤ 30%)	Variable	Highly variable
Mix screening ability	Moderate	Moderate to Poor
Sensitivity to AC variations	Moderate	Poor
Correlation to field data	Needs validation	
Practicality of implementation	Fair	No (it's difficult)

SUMMARY

This chapter provided a comparative exploration of two of the prospective surrogate test methods, namely the semi-circular bending test (SCB) and the repeated loading semi-circular bending test (R-SCB). From the overall findings of the study, the researchers have concluded that neither of these two test methods is ready to be used as a routine HMA cracking test at this point. The tests are problematic with poor repeatability and high variability (COV > 30 percent) in the test results, particularly with high AC mixes tested at room temperature (i.e., 77°F). However, these test methods (particularly the SCB) can be a viable option for low AC mixes and low temperature testing (i.e., less than 77°F).

CHAPTER 7: THE DSCTT TEST METHOD

The Disc Shaped Compact Tension Test (DSCTT) in monotonic loading mode was the second last crack test that was evaluated as a part of the continuing efforts for finding a surrogate crack test procedure. As discussed subsequently in this chapter, this test was only preliminarily evaluated and discontinued due to sample preparation complexity, and was deemed impractical for routine daily applications or mass production testing.

Other alternative crack test methods such as the advanced OT data analysis approach, DT, and the R-DT tests were also explored and are discussed in this chapter. A summary is then presented to conclude the chapter.

THE DSCTT TEST PROCEDURE

Wagoner et al. (2005) developed the DSCTT test as a method for obtaining the fracture energy of asphalt concrete (HMA). They based this test on the ASTM E399 (ASTM, 2002) Standard Test Method for obtaining plain-strain fracture toughness of metallic specimens. Figure 7-1 presents the test specimen dimensions and the pictorial test setup, and Table 7-1 presents the test loading parameters.

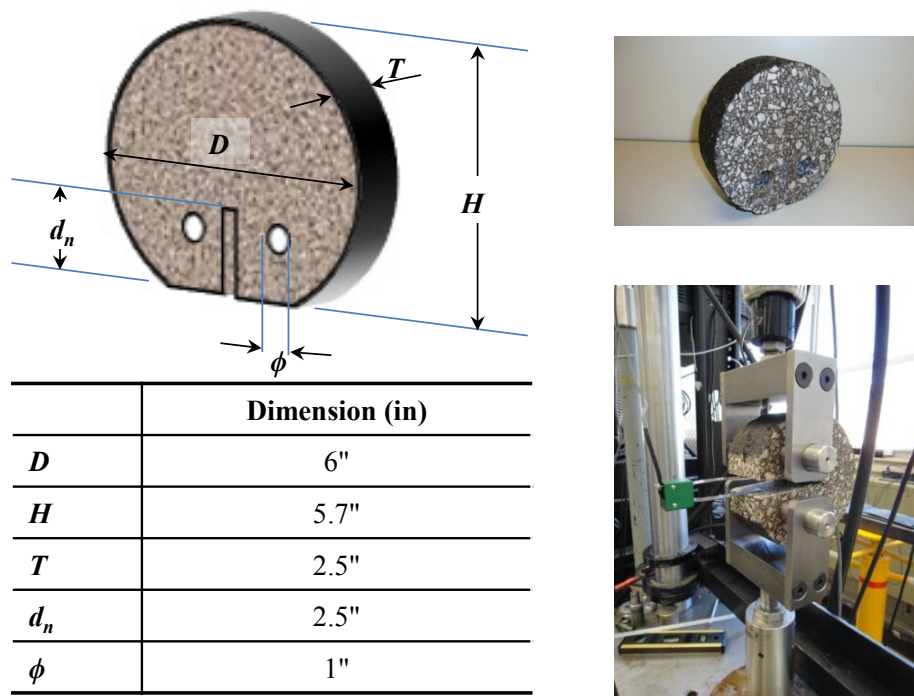



Figure 7-1. DSCTT Testing Setup and Specimen Dimensions.

Table 7-1. DSCTT Loading Parameters.

	DSCTT
Test configuration	
Sample dimensions	6"φ × 5.7" H × 2.5" T (2.5" notch, 2@1"φ drill)
Loading mode	Displacement controlled monotonic tensile loading
Test parameters	Loading rate = 0.04 inch/min, Temperature = 77°F
Output data	Strength (σ_t), Strain (ε_t), Stiffness (E_t), FE (G_f), & FE Index
Test time per specimen	≤ 10 minutes

The specimen is loaded using a couple of testing jigs that are attached to a servo-hydraulic closed-loop testing machine capable of applying axial tensile load (Figure 7-1). Loading is applied in a controlled displacement mode at a predetermined rate (Table 7-1). A Linear Variable Displacement Transducer (LVDT) is attached at the notch opening to measure the notch opening displacement.

It is immediately noticed from the specimen description that the specimen preparation for this test is fairly complex. The trimming of the specimen base, notching, and drilling, all require an expert technician and are time- and resource-consuming. Also, the complexity of the specimen preparation dictates that there is a high possibility of varying specimen dimensions, leading to high test result variability.

THE DSCTT DATA ANALYSIS MODELS

As discussed in the preceding section, the DSCTT test was developed as a means to characterizing the fracture energy of HMA mixes. Like the other monotonic loading tests discussed in the preceding chapters, the outputs from the DSCTT test include the load-displacement response. Figure 7-2 shows a typical load-displacement response from a DSCTT test. Several HMA fracture parameters are calculated from this output response curve.

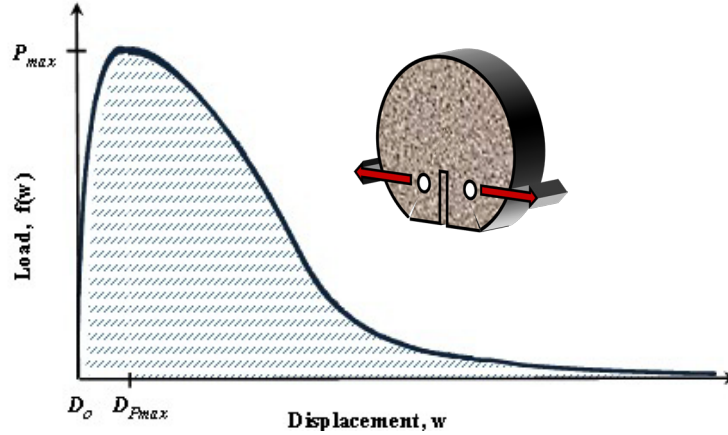


Figure 7-2. Load-Displacement Response Curve: DSCTT Testing.

The fracture parameters measured from the DSCTT tests in this study include:

- HMA tensile strength (σ_t).
- HMA tensile strain at peak failure load or ductility potential (ε_t).
- HMA tensile modulus or stiffness in tension (E_t).
- HMA fracture energy or FE (G_f).
- Fracture energy index or FE Index.

The tensile strength is determined following standard models of mechanics as the ratio of the peak failure load and the area of the cracked section as follows:

$$\sigma_t = \frac{P_{\max}}{T(H - d_n)} \quad 6-1$$

where T and H are the thickness and the height of the specimen, respectively, with the notch depth denoted as d_n (Figure 7-1), and P_{\max} is the axial peak load (see Figure 7-2). The tensile strain at peak load or the ductility potential is calculated as follows:

$$\varepsilon_t = \frac{\text{Disp. @ peak load}}{\text{Initial disp. @ zero load}} = \frac{D_{P_{\max}} - D_o}{D_o} \quad 6-2$$

where $D_{P_{\max}}$ and D_o are the displacement at peak load and initial displacements, respectively (Figure 7-2).

The ratio of the tensile strength and the tensile strain is denoted as the tensile modulus or the stiffness in tension.

$$E_t = \frac{\text{HMA tensile strength}}{\text{Tensile strain}} = \frac{\sigma_t}{\varepsilon_t} \quad 6-3$$

The fracture energy is defined as the work required to produce a crack of unit surface area, measured in J/m². The work required to fracture the sample is represented by the area under the load versus displacement curve (see Figure 7-2). Therefore, a general expression for fracture energy (G_f or FE) can be written as follows:

$$G_f = \frac{\text{Work}}{\text{Area of cracked section}} = \frac{1}{A} \int f(x) dx = \frac{1}{T(H - d_n)} \int f(x) dx \quad 6-4$$

Finally, the fracture energy index (FE Index), which is a new parameter derived in this study, is defined as a parametric ratio of the fracture energy to the HMA tensile strength and tensile strain at peak failure load per unit crack length and was computed as follows:

$$FE \text{ Index} = 1 \times 10^5 \frac{G_f}{l_{cr} \sigma_t} \varepsilon_t \quad 6-5$$

where l_{cr} is the length traversed by the crack.

DSCTT TEST RESULTS

A Type D mix with 5.5 percent asphalt binder content was tested in the DSCTT setup; Figure 7-3 presents the obtained average load-displacement response curve.

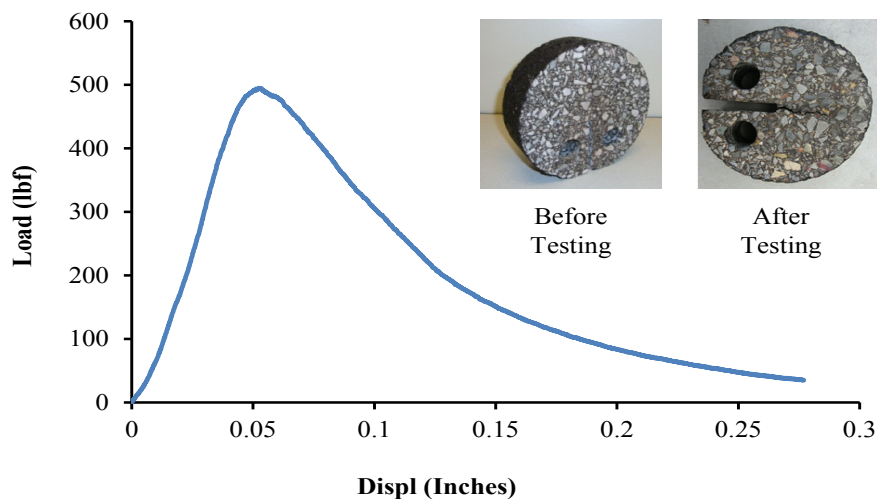


Figure 7-3. DSCTT Load-Displacement Response Curve: Type D (5.5% AC).

Data analysis models 6-1 through 6-5 were used to evaluate the fracture parameters for the mix and the results are presented in [Table 7-2](#).

Table 7-2. DSCTT Results Summary: Type D Mix.

Mix Type	Fracture Energy		Tensile Str.		Strain	FE Index
	(J/m ²)	(lb-in/in ²)	(psi)	(MPa)	(mm/mm)	
Type D (5.5%)	1139	6.50	96	0.66	0.053	4.22
	<i>19.2%</i>	<i>19.2%</i>	<i>7.2%</i>	<i>7.2%</i>	<i>9.2%</i>	<i>21.3%</i>

* COV values are shown in *italic*.

The results presented in the above table show acceptable repeatability for the DSCTT monotonic test method with COV values less than 30 percent; which is also consistent with the monotonic loading OT_M and IDT tests ([Chapters 4 and 5](#)). The evaluated parameters also seem to be within reasonable range.

However, after testing only one mix type, the researchers decided to discontinue this test procedure due to the highly challenging and laborious sample preparation procedures. The test is deemed better suited for research-level testing and not as a routine HMA crack test for regular use; even then, a highly experienced technician/operator is needed for both sample preparation and testing. Compared to the OT, IDT, and SCB test specimens, it takes an additional of 2 to 3 hours to fabricate one DSCTT specimen.

OTHER DATA ANALYSIS AND TEST METHODS EVALUATED

In addition to the DSCTT and the crack test methods discussed in the preceding chapters, other crack data analysis and test methods were also explored and are included in [Appendices D and E](#) of this report, namely:

- Advanced OT data analysis methods based on energy concepts and numerical modelling ([Appendix D](#)).
- The DT and R-DT test methods ([Appendix E](#)).

Like the DSCTT, the DT and R-IDT tests with sample dimensions of 4-inch diameter by 6-inch in height, were discontinued from further evaluation just after testing a few mixes due to the complexity of sample fabrication and setup, which are both very laborious (coring) and requires experienced technicians. Sample setup requires gluing the end platens with minimum 12 hrs curing time. Also, quite often, failures will occur in the glue or at the sample edges and not in the middle zone of the sample. Additionally, testing field cores or slabs is very tricky with these test setups. To summarize, the DT and R-DT test methods, while they may be ideal for research-level testing, are not practical nor implementable for daily routine HMA mix-designs and screening.

SUMMARY

The monotonic loading DSCTT was evaluated as a prospective surrogate test for HMA routine testing in the laboratory. After conducting one set of tests, the research team saw that the results showed promising repeatability just like the OT_M and IDT monotonic loading tests. However, due to highly complex sample preparation procedures involved, just like the DT and R-DT tests, the research team decided to discontinue evaluating this test. Like the DT and R-DT test methods, the DSCTT test requires highly experienced technicians/operators and is better suited for research-level testing, not as routine HMA mix-design and screening test.

CHAPTER 8: COMPARISON OF THE CRACK TEST METHODS

As discussed in the preceding chapters, nine different HMA crack test methods of both monotonic and dynamic loading mode were evaluated in this two-year study. This chapter provides a comprehensive comparison of the evaluated crack test methods based on various considerations. Finally the tests will be ranked based on their order of preference and practicality of implementation.

HMA CRACK TESTS EVALUATED

The tests evaluated as part of this study included four monotonic loading tests and three repeated loading tests. The four monotonic loading tests were:

- The Monotonic Overlay Tester (OT_M) test.
- The Indirect Tension (IDT) tests.
- The Semicircular Bending (SCB) test.
- The Disc Shaped Compact Tension Test (DSCTT).
- The Direct-Tension (DT) test (Appendix E)

The three repeated loading tests were:



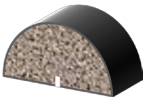

- The Repeated Overlay Tester (OT_R) test.
- The Repeated Indirect Tension (R-IDT) tests.
- The Repeated Semicircular Bending (R-SCB) test.
- The Repeated Direct-Tension (R-DT) test (Appendix E).

These tests were comparatively analyzed based on several specific criteria and are discussed in the subsequent sections. However, the DSCTT, DT, and R-DT tests were not of primary consideration in this comparative evaluation as they were already ruled out to be impractical in the preceding [Chapter 7](#).

TEST LOADING PARAMETERS AND OUTPUT DATA

[Table 8-1](#) compares the specimen dimensions and test loading parameters used in this study along with the output data for the each test.

Table 8-1. Summary of HMA Cracking Tests Evaluated: Loading Parameters and Output Data.

#	Test	Sample	Notching/ Drilling	Gluing/ Curing	Loading Parameters Used	Output Data
1	OT _R	 6" L × 3" W × 1.5" T	No	Yes (≥12 hrs)	Repeated tension loading. Displacement controlled. Maximum opening disp. = 0.025" Load frequency = 10 sec/cycle Temperature = 77°F. Sample test time = varies (up to 3.0 hrs; ≤ 1 000 cycles)	Peak load & number of cycles to failure (93% load drop)
2	OT _M		No	Yes (≥12 hrs)	Monotonic tension loading. Displacement controlled. Loading rate = 0.125 inch/min Temperature = 77°F. Sample test time ≤ 10 min	P _{max} , σ _t , ε _f , E _t , G _f (FE), FE Index
3	IDT		No	No	Monotonic compressive loading. Displacement controlled. Loading rate= 2 inch/min Temperature = 77°F. Sample test time ≤ 10 min	
4	R-IDT	6" φ × 2.5" T	No	No	Repeated compressive loading. Load controlled. Load = 25% IDT peak load (630 lb) Load frequency = 1 Hz (≤ 10,000 cycles) Temperature = 77°F. Sample test time ≤ 180 min (3 hrs)	Cycles, Cycle Index
5	SCB		Yes (Notch = 1/4")	No No	Monotonic compress loading. Displacement controlled. Loading rate = 0.05 inch/min Temperature = 77°F. Sample test time < 10 min	P _{max} , σ _t , ε _f , E _t , G _f (FE), FE Index
6	R-SCB	3" H × 2.5" T			Repeated compressive loading. Load controlled. Load = 50% SCB peak load (175 lb) Load frequency = 1 Hz (≤ 10,000 cycles) Temperature = 77°F. Sample test time ≤ 180 min (3 hrs)	Cycles, Cycle Index
7	DSCTT	 6" φ × 5.7" H × 2.5" T	Yes (Notch = 2.5") (Drill = 1"φ)	No	Monotonic tension loading. Displacement controlled. Loading rate = 0.04 inch/min Temperature = 77°F. Sample test time ≤ 10 min	P _{max} , σ _t , ε _f , E _t , G _f (FE), FE Index

Legend: OT = Overlay Tester; IDT = Indirect Tension Test; SCB = Semi-Circular Bending Test; L = length; W = width; T = thickness, H = height; φ = diameter; P_{max} = maximum peak load (lb); σ_t = HMA tensile strength (psi); ε_f = tensile strain at peak failure load (in/in); E_t = HMA tensile modulus (psi); G_f(FE) = fracture energy (J/m²); FE Index = fracture energy index.

Based on [Table 8-1](#), it is evident that the IDT and the R-IDT tests have the easiest specimen preparation, followed by the OT_R and the OT_M tests. On the other hand, the SCB, R-SCB, and DSCTT tests require complicated specimen preparation procedures involving notching and drilling of the specimen. Similar issues were also raised for the DT and R-DT tests in [Chapter 7](#) and [Appendix E](#), respectively.

Also noticeable from the test loading parameters is that the R-IDT and the R-SCB are the only tests run in load controlled mode, while the other tests are displacement controlled. The complicated loading configurations for these two tests prevent them from being run in a displacement-controlled mode.


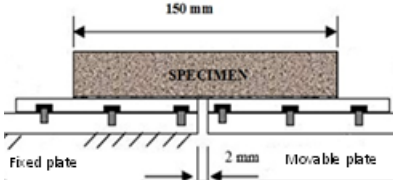


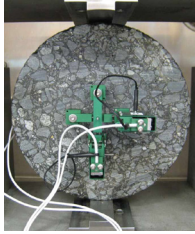
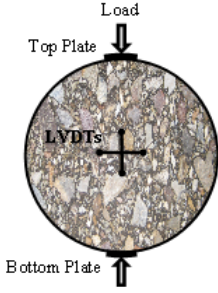

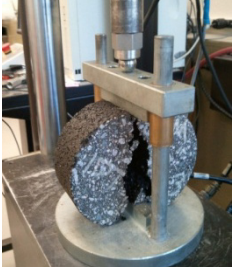
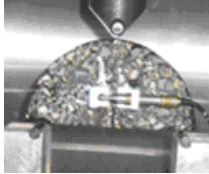
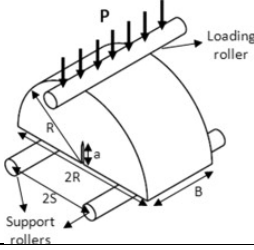



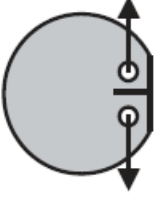




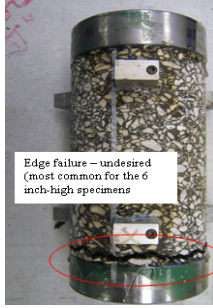
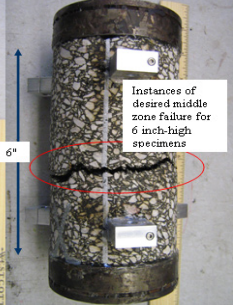
LOADING CONFIGURATION AND SPECIMEN FAILURE MODES

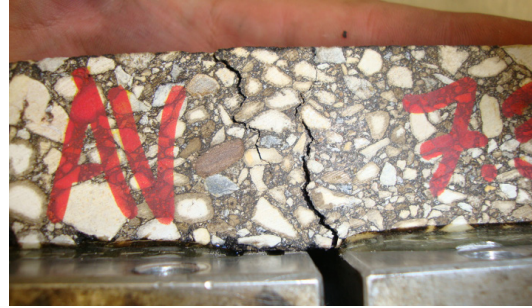
[Table 8-2](#) provides a comparative presentation of the tests based on their respective test setups, loading configurations, and specimen failure modes. Due to similarities in overall test setup, and failure modes, the monotonic and repeated loading tests are paired together in [Table 8-2](#). However, by definition, the repeated loading and monotonic loading tests have significant differences in loading configurations and input parameters ([Table 8-1](#)), which were discussed in detail in [Chapters 4](#) through [7](#), respectively.

From the [Tables 8-1](#) and [8-2](#), it is observed that the repeated and monotonic loading OT tests are simple tests considering loading configurations and overall easy test setup. In the remaining tests, the monotonic loading tests (IDT and SCB) are simpler than their repeated loading counterparts (R-IDT and R-SCB). Although the installation of the LVDTs in case of the IDT and the SCB tests can arguably complicate the test setups, the evolution of the vertical displacement to horizontal displacement conversion technique presented in [Chapter 5](#) serves to simplify this issue for practical applications. On the other hand, the R-IDT and the R-SCB tests involve complicated testing procedures using the Material Testing System (MTS) machine setup to accomplish the repeated loading mode and require skilled technicians. Like the DT and R-DT tests, the DSCTT is also a complicated test procedure requiring the MTS and skillful handling.

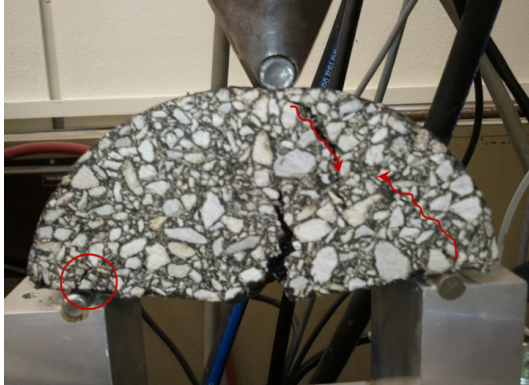
In terms of failure modes, all these tests are aimed at cracking the specimen through application of load or displacements. Ideally, the failure should occur in a single crack path. However, in some instances, multiple cracking have been observed. [Figure 8-1](#) shows some examples of multiple cracking in the OT_R , SCB, and the R-SCB tests.

Table 8-2. Crack Test Loading Configuration and Failure Modes.

Test	Pictorial Setup	Loading Configuration	Specimen Before Testing	Specimen After Testing
OT _M & OT _R				
IDT & R-IDT				
SCB & R-SCB				
DSCTT				
DT & R-DT				



Multiple cracking in OT_R specimens



Multiple cracking in SCB specimens



Multiple cracking in R-SCB specimens

Figure 8-1. Multiple Cracking in OT_R, SCB, and R-SCB Tests.

There are different reasons behind the formation of multiple cracks and they all invariably result in misleading test outputs. In case of the OT_R test, multiple cracking is mostly common in coarse-graded mixes where large aggregates often force the crack to travel through alternate paths, i.e., around the big rock. These specimens frequently show higher cycles to failure than expected. On the other hand, in case of the SCB and R-SCB tests, softer mixes with higher asphalt binder content (AC) or specimens tested at higher temperature are most susceptible to multiple cracking. Invariably, the specimens with multiple cracks show high peak failure load (SCB) or high cycles to failure (R-SCB). Like for the DT and R-DT tests, no instances of multiple cracking were observed for the OT_M, IDT, and the R-IDT tests.

TEST REPEATABILITY AND LOAD-DISPLACEMENT RESPONSE CURVES

The primary objective of this study was to address the issue of results' variability associated with the OT_R test and, subsequently, finding ways to improve repeatability. Therefore, a comparison of the surrogate crack tests in regard to their respective result repeatability was an integral part of this study. [Table 8-3](#) compares the six tests based on their coefficient of variation

values for the same three mix types, namely Type B, Type D, and CAM. The DSCTT, DT, and R-DT were discontinued after initial assessment and, therefore, are not included in this table.

Table 8-3. Comparison of Test Repeatability.

Mix Type	FE Index (Monotonic)			Cycles/Index (Repeated)		
	OT _M	IDT	SCB	OT _R	R-IDT	R-SCB
Type B	3.68	1.88	0.92	47	26.02	3.22
	<i>29.0%</i>	<i>11.8%</i>	<i>24.7%</i>	<i>22.0%</i>	<i>65.8%</i>	<i>35.9%</i>
Type D	5.44	2.76	2.46	269	41.34	5.49
	<i>17.0%</i>	<i>24.4%</i>	<i>40.9%</i>	<i>24.0%</i>	<i>12.9%</i>	<i>26.1%</i>
Type D (Chico) 4.5% AC	3.40	1.84	1.63	165	54.40	2.78
	<i>3.4%</i>	<i>1.2%</i>	<i>24.0%</i>	<i>6.6%</i>	<i>28.4%</i>	<i>24.7%</i>
Type D (Chico) 5.0% AC	5.28	2.81	1.93	210	59.83	8.01
	<i>4.2%</i>	<i>4.6%</i>	<i>33.5%</i>	<i>25.0%</i>	<i>6.4%</i>	<i>33.9%</i>
Type D (Chico) 5.5% AC	11.51	3.59	2.90	822	104.48	1.05
	<i>10.2%</i>	<i>10.7%</i>	<i>42.4%</i>	<i>31.3%</i>	<i>18.1%</i>	<i>43.2%</i>
CAM	15.32	9.21	7.63	1000	57.85	8.72
	<i>24.0%</i>	<i>10.0%</i>	<i>38.9%</i>	----	<i>49.7%</i>	<i>6.0%</i>

*COV values are in ***Bold-Italic***.

From [Table 8-3](#), it is evident that among the monotonic loading tests, the OT_M and the IDT are much more repeatable than the SCB. In the case of repeated loading tests, the OT_R is the most repeatable test compared to the R-IDT and R-SCB. In general, the monotonic loading tests were found to be more repeatable than their repeated loading counterparts, which is, according to [SHRP \(1994\)](#) and [Walubita et al \(2010\)](#), an expected behavior. Despite the inherent tendency of variability associated with its repeated loading mode, the OT_R test has in fact shown good repeatability due to the strict adherence to the specifications and procedural modifications recommended in [Chapter 3](#) and careful testing by trained technicians. The IDT test has shown good repeatability, while the SCB test has shown high variability in both repeated loading and monotonic loading modes, particularly for high AC mixes at 77°F. This behavior is nicely demonstrated in the load-displacement response curves for the three monotonic loading tests in [Figure 8-2](#). The mix compared here is the Type D mix from Chico with 4.5 percent AC. Clearly, the SCB response curves in [Figure 8-2](#) show high variability; whereas the IDT shows the best repeatability.

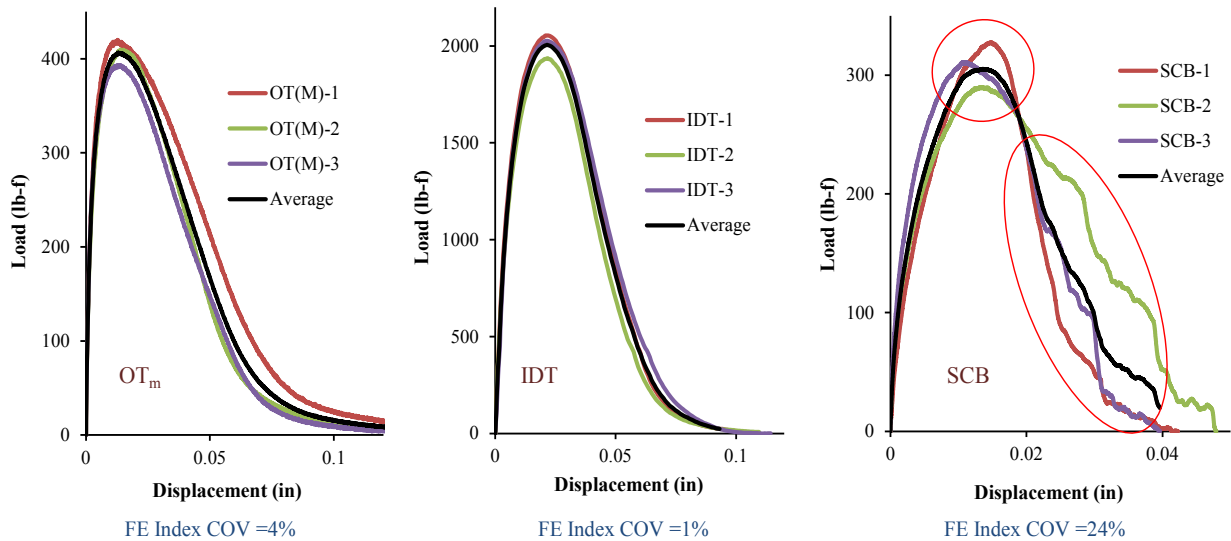


Figure 8-2. Comparison of Test Repeatability (Load-Displacement Response Curves).

POTENTIAL TO DIFFERENTIATE AND SCREEN MIXES

A crucial aspect of the potential of any HMA crack test to be involved in the HMA mix design process is its ability to differentiate the crack resistance potential of HMA mixes. To assess this aspect, two approaches were followed in this study: the discriminatory ratio (DR) concept and Tukey’s HSD statistical analysis. Table 8-4 lists the DR values comparing the same three mixes, namely Type B, Type D, and CAM, for the six evaluated crack test methods.

Table 8-4. Differentiating of HMA Mixes: Discriminatory Ratios.

Mix Type	FE Index			Cycles/Index			Comment
	OT _M	IDT	SCB	OT _R	R-IDT	R-SCB	
CAM/B	4.16	4.90	8.29	21.28	2.22	2.71	VG/M
CAM/D	2.82	3.34	3.10	3.72	1.40	1.59	VG/G
D/B	1.48	1.47	2.67	5.72	1.59	1.70	G/M

The discriminatory ratio (DR) is an arithmetic ratio of two corresponding parametric values for the same test method (e.g., FE Index, Cycles, or Cycle Index) comparing a good mix with a relatively poor mix. The larger the DR in magnitude, the greater the difference between the mixes and the more effective the corresponding test is in discriminating and differentiating the mixes. Based on the DR values computed in Table 8-4, it is evident that the OT_R provides a more superior degree of discrimination between good and poor lab crack-resistant mixes than any other crack test

method. The OT_R , with a DR value of about 21.3, shows a distinctive difference between the CAM (very good) and the Type B (moderate), and 5.7 and 3.7 are the ratio difference for Type D-Type B and CAM-Type D mixes, respectively. Apart from the OT_R , the SCB shows good potential in differentiating the mixes based on the calculated DR values for these mixes, followed by the IDT and the OT_M , while the R-IDT and R SCB tests' DR ratios are not as pronounced as the OT_R test.

Analysis of variance and Tukey's Honestly Significant Differences multiple comparison procedure at a 95 percent confidence level were used to statistically investigate the potential of the test parameters' ability to differentiate the crack resistance potential of the HMA mixes. [Table 8-5](#) shows the results of this analysis.

Table 8-5. Differentiating of HMA Mixes: Statistical Analysis.

Mix Type	FE Index (monotonic)			Cycles/Index (repeated)		
	OT_M	IDT	SCB	OT_R	R-IDT	R-SCB
CAM	A	A	A	A	A	A
Type D	B	B	B	B	A	A
Type B	B	B	B	C	A	B

The interpretation of the ANOVA results in [Table 8-5](#) is as follows: for a particular test method, the mixes having parametric values that are statistically (not significantly) different are listed in the same group (e.g., A or B). A mix categorized in Group A has higher numerical values than a mix listed in Group B for the same parameter and the difference in their numeric values are statistically significant. For example, the CAM mix has the highest FE Index value for the OT_M test and, hence, is categorized in Group A, while Type D and Type B fall in the same group (Group B), which indicates that the difference in their FE Index values is statistically insignificant. Similarly, in case of the OT_R cycles, the three mix types are categorized in three different groupings, implying that these three mixes have significantly different OT_R cycles to failure. The results in [Table 8-5](#) further demonstrate the ability and superiority of the OT_R test in screening and differentiating the HMA mixes.

SENSITIVITY TO HMA MIX-DESIGN VARIABLES

Another important aspect to consider while assessing a test's potential to be included in the mix design procedure is its sensitivity to mix design variables. To assess this potential in this study,

the research team compared the six test methods based on their sensitivity to mix asphalt binder content (AC) and, to a limited extent, temperature variations.

AC Variations

Table 8-6 compares the test methods based on their sensitivity to AC variations. The mix tested for this study was a Type D mix from Chico (PG 70-22 + Limestone) with three different AC levels, namely 4.5 percent, 5.0 percent, and 5.5 percent.

Table 8-6. Sensitivity to AC Variations.

Asphalt Content	FE Index (Monotonic)			Cycles/Index (Repeated)		
	OT _M	IDT	SCB	OT _R	R-IDT	R-SCB
5.5% AC	11.51	3.59	2.90	822	104.48	1.05
	<i>10.2%</i>	<i>10.7%</i>	<i>42.4%</i>	<i>31.3%</i>	<i>18.1%</i>	<i>43.2%</i>
5.0% AC	5.28	2.81	1.93	210	59.83	8.01
	<i>4.2%</i>	<i>4.6%</i>	<i>33.5%</i>	<i>25.0%</i>	<i>6.4%</i>	<i>33.9%</i>
4.5% AC	3.40	1.84	1.63	165	54.40	2.78
	<i>3.4%</i>	<i>1.2%</i>	<i>24.0%</i>	<i>6.6%</i>	<i>28.4%</i>	<i>24.7%</i>

*COV values are in ***Bold-Italic***.

Results in Table 8-6 show the superior degree of sensitivity of the OT_M test over the other two monotonic loading tests. Similarly, in case of the repeated loading tests, the OT_R is the most sensitive to AC changes. The results for the R-SCB tests are particularly inconsistent, where the Cycle Index for the 5.5 percent AC is lower than those at lower AC levels. This, along with the high COV values at higher AC levels, make the SCB and R-SCB tests unsuitable to test softer mixes with high AC levels at 77°F. The sensitivity of the different test methods to AC changes are better demonstrated with the DR values comparatively presented in Table 8-7.

Table 8-7. Sensitivity to AC Change: Discriminatory Ratios.

AC	FE Index (monotonic)			Cycles/Index (repeated)		
	OT _M	IDT	SCB	OT _R	R-IDT	R-SCB
5.5%/4.5%	3.39	1.95	1.78	4.98	1.92	0.38
5.5%/5.0%	2.18	1.28	1.50	3.91	1.75	0.13
5.0%/4.5%	1.55	1.53	1.18	1.27	1.10	2.88

Table 8-7 bears further evidence that in both monotonic and repeated test categories, the OT tests show superior degree of sensitivity to AC change than the other two test methods. Among the two modes of the OT test, the repeated loading mode (OT_R) is slightly more sensitive.

Additionally, a Type D (PG 64-22 + Quartzite + 20 percent RAP) mix from Atlanta District was also tested to compare the AC sensitivity of the two modes of OT loading and the results are presented in Table 8-8. The results for this particular mix also show that the OT_R test is slightly more sensitive to AC changes than its monotonic counterpart.

Table 8-8. Sensitivity to AC Change: Comparison of the OT_M and OT_R Tests.

Asphalt Content	OT _M FE Index	OT _R cycles
6.2%	7.13	655
5.6%	6.28	469
5.2%	5.44	269
6.2%/5.2%	1.31	2.43
6.2%/5.6%	1.14	1.40
5.6%/5.2%	1.15	1.74

Temperature Variations

For easy comparison, all the crack tests in this study were run at room temperature (77°F). However, the OT_M and the OT_R tests were also comparatively evaluated for sensitivity to temperature variation. The results are presented in Table 8-9. The mix evaluated for temperature sensitivity was a Type C mix (PG 64-22 + Crushed Gravel + 20 percent RAP + 1 percent Lime) and the test temperature was varied from 50°F to 77°F.

Table 8-9. Sensitivity to Temperature Change: Comparison of the OT_M and OT_R Tests.

Test Temperature (°F)	OT _M FE Index	OT _R cycles
77	1.93	25
59	0.70	3
50	0.66	2
77/50	2.92	12.50
77/59	2.76	8.33
59/50	1.06	1.50

From the above table, it is evident that both the OT_R and the OT_M tests are sensitive to temperature variation with the repeated loading mode showing significantly higher sensitivity. However, note that at low temperatures, the mixes get much more brittle, resulting in lower crack resistance. Type C, being a relatively poor crack-resistant mix, somewhat magnifies this effect for specimens tested at lower temperatures.

CASE STUDIES AND FIELD CORRELATIONS

In Texas, incorporation of HMA crack tests in mix design procedures is rather limited. Therefore, the correlations of these test methods to field performances are not widely reported. Especially for the newly developed repeated loading tests, namely R-IDT and R-SCB, no studies have been conducted so far to establish their correlation with field performances. On the other hand, for the monotonic loading tests, the FE Index parameter has been introduced as a novel concept. The use of the IDT and the SCB tests as a means to evaluate only HMA tensile strength means that, despite being relatively common HMA crack test methods, they lack sufficient field correlation data. However, in recent years, efforts have been taken to incorporate HMA crack tests, namely the OT_R test, into the mix design process through development of new and more practical mix design methods. Several highways have been constructed in Texas where these new mix design methods have been implemented, subsequently providing field correlation data for review. [Table 8-10](#) compares two such highways where the mix design was developed at TTI based on the OT_R and Hamburg Wheel Tracking Test (HWTT).

Both these two highways are showing satisfactory performances against cracking after two years of service as can be observed from the pictures (see [Table 8-10](#)). [Table 8-11](#) shows another case study, where the HMA mix (Type C) was subjected to accelerated pavement testing (APT) on a pavement structure consisting of 2 inches thick Type C mix over 8 inches thick JCP over 7 inches thick CTB (5 percent cement) resting on a compacted subgrade soil material.

[Table 8-11](#) is another example that serves as a significant evidence of the satisfactory correlation of the OT_R test with a mix's field performance. The Control mix with poor lab performance in the OT_R test failed when subjected to APT testing, while the Modified mix showed no cracks after being subjected to an equivalent level of APT traffic loading.

Table 8-10. Field Correlation: OT_R Test.





Item	US 59 S (Atlanta District)	Loop 20 (Laredo District)
		
Mix Type	Type D	Type C
Mix Design	5.1% AC PG 64-22 + Quartzite + 20% Rap	5.0% AC PG 64-22 + Gravel + 1% Lime + 20% Rap
Overlay Thickness	1¾ inches	2 inches
Construction Year	2010	2010
Date Picture Taken	May 17, 2012	June 26, 2012
OT _R Cycles	269	200
OT _M FE Index	5.44	4.13
IDT FE Index	2.76	1.97
ADT	3 711	-
Trucks (%)	40%	-

Table 8-11. Field Correlation: APT Testing.

Item	Control	Modified
Type C mix	4.3% AC PG 76-22 + Limestone	5.2% AC PG 76-22 + Limestone
OT _R Cycles	41 (< 300)	446 (> 300)
OT _M FE Index	2.93	5.83
IDT Strength	165 psi	130 psi
SCB Strength	177 psi	159 psi
IDT Strain	0.011	0.021
SCB Strain	0.030	0.047
Field performance after 75 000 ALF load passes	 Cracked	 No Cracking

COMPARATIVE EVALUATION AND RANKING OF THE TEST METHODS

Based on the discussion in the preceding sections, a comparative evaluation of the crack test methods is presented in [Table 8-12](#). Following the test method comparisons presented in [Table 8-12](#), [Table 8-13](#) presents a ranking of the seven test methods.

Table 8-12. Comparative Evaluation of the Crack Test Methods.

	Monotonic Loading				Repeated Loading		
	OT _M	IDT	SCB	DSCTT	OT _R	R-IDT	R-SCB
Sample preparation	Easy	Very easy	Requires notching	Challenging (drill holes)	Easy	Very easy	Requires notching
Potential to test field cores	Yes	Yes	Yes	Yes	Yes	Yes	Yes
Overall test Simplicity	Very simple	Very simple	Simple	Challenging	Very simple	Fair	Complex
Test time	≤ 1 0 m i n u t e s				≤ 1 8 0 m i n u t e s		
Data analysis & result interpretation	Fairly simple; but needs post-processing of data				Straight-forward (The machine directly reports the cycles to failure)		
Repeatability & variability in the test results	Repeatable	Repeatable	Variable	Was reasonable for the one mix tested	Acceptable*	Variable	Highly variable
Screening ability	Good	Moderate	Moderate	Test not evaluated	Very good	Moderate	Moderate to poor
Sensitivity to AC & temperature variations	Good	Good	Moderate		Very good	Moderate	Poor
Routine applications	Very Good	Very Good	Moderate	-	Very good	Fair	-
Correlation to field data	N e e d s V a l i d a t i o n				Yes	Needs validation	
Practicality & implementation	Yes	Yes	Fair	-	Yes	Possible	-

*OT_R repeatability becomes reasonably acceptable if the Tex-248-F recommendations in [Chapter 3](#) are adhered to.

Table 8-13. Crack Test Ranking, Practicality, and Implementation.

Rank #	Test	Loading Mode	Key Advantages	Key Challenges
1	OT _R	Dynamic	<ul style="list-style-type: none"> - Proven correlation with field data - Simple data analysis 	Repeatability & variability
2	OT _M	Monotonic	<ul style="list-style-type: none"> - Short & repeatable - Ideal for routine use & production testing - Use existing equip. 	<ul style="list-style-type: none"> - FE Index requires validation with field data
3	IDT	Monotonic	<ul style="list-style-type: none"> - Short & repeatable - Ideal for routine use & production testing - Use existing equip. - Simplest sample prep 	<ul style="list-style-type: none"> - FE Index requires validation with field data - Loading strips - High AC levels - High temperatures
4	R-IDT	Dynamic		<ul style="list-style-type: none"> - High variability
5	SCB	Monotonic	<ul style="list-style-type: none"> - Short test 	<ul style="list-style-type: none"> - Experienced operator/technician - Test setup not easy
6	R-SCB	Dynamic		<ul style="list-style-type: none"> - High variability - Very problematic @ high AC & high temperatures
7	DT	Monotonic	<ul style="list-style-type: none"> - Applies direct tension - Simple data analysis 	<ul style="list-style-type: none"> - Sample prep → very laborious & quite challenging - Potential for end failure or in the glue - Impractical for daily routine applications - Requires validation with field data
8	R-DT	Dynamic	<ul style="list-style-type: none"> - Applies direct tension - Simple data analysis 	<ul style="list-style-type: none"> - Sample prep → very laborious & quite challenging - Potential for end failures or in the glue - Impractical for daily routine applications - Requires validation with field data
9	DCSTT	Monotonic	<ul style="list-style-type: none"> - Repeatability seemed reasonable for the one mix evaluated 	<ul style="list-style-type: none"> - Sample prep → laborious & challenging - Test setup - Experienced operator/technician

SUMMARY

This chapter compared the nine HMA crack test methods evaluated throughout the course of this study based on several criteria, namely:

- The test loading parameters and configurations.
- Test repeatability.
- Potential to screen and discriminate mixes.

- Sensitivity to HMA mix design variables.
- Case studied and field correlations.

Finally, the test methods were ranked based on the comparative evaluations and the various advantages and challenges that these tests present. Overall, the key findings and recommendations drawn from this chapter are as follows:

- The OT cycles from the repeated loading OT test was found to be the best screener of different mixes, followed by monotonic IDT and OT_M tests, respectively. Therefore, these two test methods along with the FE Index concept can be considered as candidates to serve as supplementary and/or surrogate crack tests to the repeated loading OT test.
- Monotonic crack tests, irrespective of the crack test method, are more repeatable and less variable than their dynamic counterparts that are inherently associated with high variability.
- The OT repeatability and variability can be improved to reasonably acceptable levels if the recommended updates and modifications to Tex-248-F as suggested in [Chapter 3](#) are adhered to.
- For the temperature conditions considered and the HMA mixes evaluated, the SCB, R-SCB, and R-IDT were found to be problematic with the poorest repeatability and high variability (i.e., $COV > 30$ percent, particularly for higher AC level mixes at 77°F). Therefore, these tests may not be readily applicable for routine HMA mix-designs that involve AC variations.
- The SCB, R-SCB, and DSCTT were found to be impractical for daily routine mix-designs at room temperature. These tests are better applicable for low temperature and low AC testing. Additionally, the DSCTT, just like the DT and R-DT tests, is associated with complicated and laborious sample fabrication and setting procedures, which is not ideal for daily routine applications.
- OT monotonic FE Index exhibited good correlations with OT repeated loading cycles. Therefore, the monotonic loading OT test and the FE Index concept should be explored further.
- The R-IDT and R-SCB Cycle Index concept yielded promising results. This concept should be investigated further, particularly for low temperature and low AC mix testing.

CHAPTER 9: SUMMARY, CONCLUSIONS, AND RECOMMENDATIONS

As part of the new generation HMA mix-design procedures, TxDOT routinely uses the OT to evaluate the cracking susceptibility of HMA mixes in the laboratory. However, while the OT has exhibited good correlations with field performance data, repeatability and variability in the test results have been major challenges hampering the statewide implementation of the OT test. This is particularly true for most conventional TxDOT dense-graded mixes such as Type C and D mixes that constitute approximately 75 percent of all HMA produced for TxDOT.

As a step toward addressing the OT variability issues and exploring new supplementary and/or surrogate crack tests, these researchers undertook this study to conduct a comprehensive step-by-step sensitivity evaluation of the OT testing procedure. The findings of this study were presented in detail in the preceding chapters of this report. This final chapter provides a summation of the overall findings and recommendations drawn from this study.

OT SENSITIVITY EVALUATION

While taking due cognizance of the fact that repeated loading crack tests, irrespective of the test method, are by their nature inherently associated with high variability (particularly for coarse-graded, RAP, and RAS mixes) and that the OT is no exception, the work presented in this report showed promise to optimize the OT repeatability and minimize variability in the test results. Summarized, the key findings and recommendations derived from the OT sensitivity evaluation are as follows:

- Adhering to the recommended Tex-248-F updates and modifications, including use of trained technicians/operators on well-calibrated OT machines, yielded satisfactory results with acceptable variability, i.e., $COV \leq 30$ percent. Therefore, the recommended Tex-248-F updates and modifications should be implemented and enforced.
- To optimize the OT operational accuracy, calibrations and service maintenance should be performed regularly on the OT machines, at most on a yearly basis.
- Given the criticalness of the OT test to the TxDOT HMA mix-design process, all OT operators and technicians must be trained and certified. At a minimum, two technicians/operators must be trained per laboratory.

- In addition to the available ShedWorks machines, TTI and/or TxDOT should seriously consider buying and evaluating one of the new OT machines that other suppliers are manufacturing.
- For consistency and ease of calibration and maintenance, a similar version of the OT software should be installed on all the TTI and TxDOT OT machines. Thereafter, Round-robin testing should be conducted to verify the consistency and repeatability/accuracy of the machines.
- The FE Index determined from the OT_M test exhibited good correlation with the OT cycles from the OT_R test. From the OT_R - OT_M linear relationship, the computed coefficient of correlation was over 95 percent. Therefore, the monotonic loading OT_M test and FE Index concept should be investigated further relative to field data and in parallel with OT_R (Tex-248-F) testing.

SUPPLEMENTARY AND SURROGATE CRACK TESTS

The research team comparatively evaluated nine crack test methods, namely:

- The standard repeated (OT_R , Tex-248-F) and monotonic loading OT test (OT_M).
- The monotonic (IDT) and repeated loading indirect-tension (R-IDT) test.
- The monotonic (SCB) and repeated loading semi-circular bending (R-SCB) test.
- The disk-shaped compaction tension test (DSCTT).
- The monotonic (DT) and repeated loading direct-tension (R-DT) test.

Comparative evaluation of the crack test methods yielded the following conclusions and recommendations:

- Compared to their monotonic loading counter parts, repeated loading crack tests (irrespective of the test method) are, by their loading nature, inherently associated with high variability in the test results. As observed in this study, the OT_R even exhibited better repeatability with lower COV values compared to the R-IDT and R-SCB tests.
- Although much simpler, more repeatable, and have a shorter test time, monotonic crack tests are not as effective as their dynamic loading counterparts in terms of discriminating and screening mixes as well as capturing the effects of HMA mix-design variables such as AC and temperature variations.

- Compared to the other repeated loading crack tests that were evaluated, namely the R-IDT and R-SCB, the repeated loading OT_R test exhibited statistical superiority in terms of repeatability, variability (lower COV values), potential to differentiate and screen mixes, and sensitivity to changes in AC variations. Therefore, the OT_R tentatively qualifies to be used as a routine crack test for HMA mix-designs and screening purposes, subject to implementing the proposed Tex-248-F updates and modifications.
- The OT_M and IDT, through the use of the FE Index concept, exhibited promising potential both in terms of repeatability and mix screening capabilities. These tests are also fairly simple with a relatively short test time (< 10 minutes) that cost-effectively allows for numerous specimens to be tested within a day. Therefore, the OT_M and/or IDT test methods along with the FE Index concept constitute potential candidates as supplementary and/or surrogate test(s) to the OT_R (Tex-248-F) test method and should be investigated further.
- For the mixes evaluated at room temperature (77°F), the SCB and R-SCB exhibited problems with poor repeatability and high variability (COV > 30 percent) for high AC mixes. Additionally, specimen fabrication just like the DSCTT (and the DT and R-DT tests) is also very tedious. Therefore, these tests are impractical for daily routine HMA mix-designs at room temperature. The tests appear to be better suited for research-level, low temperature, and low AC mix testing.
- While the OT_M and IDT tests (with the FE Index) exhibited promising potential as supplementary and/or surrogate crack tests, validation with field data still remains one of the key challenges. Therefore, performance monitoring of field test sections should be continued so as to validate these crack test methods and develop some screening criteria.

REFERENCES

- Abu Al-Rub, R. K., M. K. Darabi, D. N. Little, and E. A. Masad, (2010). “A micro-damage healing model that improves prediction of fatigue life in asphalt mixes.” *International Journal of Engineering Science*, 48 (Copyright 2011, The Institution of Engineering and Technology), pp. 966–990.
- ASTM D6931, (2005), “Standard Test Method for Indirect Tensile (IDT) Strength of Bituminous Mixtures.”
- ASTM D7313 (2008). “Standard Test Method for Determining Fracture Energy of Asphalt Aggregate Mixtures Using the Disk Shaped Compact Tension Geometry.”
- ASTM E399-90 (2002). “Standard Test Method for Plane-strain Fracture Toughness of Metallic Materials.” Annual Book of ASTM Standards, Vol. 03.01, ASTM International, pp. 443–473.
- Atzori, B., P. Lazzarin, and G. Meneghetti, (2008). “Fatigue strength assessment of welded joints: From the integration of Paris’ law to a synthesis based on the notch stress intensity factors of the uncracked geometries.” *Engineering Fracture Mechanics*, 75 (Compendex), pp. 364–378.
- Bennert, T. (2009). “Lab Overlay Testers for Characterizing HMA Crack Resistance.” 2009 Northeast Asphalt User Producer Group, South Portland, Maine, October 7–8, 2009.
- Bennert, T. and M. Ali, (2008). “Field and Laboratory Evaluation of a Reflective Crack Interlayer in New Jersey,” Transportation Research Board.
- Bennert, T. and R. Dongré, (2010). “A Back Calculation Method to Determine ‘Effective’ Asphalt Binder Properties of RAP Mixtures.” Transportation Research Board.
- Bennert, T., M. Ali, and R. Sauber, (2011). “Influence of Production Temperature and Aggregate Moisture Content on the Performance of Warm Mix Asphalt (WMA).” TRB, Paper Submitted for Presentation and Publication to the 90th Annual Meeting of the Transportation Research Board.
- Bennert, T., M. Worden, and M. Turo, (2009). “Field and Laboratory Forensic Analysis of Reflective Cracking on Massachusetts Interstate 495.” Transportation Research Board.
- Bilir, O. G. (1990). “Relationship between the parameters c and n of Paris’ law for fatigue crack growth in a SAE 1010 steel.” *Engineering Fracture Mechanics*, 36 (Compendex), pp. 361–364.
- Brown, E. N., N. R. Sottos, and White, S. R. (2002). “Fracture testing of a self-healing polymer composite.” *Experimental Mechanics*, 42 (Copyright 2003, IEE), pp. 372–379.

- Buttlar, W. G., R. Roque, and N. Kim, (1996). "Accurate Asphalt Mixture Tensile Strength." Proceedings of the Materials Engineering Conference, Vol. 1, pp. 163–172.
- Chowdary, V., and J. M. Krishnan, "Characterization of healing in sand asphalt mixtures using a thermomechanical framework." Proc., 2006 Airfield and Highway Pavement Specialty Conference, April 30, 2006 – May 3, 2006, American Society of Civil Engineers, pp. 467–478.
- Christensen Jr, D. W., R. Bonaquist, E. Masad, G. Rowe, S. Brown, G. Chehab, and B. Radovsky, "Practical application of continuum damage theory to fatigue phenomena in asphalt concrete mixtures." Proceedings, 2005 Meeting of the Association of Asphalt Paving Technologists, March 7, 2005 – March 9, 2005, Association of Asphalt Paving Technologists, pp. 963–1001.
- Cleveland, G. S., J. W. Button, and R. L. Lytton, (2002). "Geosynthetics in flexible and rigid pavement overlay systems to reduce reflection cracking." Texas A&M Transportation Institute, 298 p.
- Cleveland, G., R. Lytton, and J. Button, (2003). "Reinforcing Benefits of Geosynthetic Materials in Asphalt Concrete Overlays Using Pseudo Strain Damage Theory." 2003, Transportation Research Board.
- Cleveland, G., R. Lytton, and J. Button, (2003). "Using pseudostrain damage theory to characterize reinforcing benefits of geosynthetic materials in asphalt concrete overlays." *Transportation Research Record: Journal of the Transportation Research Board*, No. 1849(-1), pp. 202–211.
- Darabi, M. K., R. K. Abu Al-Rub, E. A. Masad, H. Chien-Wei, D. N. and Little, (2011). "A thermo-viscoelastic-viscoplastic-viscodamage constitutive model for asphaltic materials." *International Journal of Solids and Structures*, 48 (Copyright 2010, The Institution of Engineering and Technology), pp. 191–207.
- Dave, E. V., W. G. Buttlar, G. H. Paulino, and H. H. Hilton, "Graded viscoelastic approach for modeling asphalt concrete pavements." Proceedings, Multiscale and Functionally Graded Materials 2006: 15–18 Oct. 2006, AIP, pp. 736–741.
- Fang, X. Q., C. Hu, and W. H. Huang, (2007). "Determination of dynamic effective properties in functionally graded materials." *Acta Mechanica*, 192 (1–4), pp. 49–63.
- Germann, F. P., and R. L. Lytton, (1979). "Methodology for predicting reflection cracking life of asphalt concrete overlays."

- Hajj, E., P. Sebaaly, J. Porras, and J. Azofeifa, (2010). “Reflective Cracking of Flexible Pavements Phase III: Field Verification.” Research Report No. 13KJ-1, Nevada Department of Transportation, Research Division, University of Nevada, Reno.
- Harvey, J., and C. L. Monismith, (1993). “Effects of laboratory asphalt concrete specimen preparation variables on fatigue and permanent deformation test results using Strategic Highway Research Program a-003a proposed testing equipment,” pp. 38–48.
- Huang, L., K. Cao, and M. Zeng, (2009). “Evaluation of Semicircular Bending Test for Determining Tensile Strength and Stiffness Modulus of Asphalt Mixtures.” *Journal of Testing and Evaluation*, Vol. 37, pp. 122–128.
- Huang, G., Y. Wang, and S. Yu, (2005). “A new multilayered model for in-plane fracture analysis of functionally graded materials (fgms).” *Acta Mechanica Sinica*, 37(1), pp. 1–8.
- Huang, B., X. Shu, and Y. Tang, (2005). “Comparison of Semi-Circular Bending and Indirect Tensile Strength Tests for HMA Mixtures.” *Advances in Pavement Engineering*, GSP 130.
- Jacobs, M. M. J. (1995). “Crack growth in asphaltic mixes.” PhD Thesis, University of Technology, the Netherlands.
- Kallas, B. F., and V. P. Puzinauskas, (1971). “Flexure fatigue tests on asphalt paving mixtures.” ASTM Special Technical Publication(Compendex), pp. 47–66.
- Kessler, M. R. (2007). “Self-healing: A new paradigm in materials design.” Proceedings of the Institution of Mechanical Engineers, *Part G: Journal of Aerospace Engineering*, 221 (Compendex), pp. 479–495.
- Kim, Y. R., and D. N. Little, (1989). “Evaluation of healing in asphalt concrete by means of the theory of nonlinear viscoelasticity.” *Transportation Research Record* (Compendex), pp. 198–210.
- Kim, R. and H. Wen, (2002). “Fracture Energy from Indirect Tension Testing,” *Journal of the Association of Asphalt Paving Technologists*, Vol. 71, pp. 779–793.
- Koohi, Y., J. J. Lawrence, R. Luo, and R. L. Lytton, (2011). “Complex stiffness gradient estimation of field-aged asphalt concrete layers using the direct tension test.” *Journal of Materials in Civil Engineering*, 1 (Compendex), 401.
- Kuai, H., H. J. Lee, G. Zi, and S. Mun, (2009). “Application of generalized j-integral to crack propagation modeling of asphalt concrete under repeated loading.” *Transportation Research Record* (2127), pp. 72–81.

- Li, X. and M. Marasteanu, (2004). "Evaluation of the Low Temperature Fracture Resistance of Asphalt Mixtures using the Semi-Circular Bending Test." *Journal of the Association of Asphalt Paving Technologists*, 73, pp. 401–426.
- Loria-Salazar, L. (2008). "Reflective Cracking of Flexible Pavements: Literature Review, Analysis Models, and Testing Methods." Master's Thesis, University of Nevada, Reno.
- Majidzadeh, K., E. M. Kaufmann, and D. V. Ramsamooj, (1970). "Application of Fracture Mechanics in the Analysis of Pavement Fatigue, Proceedings of Association of Asphalt Pavement Technologists, 1970, Vol. 40, pp. 227–246.
- Masad, E., E. Kassem, and A. Chowdhury, (2009). "Application of Imaging Technology to Improve the Laboratory and Field Compaction of HMA." Technical Research Report FHWA/TX-09/0-5261-1.
- Molenaar, A., A. Scarpas, X. Liu, and S. Erkens, (2002). "Semi-Circular Bending Test: Simple but Useful?" *Journal of the Association of Asphalt Paving Technologists*, Vol. 71, pp. 794–815.
- Mukherjee, S. and G. H. Paulino, (2003). "The elastic-viscoelastic correspondence principle for functionally graded materials, revisited." *Transactions of the ASME. Journal of Applied Mechanics*, 70(3), pp. 359–363.
- Paris, P. and E. Erdogan, (1963). "A Critical Analysis of Crack Propagation Laws." *Journal of Basic Engineering*. Transaction of the American Society of Mechanical Engineering, Series D, 1963, Vol. 85, pp. 528–883.
- Pugno, N., M. Ciavarella, P. Cornetti, and A. Carpinteri, (2006). "A generalized Paris' law for fatigue crack growth." *Journal of the Mechanics and Physics of Solids*, 54 (Copyright 2006, The Institution of Engineering and Technology), pp. 1333–1349.
- Ramsamooj, D. V. (1991). "Prediction of fatigue life of asphalt concrete beams from fracture tests." *Journal of Testing and Evaluation*, 19 (3), 231–239.
- Ramsamooj, D. V. (1991). "Prediction of fatigue life of asphalt concrete beams from fracture tests." *Journal of Testing and Evaluation*, 19 (Compendex), pp. 231–239.
- Schapery, R. A. (1984). "Correspondence principles and a generalized j integral for large deformation and fracture analysis of viscoelastic media." *International Journal of Fracture*, 25 (3), pp. 195–223.
- Schapery, R. A. (1989). "On the mechanics of crack closing and bonding in linear viscoelastic media." *International Journal of Fracture*, 39 (1–3), pp. 163–189.

- Schapery, R. A. (1975). "A theory of crack initiation and growth in viscoelastic media." *International Journal of Fracture*, 11.
- Shen, S., H.-M. Chiu, and H. Huang, (2010). "Characterization of fatigue and healing in asphalt binders." *Journal of Materials in Civil Engineering*, 22 (Compendex), pp. 846–852.
- SHRP. (1994). "Level One Mix Design: Material Selection, Compaction, and Conditioning" SHRP-A-408, Strategic Highway Research Program, National Research Council, DC.
- Tayebali, A. A., J. A. Deacon, and C. L. Monismith, (1996). "Development and evaluation of dynamic flexural beam fatigue test system." *Transportation Research Record (1545)*, pp. 89–97.
- Tex-226-F. (2004). "Indirect Tensile Strength Test."
- Tex-241-F. (2009). "Superpave Gyratory Compacting of Test Specimens of Bituminous Materials."
- Tex-242-F. (2009). "Hamburg Wheel-tracking Test."
- Tex-248-F. (2009). "Overlay Test."
- T.O. Medani, and A. A. A. Molenaar, (2000). "A simplified practical procedures for estimation of fatigue and crack growth characteristics of asphaltic mixes." *International Journal of Road Materials and Pavement Design*, 10.
- TxDOT. (2004). "Standard Specifications for Construction and Maintenance of Highways, Streets, and Bridges." Austin, Texas.
- TxDOT. (2009). "Texas Department of Transportation. Crack-Attenuating Mixture." Statewide Special Specification 3165 (04). Austin, Texas.
- TxDOT. (2011). *Pocket Facts: TxDOT Test Specification Manuals*.
http://www.txdot.gov/business/contractors_consultants/test_procedures/tms_series.htm?series=200-F Accessed October 2011.
- Wagoner, M., W. Buttlar, and G. Paulino, (2005). "Disk-shaped Compact Tension Test for Asphalt Concrete Fracture." *Experimental Mechanics*. Vol. 45, No. 3, 2005.
- Walubita, L., A. Epps Martin, S. Jung, C. Glover, E. Park, A. Chowdhury, and R. Lytton, (2004). "Comparison of Fatigue Analysis Approaches for Two Hot Mix Asphalt Concrete (HMAC) Mixtures." Research Report No. FHWA/TX-05/0-4468-2, Texas A& M Transportation Institute, Texas A&M University System, College Station, Texas.

- Walubita, L. F. (2006). Comparison of fatigue analysis approaches for predicting fatigue lives of hot-mix asphalt concrete (HMAC) mixtures, PhD Dissertation, Texas A&M University, College Station, Texas.
- Walubita, L., V. Umashankar, X. Hu, B. Jamison, F. Zhou, T. Scullion, A. Epps Martin, and S. Dessouky, (2010). “New Generation Mix-Designs: Laboratory Testing and Construction of the APT Test Sections.” Technical Research Report FHWA/TX-10/0-6132-1. Texas A&M Transportation Institute.
- Walubita, L. F., A. N. M. Faruk, G. Das, H. A. Tanvir, J. Zhang, and T. Scullion (2012). *The Overlay Tester: A Sensitivity Study to Improve OT Repeatability and Minimize Variability in the OT Test Results*. Technical Research Report FHWA/TX-12/0-6607-1. Texas A&M Transportation Institute.
- Wen, H., and H. Bahia, (2009). “Characterizing fatigue of asphalt binders with viscoelastic continuum damage mechanics.” *Transportation Research Record (Compendex)*, pp. 55–62.
- Wu, X., and Y.-X. Luo, (2011). “Dynamic responses of a beam with functionally graded materials with Timoshenko beam correction theory.” *Zhendong yu Chongji/Journal of Vibration and Shock*, 30 (10), pp. 245–248.
- Yoda, M. (1980). “The j-integral fracture toughness for mode ii.” *International Journal of Fracture*, 16 (4), R175–R178.
- Yufeng, G., and G. Wanlin, (2006). “Self-healing properties of flaws in nanoscale materials: Effects of soft and hard molecular dynamics simulations and boundaries studied using a continuum mechanical model.” *Physical Review B (Condensed Matter and Materials Physics)*, 73 (Copyright 2006, The Institution of Engineering and Technology), 085411 (2006).
- Zhang, J., and X. Huang, (2010). “Viscoelastoplastic-damage mechanics model of permanent deformation in asphalt mixture.” *Journal of Southeast University (Natural Science Edition)*, 40 (Copyright 2010, The Institution of Engineering and Technology), pp. 185–189.
- Zhao, Y., and Y. R. Kim, “Time-temperature superposition for asphalt mixtures with growing damage and permanent deformation in compression.” National Research Council, pp. 161–172.
- Zhou, F. and T. Scullion, (2003). “Upgraded Overlay Tester and Its Application to Characterize Reflection Cracking Resistance of Asphalt Mixtures.” Research Report No. FHWA/TX-04/0-4467-1, Texas A&M Transportation Institute, Texas A&M University System, College Station, Texas.

- Zhou, F. and T. Scullion, (2005). "Overlay Tester: A Rapid Performance Related Crack Resistance Test." Research Report No. FHWA/TX-04/0-4467-2, Texas A&M Transportation Institute, Texas A&M University System, College Station, Texas.
- Zhou, F., T. Scullion, and R. Williammee, (2004). "Upgraded TTI Overlay Tester: A Simple Reflective Cracking Simulation Test," In *Pavement Management, Design, and Testing*. CD-ROM. Transportation Research Board of the National Academies, Washington, D.C.
- Zhu, G., S. Wu, R. Liu, and L. Zhou, (2009). "Study on the fatigue property for aged asphalt mixtures by using four point bending tests." 6th International Forum on Advanced Material Science and Technology, IFAMST 2008, June 12, 2008 – June 14, 2008, Trans Tech Publications Ltd, Hong Kong, China, pp. 289–294.

APPENDIX A: OT MACHINE CHECK, CALIBRATION, AND VERIFICATION PRIOR TO ROUND-ROBIN TESTING

OT machines		Error from 0.025"	Comment
1) TxDOT Old	6007	+0.0011"	Higher displacement less cycles
2) TxDOT New	7001	-0.0001"	Same as 1002
3) TTI Old	7002	-0.0002"	Lower displacement more cycles
4) TTI New	1002	-0.0001"	Same as 7001

Figure A-1. Example OT Displacement Error Deviation prior to Calibration.

	TxDOT Old	TxDOT New	TTI Old	TTI New
Sample# 1	531	639	549	203
Sample# 2	540	502	461	478
Sample# 3	488	448	499	470
Sample# 4	576	382	546	408
Sample# 5	504	591	518	489
Avg (best 3)	525	577	538	479
CV % (best 3)	4	12	3	2
Avg (all)	528	512	515	410
CV % (all)	6	20	7	29
Avg overall	491			
Stdev overall	55			
COV overall	11.1%			

Figure A-2. Comparison of OT Machine Peak Loads (Type D Mix).

	TxDOT Old (%P_{max})	TxDOT New (%P_{max})	TTI Old (%P_{max})	TTI New (%P_{max})
Sample# 1	37 (7%)	45 (7%)	17 (3%)	15 (7%)
Sample# 2	38 (7%)	35 (7%)	32 (7%)	34 (7%)
Sample# 3	34 (7%)	31 (7%)	47 (9%)	33 (7%)
Sample# 4	40 (7%)	27 (7%)	59 (11%)	33 (7%)
Sample# 5	35 (7%)	41 (7%)	37 (7%)	29 (7%)
Avg (best 3)	38 (7%)	40 (7%)	39	33 (7%)
CV % (best 3)	4	13	20	2
Avg (all)	37 (7%)	36 (7%)	38 (7%)	29 (7%)
CV % (all)	7	20	42	27
Avg overall	35			
Stdev overall	10			
COV overall	27.5%			

Figure A-3. Comparison of Loads Reduction at Test Termination (Type D Mix).

Table A-1. Comparison of AV and OT Cycle Results (Type D Mix).

Item	TxDOT Old	TxDOT New	TTI Old	TTI New
AV (avg, all 5 replicates)	7	7	7	7
COV (all 5 replicates)	2%	2%	2%	6%
OT cycles (avg, all 5 replicates)	273	260	319	209
COV (all 5 replicates)	49%	50%	59%	19%

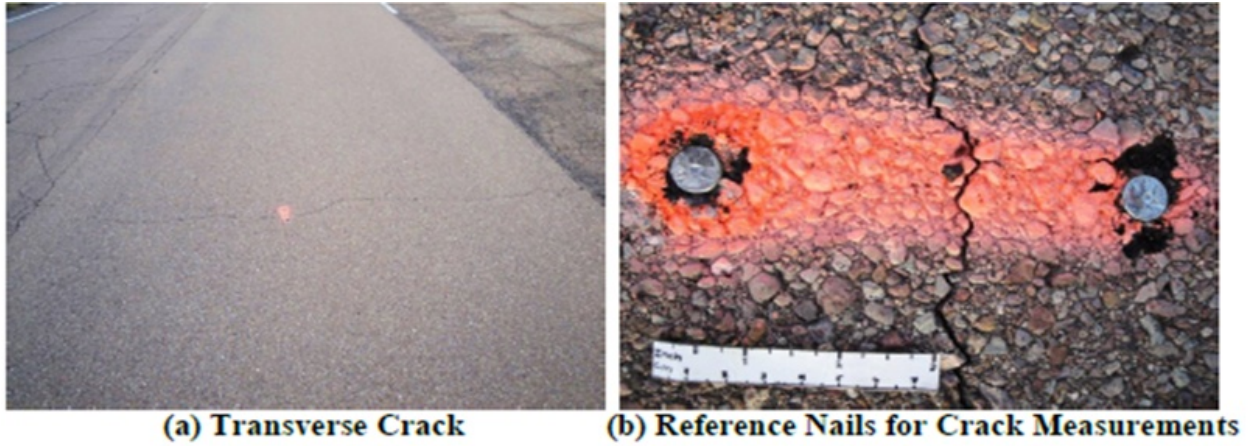


Figure A-4. Method Adapted for Measuring Crack Widths in the Field (by Bryan Wilson).

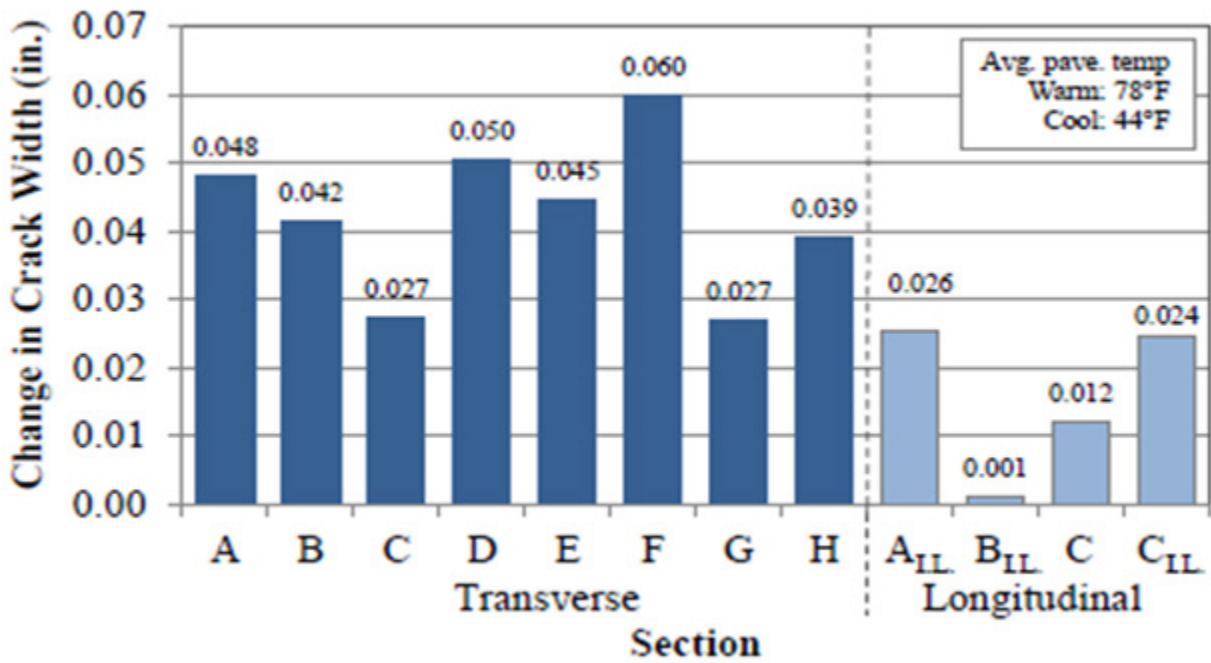


Figure A-5. Average Crack Widths (Inches) Measured at Different Field Sections (by Bryan Wilson).



Figure A-6. Transverse Cracked Pavement Sections at Riverside Campus and Pecos RTC (by Bryan Wilson).

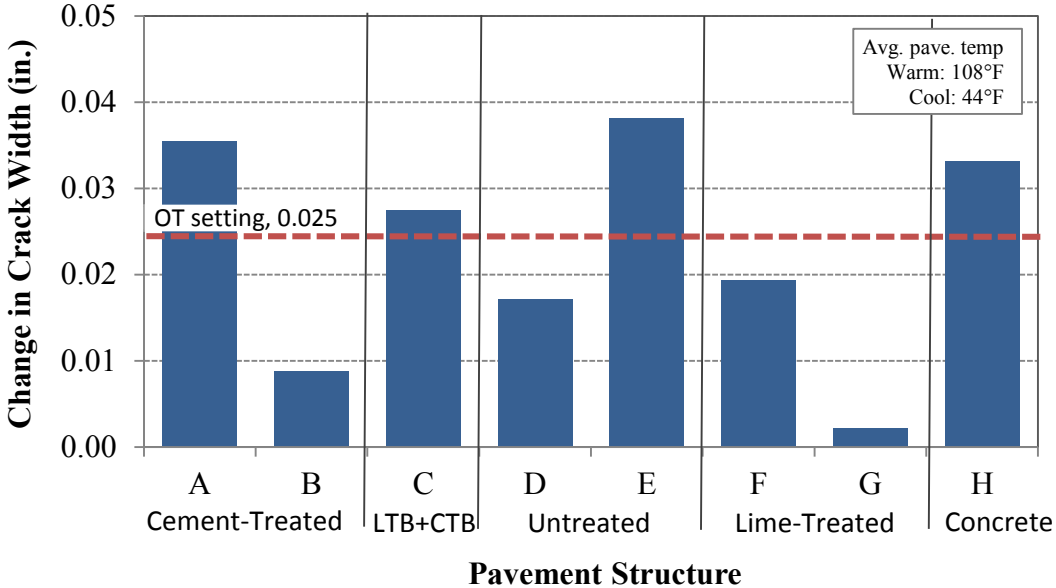


Figure A-7. Crack Movement (Inches) of Various Pavements at Riverside Campus (by Bryan Wilson).

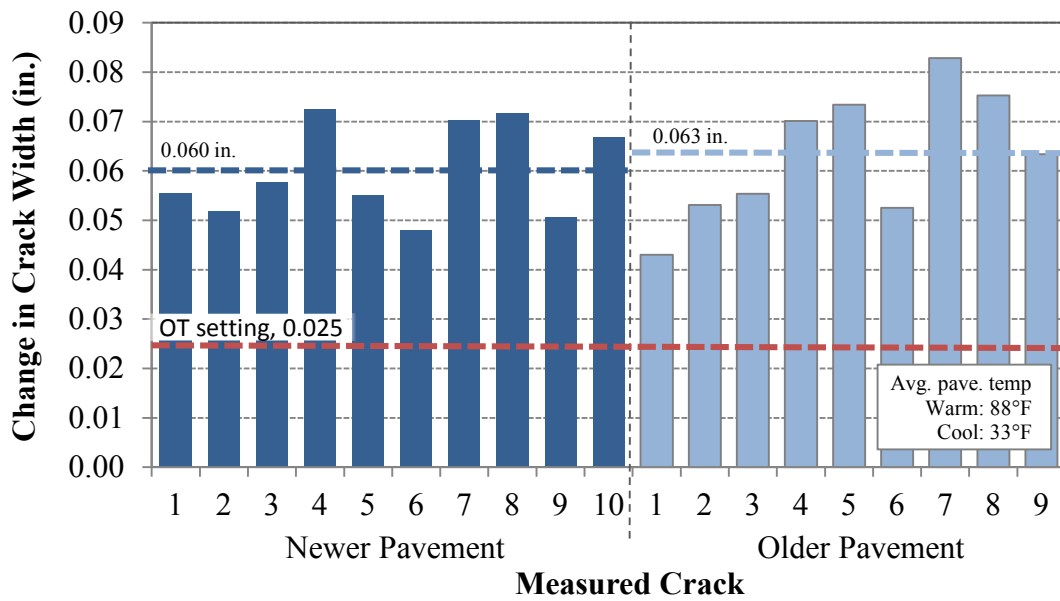


Figure A-7. Crack Movement Measurements (Inches) at Pecos RTC (by Bryan Wilson).

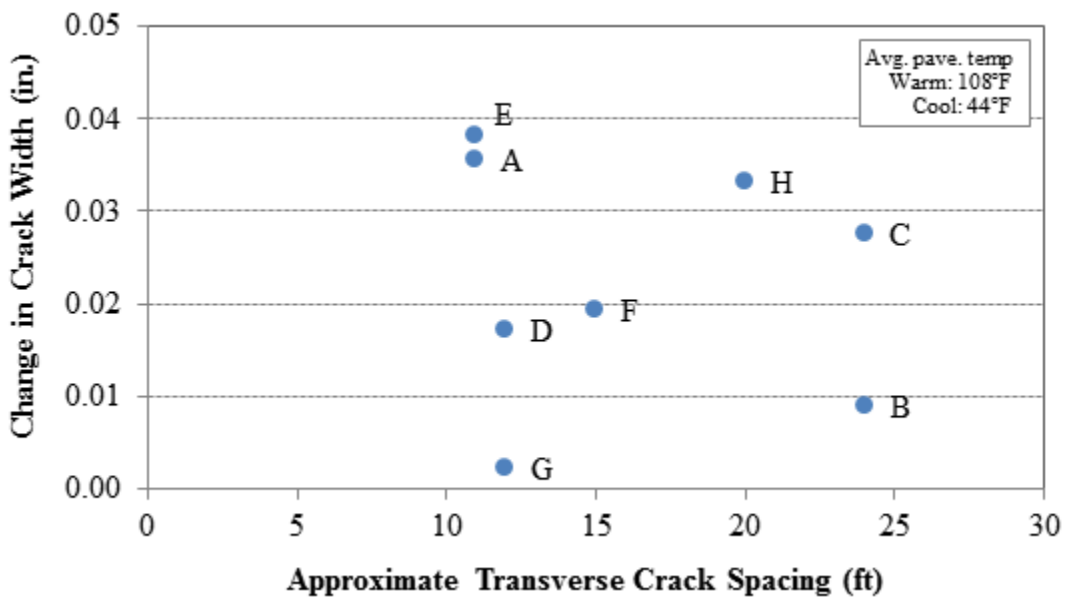


Figure A-7. Transverse Spacing (ft) versus Crack Movement (Inches) at Riverside Campus (by Bryan Wilson).

APPENDIX B: OT PARALLEL TESTING WITH TXDOT-CST (AUSTIN)

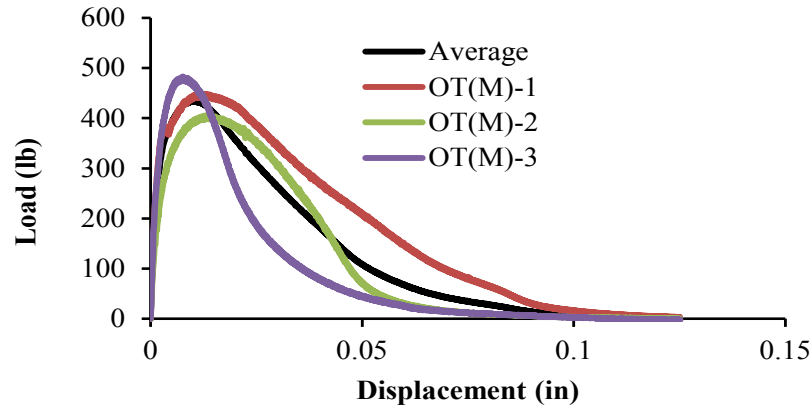
**Table B-1. Work Plans for Parallel OT Testing with TxDOT-CST.
(All aggregate batching done at TTI)**

Phase	Samples	TTI Tasks	TxDOT Tasks
Ia	5	-Mixing, molding -Cutting, drying, AV, gluing -Testing	---
Ib	5	---	-Mixing, molding -Cutting, drying, AV, gluing -Testing
IIa	5	-Testing	-Mixing, Molding -Cutting, drying, AV, gluing
IIb	5	-Mixing, molding -Cutting, drying, AV, gluing	-Testing
IIIa	5	-Cutting, drying, AV, gluing -Testing	-Mixing, molding
IIIb	5	-Mixing, molding	-Cutting, drying, AV, gluing -Testing

Table B-2. Example of Parallel OT Testing Results for a Type D Mix.

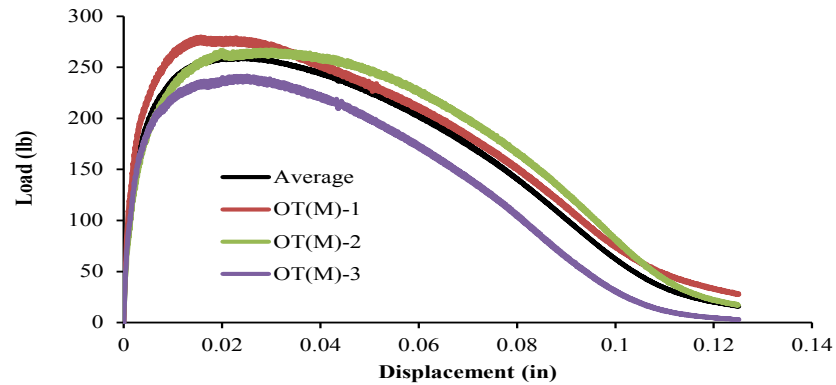
Atlanta Type D: 5.1%PG 64-22 + Quartzite + 20% RAP US 59 SB (Atlanta District; Panola County)	OT Cycles	
	TxDOT-CST	TTI
Sample# 1	294	309
Sample# 2	241	121
Sample# 3	197	334
Sample# 4	257	269
Sample# 5	306	240
Avg (all)	286	255
COV (all)	9.0%	32.6%
Avg (best 3)	259	304
COV (best 3)	17%	11%

APPENDIX C: LOAD-DISPLACEMENT RESPONSE CURVES FOR MONOTONIC LOADING CRACK TESTS



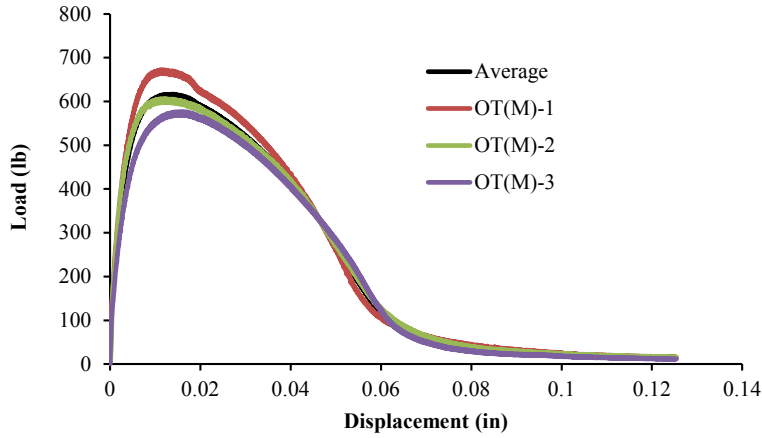
Sample#	Fracture Energy		Tensile Str.		Strain (mm/mm)	FE Index
	(J/m ²)	(lb-in/in ²)	(psi)	(Mpa)		
OT _M 1	855	4.882	100	0.689	0.1513	4.94
OT _M 2	592	3.379	90	0.623	0.1789	4.47
OT _M 3	472	2.697	107	0.742	0.0969	1.62
Average	640	3.653	99	0.685	0.1423	3.68
COV	30.6%	30.6%	8.7%	8.7%	29.3%	48.8%

Figure C-1. OT_M Testing – IH 35 Type B Mix.



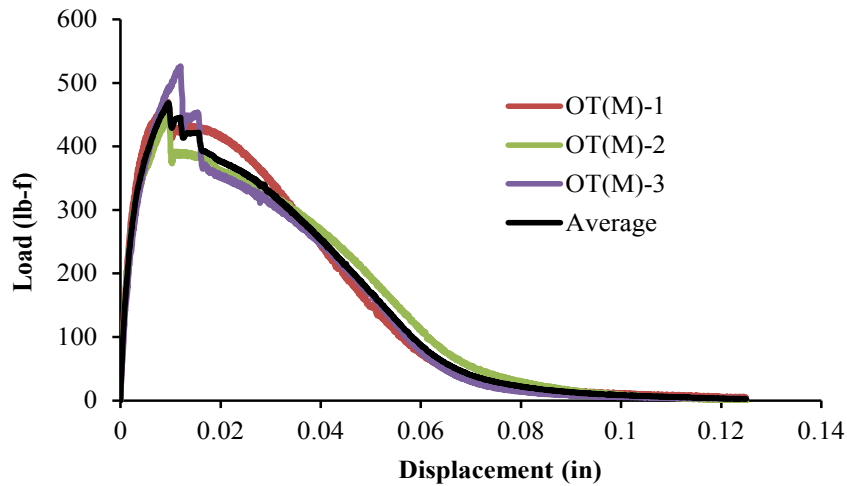
Sample#	Fracture Energy		Tensile Str.		Strain (mm/mm)	FE Index
	(J/m ²)	(lb-in/in ²)	(psi)	(Mpa)		
OT _M 1	848	4.841	62	0.430	0.1989	10.31
OT _M 2	849	4.849	59	0.411	0.3807	20.70
OT _M 3	663	3.784	54	0.372	0.3189	14.96
Average	786	4.491	58	0.404	0.2995	15.32
COV	13.6%	13.6%	7.4%	7.4%	30.9%	34.0%

Figure C-2. OT_M Testing – SH 121 CAM Mix.



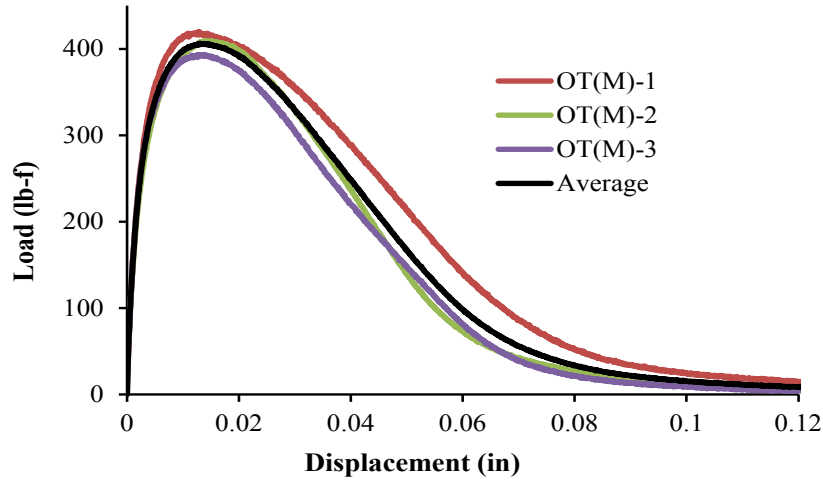
Sample#	Fracture Energy		Tensile Str.			FE Index
	(J/m ²)	(lb-in/in ²)	(psi)	(Mpa)	Strain (mm/mm)	
OT _M 1	1275	7.28	183	1.26	0.131	5.85
OT _M 2	1438	8.21	210	1.45	0.125	4.38
OT _M 3	1711	9.78	185	1.28	0.198	6.10
Average	1475	8.42	193	1.33	0.151	5.44
COV	14.9%	14.9%	7.9%	7.9%	27.0%	17.0%

Figure C-3. OT_M Testing – US 59 Type D Mix.



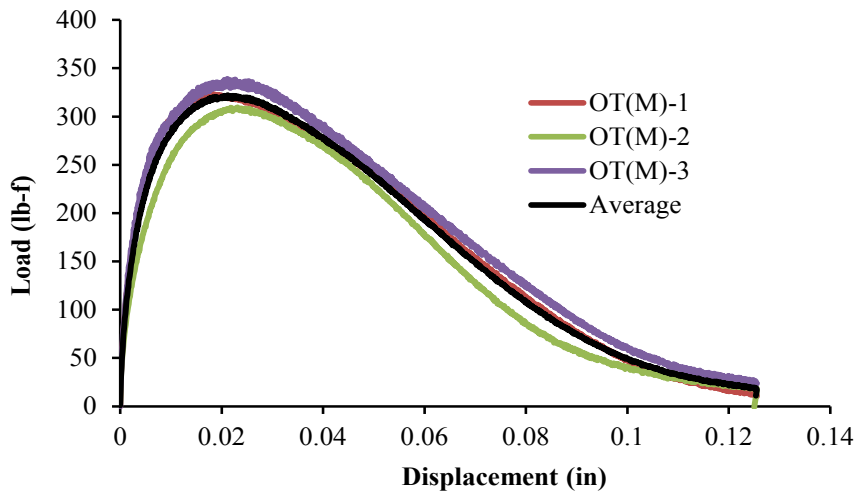
Sample#	Fracture Energy		Tensile Str.			FE Index
	(J/m ²)	(lb-in/in ²)	(psi)	(Mpa)	Strain (mm/mm)	
OT _M 1	742	4.235	105	0.721	0.1213	3.2739
OT _M 2	740	4.228	100	0.69	0.1225	3.4506
OT _M 3	703	4.014	117	0.807	0.1525	3.4893
Average	728	4.159	107	0.739	0.1321	3.4046
COV	3.0%	3.0%	8.2%	8.2%	13.4%	3.4%

Figure C-4. OT_M Testing – Chico Type D (4.5% AC) Mix.



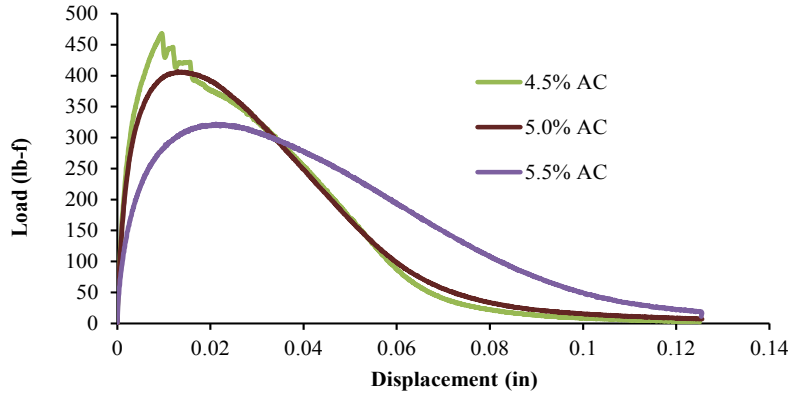
Sample#	Fracture Energy		Tensile Str.		Strain (mm/mm)	FE Index
	(J/m ²)	(lb-in/in ²)	(psi)	(Mpa)		
OT _M 1	839	4.792	93	0.643	0.1615	5.5298
OT _M 2	696	3.972	91	0.628	0.1764	5.1277
OT _M 3	668	3.816	87	0.603	0.1776	5.1693
Average	734	4.193	91	0.625	0.1718	5.2756
COV	12.5%	12.5%	3.3%	3.3%	5.2%	4.2%

Figure C-5. OT_M Testing – Chico Type D (5.0% AC) Mix.



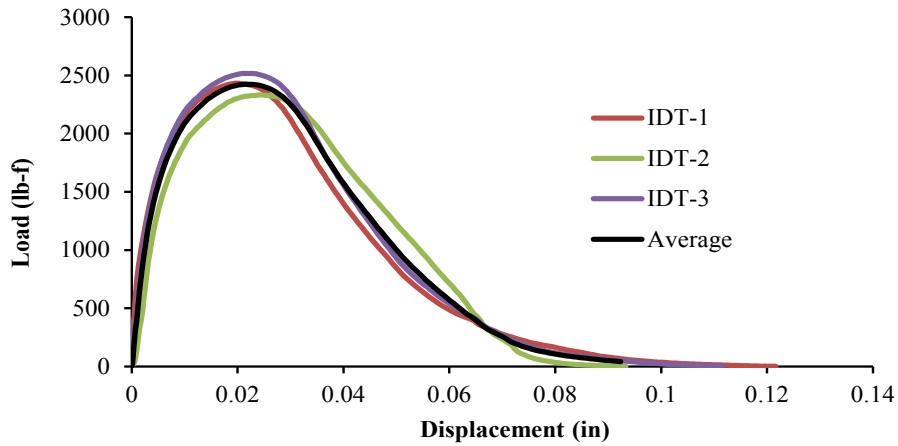
Sample#	Fracture Energy		Tensile Str.		Strain (mm/mm)	FE Index
	(J/m ²)	(lb-in/in ²)	(psi)	(Mpa)		
OT _M 1	834	4.760	72	0.496	0.2304	10.1659
OT _M 2	758	4.330	69	0.474	0.2935	12.3180
OT _M 3	887	5.067	75	0.52	0.2686	12.0359
Average	826	4.719	72	0.497	0.2642	11.5066
COV	7.8%	7.8%	4.6%	4.6%	12.0%	10.2%

Figure C-6. OT_M Testing – Chico Type D (5.5% AC) Mix.



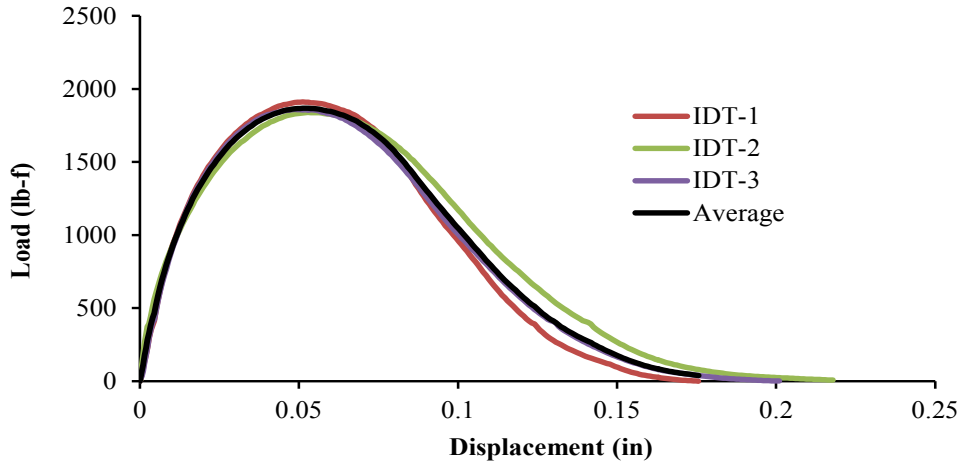
AC	Fracture Energy		Tensile Str.		Strain (mm/mm)	FE Index
	(J/m ²)	(lb-in/in ²)	(psi)	(Mpa)		
4.5%	728	4.159	107	0.739	0.1321	3.40
5.0%	734	4.193	91	0.625	0.1718	5.28
5.5%	826	4.719	72	0.497	0.2642	11.51

Figure C-7. OT_M Testing – Chico Type D Mix – AC Variation Summary.



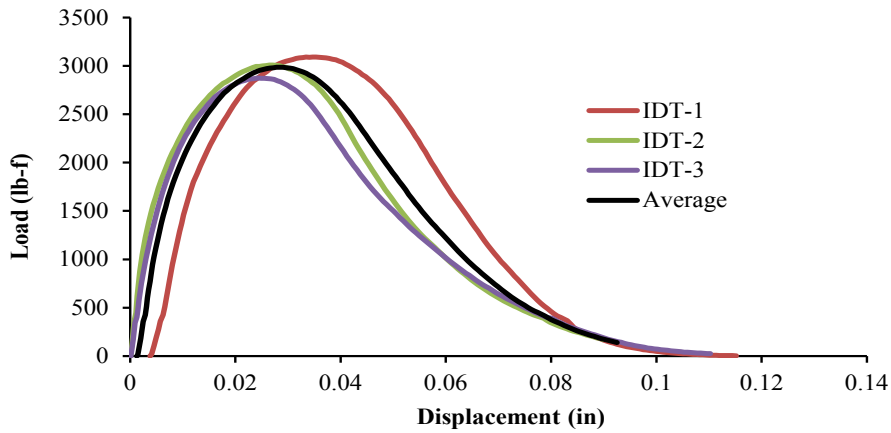
Sample#	Fracture Energy		Tensile Str.		Strain (mm/mm)	FE Index
	(J/m ²)	(lb-in/in ²)	(psi)	(Mpa)		
IDT1	135	0.771	103	0.712	0.0135	1.6762
IDT2	134	0.766	99	0.682	0.0164	2.1158
IDT3	140	0.799	107	0.736	0.0148	1.8443
Average	136	0.779	103	0.710	0.0149	1.8788
COV	2.3%	2.3%	3.8%	3.8%	9.9%	11.8%

Figure C-8. IDT Testing – IH 35 Type B Mix.



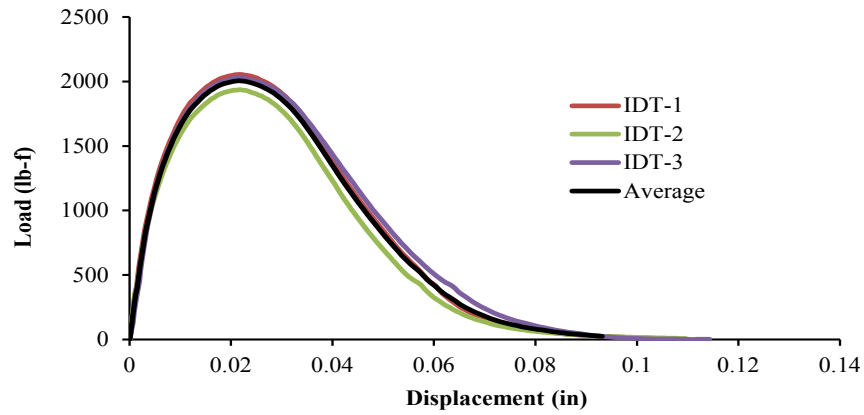
Sample#	Fracture Energy		Tensile Str.			FE Index
	(J/m ²)	(lb-in/in ²)	(psi)	(Mpa)	Strain (mm/mm)	
IDT1	216	1.235	81	0.559	0.0341	8.6595
IDT2	239	1.365	78	0.538	0.0353	10.2769
IDT3	222	1.269	79	0.544	0.0325	8.7048
Average	226	1.290	79	0.547	0.0340	9.2138
COV	5.2%	5.2%	2.0%	2.0%	4.1%	10.0%

Figure C-9. IDT Testing – SH 121 CAM Mix.



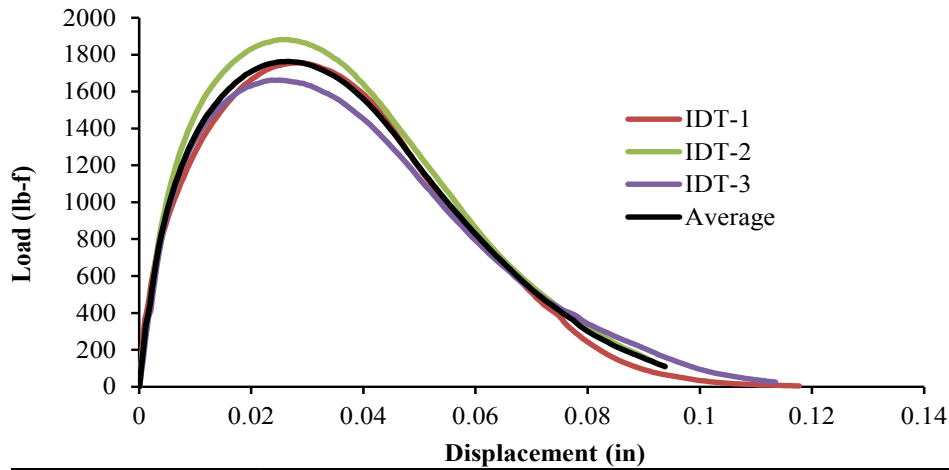
Sample#	Fracture Energy		Tensile Str.			FE Index
	(J/m ²)	(lb-in/in ²)	(psi)	(Mpa)	Strain (mm/mm)	
IDT1	210	1.199	131	0.905	0.0231	3.5214
IDT2	189	1.077	128	0.881	0.0177	2.4818
IDT3	180	1.027	122	0.841	0.0161	2.2634
Average	193	1.101	127	0.876	0.0190	2.7555
COV	8.1%	8.1%	3.7%	3.7%	19.4%	24.4%

Figure C-10. IDT Testing – US 59 Type D Mix.



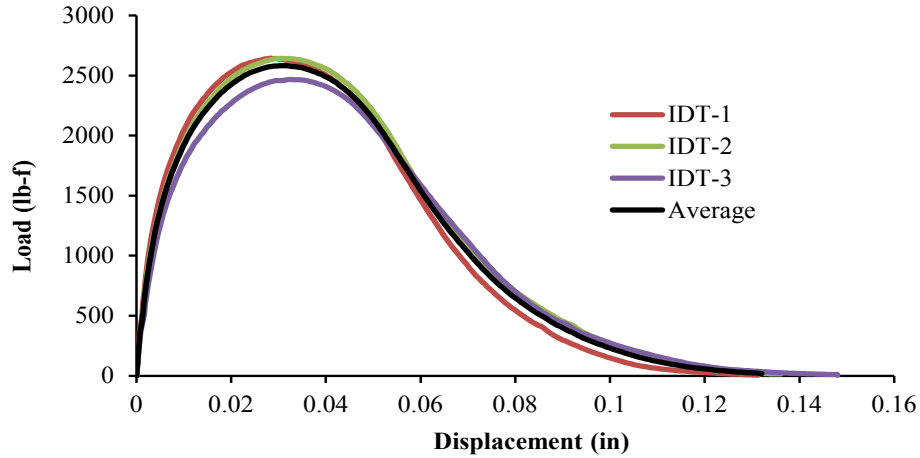
Sample#	Fracture Energy		Tensile Str.		Strain (mm/mm)	FE Index
	(J/m ²)	(lb-in/in ²)	(psi)	(Mpa)		
IDT1	113	0.647	87	0.601	0.0147	1.8214
IDT2	111	0.637	82	0.567	0.0145	1.8669
IDT3	116	0.664	86	0.593	0.0143	1.8455
Average	114	0.649	85	0.587	0.0145	1.8446
COV	2.2%	2.2%	3.1%	3.1%	1.4%	1.2%

Figure C-11. IDT Testing – Chico Type D (4.5% AC) Mix.



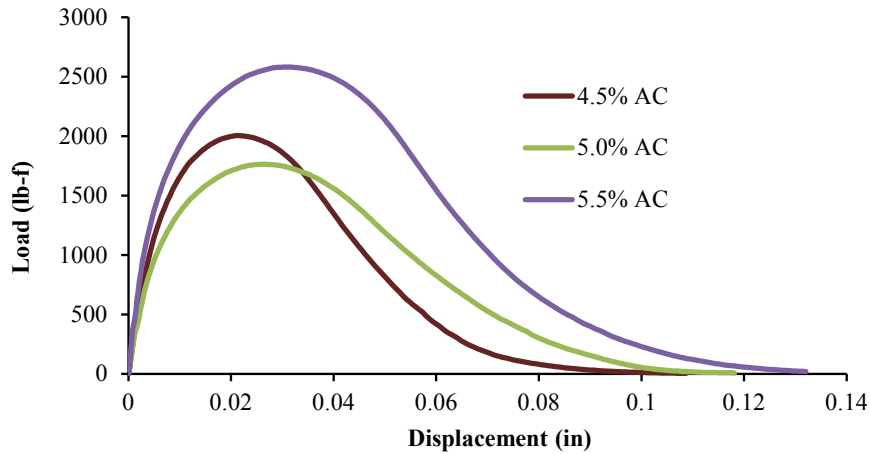
Sample#	Fracture Energy		Tensile Str.		Strain (mm/mm)	FE Index
	(J/m ²)	(lb-in/in ²)	(psi)	(Mpa)		
IDT1	120	0.686	75	0.514	0.0193	2.9564
IDT2	131	0.746	80	0.551	0.0177	2.7610
IDT3	121	0.692	71	0.487	0.0166	2.7104
Average	124	0.708	75	0.517	0.0179	2.8093
COV	4.7%	4.7%	6.2%	6.2%	7.5%	4.6%

Figure C-12. IDT Testing – Chico Type D (5.0% AC) Mix.



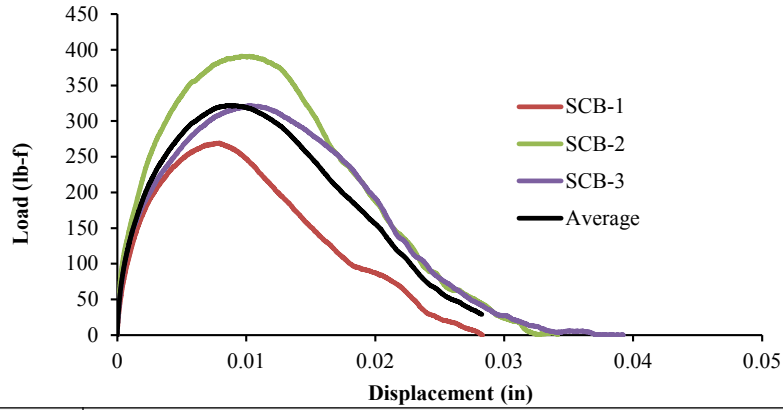
Sample#	Fracture Energy		Tensile Str.			FE Index
	(J/m ²)	(lb-in/in ²)	(psi)	(Mpa)	Strain (mm/mm)	
IDT1	199	1.138	112	0.774	0.0189	3.1873
IDT2	209	1.193	112	0.773	0.0205	3.6402
IDT3	201	1.147	105	0.722	0.0217	3.9548
Average	203	1.159	110	0.756	0.0204	3.5941
COV	2.6%	2.6%	3.9%	3.9%	6.9%	10.7%

Figure C-12. IDT Testing – Chico Type D (5.5% AC) Mix.



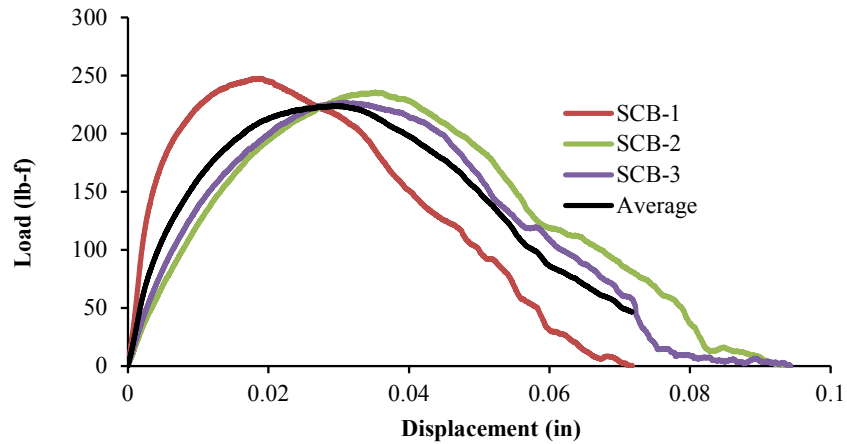
AC	Fracture Energy		Tensile Str.			FE Index
	(J/m ²)	(lb-in/in ²)	(psi)	(Mpa)	Strain (mm/mm)	
4.5%	114	0.649	85	0.587	0.0145	1.84
5.0%	124	0.708	75	0.517	0.0179	2.81
5.5%	203	1.159	110	0.756	0.0204	3.59

Figure C-13. IDT Testing – Chico Type D Mix – AC Variation Summary.



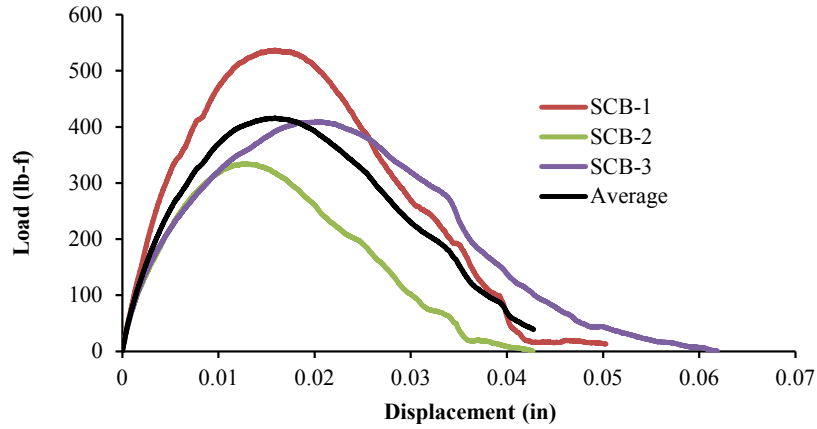
Sample#	Fracture Energy		Tensile Str.		Strain (mm/mm)	FE Index
	(J/m ²)	(lb-in/in ²)	(psi)	(Mpa)		
SCB1	102	0.585	167	1.152	0.0053	0.67
SCB2	177	1.008	243	1.672232	0.0064	0.97
SCB3	156	0.891	200	1.375638	0.0069	1.12
Average	145	0.828	203	1.400	0.0062	0.92
COV	26.4%	26.4%	18.6%	18.6%	13.3%	24.7%

Figure C-14. SCB Testing – IH 35 Type B Mix.



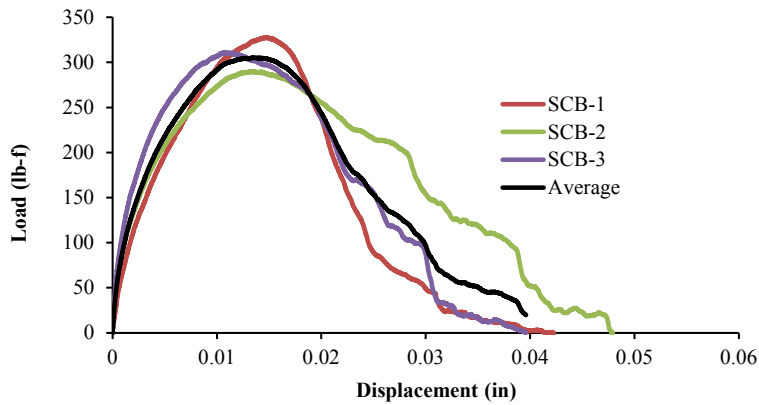
Sample#	Fracture Energy		Tensile Str.		Strain (mm/mm)	FE Index
	(J/m ²)	(lb-in/in ²)	(psi)	(Mpa)		
SCB1	258	1.475	154	1.059	0.0124	4.3298
SCB2	301	1.721	146	1.008	0.0235	10.0710
SCB3	281	1.607	141	0.971	0.0205	8.4945
Average	280	1.601	147	1.013	0.0188	7.6318
COV	7.7%	7.7%	4.4%	4.4%	30.6%	38.9%

Figure C-15. SCB Testing – SH 121 CAM Mix.



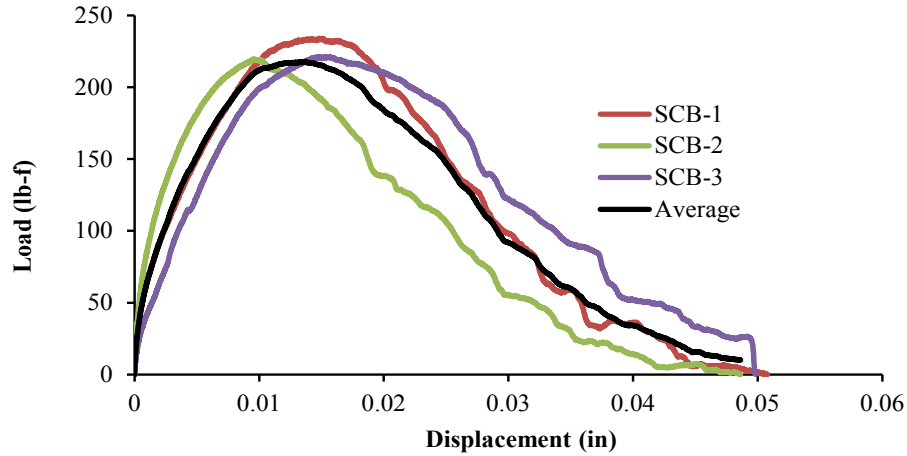
Sample#	Fracture Energy		Tensile Str.			FE Index
	(J/m ²)	(lb-in/in ²)	(psi)	(Mpa)	Strain (mm/mm)	
SCB1	347	1.983	333	2.298	0.0105	2.28
SCB2	186	1.063	207	1.429	0.0083	1.55
SCB3	322	1.836	254	1.751	0.0135	3.54
Average	285	1.627	265	1.826	0.0108	2.46
COV	30.4%	30.4%	24.1%	24.1%	23.9%	40.9%

Figure C-16. SCB Testing – US 59 Type D Mix.



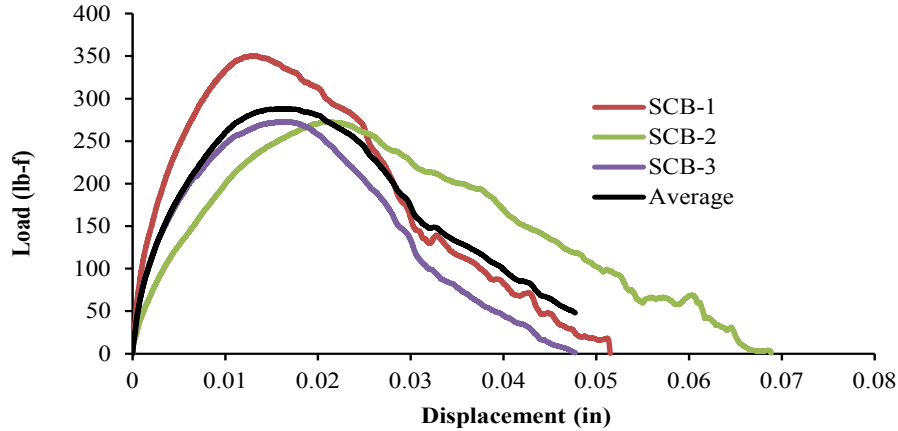
Sample#	Fracture Energy		Tensile Str.			FE Index
	(J/m ²)	(lb-in/in ²)	(psi)	(Mpa)	Strain (mm/mm)	
SCB1	152	0.869	203	1.401	0.0099	1.5340
SCB2	201	1.151	180	1.24	0.0089	2.0626
SCB3	170	0.973	193	1.329	0.0071	1.2964
Average	175	0.997	192	1.324	0.0086	1.6310
COV	14.3%	14.3%	6.1%	6.1%	16.5%	24.0%

Figure C-17. SCB Testing – Chico Type D (4.5% AC) Mix.



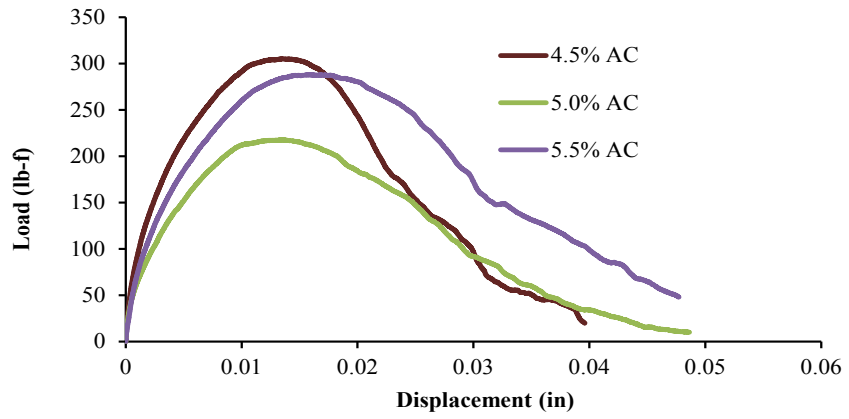
Sample#	Fracture Energy		Tensile Str.			FE Index
	(J/m ²)	(lb-in/in ²)	(psi)	(Mpa)	Strain (mm/mm)	
SCB1	146	0.834	145	1.001	0.0100	2.0897
SCB2	125	0.715	136	0.94	0.0064	1.2216
SCB3	157	0.897	137	0.946	0.0105	2.4879
Average	143	0.816	140	0.962	0.0090	1.9331
COV	11.3%	11.3%	3.5%	3.5%	24.8%	33.5%

Figure C-18. SCB Testing – Chico Type D (5.0% AC) Mix.



Sample#	Fracture Energy		Tensile Str.			FE Index
	(J/m ²)	(lb-in/in ²)	(psi)	(Mpa)	Strain (mm/mm)	
SCB1	241	1.375	217	1.499	0.0085	1.9625
SCB2	256	1.460	169	1.167	0.0137	4.2853
SCB3	177	1.014	169	1.167	0.0112	2.4378
Average	225	1.283	185	1.278	0.0111	2.8952
COV	18.5%	18.5%	15.0%	15.0%	23.1%	42.4%

Figure C-19. SCB Testing – Chico Type D (5.5% AC) Mix.



AC	Fracture Energy		Tensile Str.			<i>FE Index</i>
	(J/m ²)	(lb-in/in ²)	(psi)	(Mpa)	Strain (mm/mm)	
4.5%	175	0.997	192	1.324	0.0086	1.63
5.0%	143	0.816	140	0.962	0.0090	1.93
5.5%	225	1.283	185	1.278	0.0111	2.90

Figure C-20. SCB Testing – Chico Type D Mix – AC Variation Summary.

APPENDIX D: ADVANCED OT DATA ANALYSIS METHODS USING ENERGY CONCEPT AND NUMERICAL MODELING

The methodology that will be described in this chapter is a novel approach to analyze the OT test results based on the linear viscoelasticity and fracture mechanics principles. The methodology uses a Finite Element code integrated with a user-defined material to find the strain profiles above the tip of the crack for both laboratory and aged specimen.

HMA layers under different repeated loading and rest periods experience both fatigue and healing processes. The tests are costly and time-consuming, and the results are highly variable. Current methods of evaluating these phenomena using the OT rely on counting the number of load repetitions until the crack breaks through the sample.

This research provides a novel analysis method based on the viscoelastic fracture mechanics and Finite Element modeling to predict the actual crack growth rate in asphalt mixes both in the laboratory compacted and field samples using the Overlay Tester. Furthermore, the new method uses viscoelastic fracture mechanics principles to find the fracture and healing properties of the asphalt mixes. The resulting test is fast, less costly and more repeatable than the previous methods using the Overlay Tester.

Testing lab compacted specimens have determined and improved the precision of the test method. The COV of the laboratory compacted mixture undamaged properties are comparable with the test results.

THE BACKGROUND OF THE OT DATA ANALYSIS METHODS

Asphalt layers experience the repeated loading, unloading as well as the rest periods because of the traffic and environmental conditions. The crack propagation from the bottom to the top and vice versa is a prominent distress in the asphalt layers. Fortunately, each one of these phenomena can be well explained by mechanistic-based models and various research projects have been conducted to develop and use such models.

Different approaches have been used to characterize the crack initiation and propagation in asphalt layers, namely, conventional fatigue crack analysis ([Harvey and Monismith, 1993](#), [Ramsamooj, 1991](#), [Tayebali et al., 1996](#)), continuum damage mechanics, and fracture mechanics.

The traditional tests to measure the fatigue cracking susceptibility of mixes such as the four-point bending beam test, are very expensive and time-consuming (Kallas and Puzinauskas, 1971, Ramsamooj, 1991, Zhu et al., 2009)

The continuum damage mechanics approach basically states that the micro structure of materials changes with deformations caused by external loadings without focusing on the crack initiation and propagation. Subsequently, the micro damage process results in the loss in material properties such as stiffness. Various models have been developed to explain these phenomena in different materials including some recent studies in HMA (Abu Al-Rub et al., 2010, Christensen Jr. et al., 2005, Darabi et al., 2011, Wen and Bahia, 2009, Zhang and Huang, 2010, Zhao and Kim, 2003).

This study is based on viscoelastic fracture mechanics. The fracture mechanics approach focuses directly on the crack geometry, initiation, and propagation mechanisms. This approach is based on Paris's law for crack propagation theory. However, the stress intensity factor in Paris's law applies only to elastic materials (Paris and Erdogan, 1963).

In viscoelastic media, the generalized J-integral based on the correspondence principle and pseudo strain energy concepts proposed by Schapery, is a powerful principle to address the crack propagation process (Cleveland et al., 2003, Kuai et al., 2009, Schapery, 1984, Schapery, 1975).

Asphalt like other viscoelastic materials restores part of its strength by healing. The study of the fracture or damage properties without considering the healing is incomplete and results in an underestimation of the number of load cycles to reach failure. Various research studies focused on the self-healing in different materials namely polymers and asphalt in recent years (Abu Al-Rub et al., 2010, Brown et al., 2002, Chowdary and Krishnan, 2006, Kessler, 2007, Kim and Little, 1989, Schapery, 1989, Shen et al., 2010, Yufeng and Wanlin, 2006).

The Texas OT is a capable multipurpose test apparatus. The OT was originally developed to determine the reflection cracking resistance of hot mix asphalt mixtures used in overlays over concrete joints (Germann and Lytton, 1979). This machine also has been used to study the behavior of the geosynthetic fabrics and grids inside the asphalt layers based on fracture mechanics concepts (Cleveland et al., 2003, Cleveland et al., 2002).

As shown in Figure D-1, the OT machine consists of two steel plates. One plate is fixed and the other can move back and forth to apply the desired repeating displacement. This machine

has been modified several times since its first prototype (Germann and Lytton, 1979) and the latest version is more precise and portable. In this later model, specimens with the standard size of 150 mm long, 75 mm wide and 38 mm high can be tested. These specimens with this size can be easily cut from the cylindrical mixes that the Gyratory compactor has compacted in the laboratory or cores taken from the field. Still in the same Figure D-1, the specimen is glued on the aluminum plates and subsequently the plates are mounted and fixed on the machine's steel platforms using pins (Zhou and Scullion, 2005). The data acquisition system records the time, load, opening displacement, and temperature during the OT test. Figure D-2 shows the OT machine during the test.

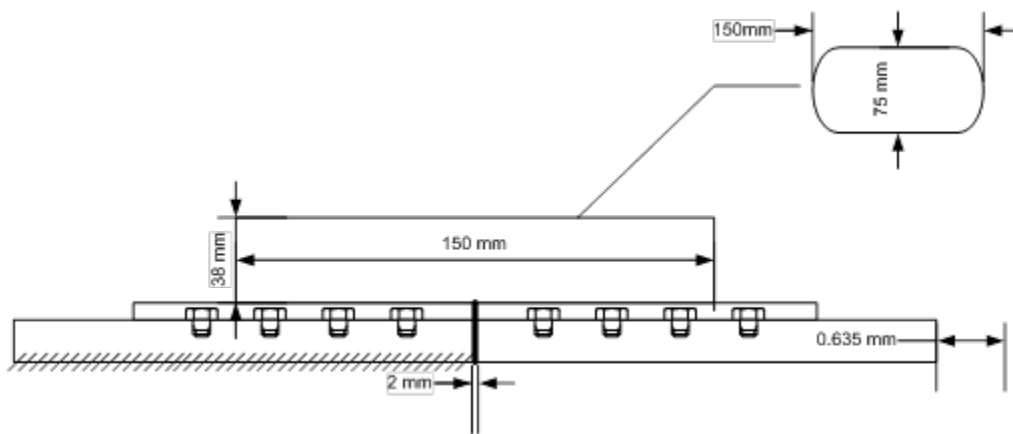


Figure D- 1. The OT Test Setup.

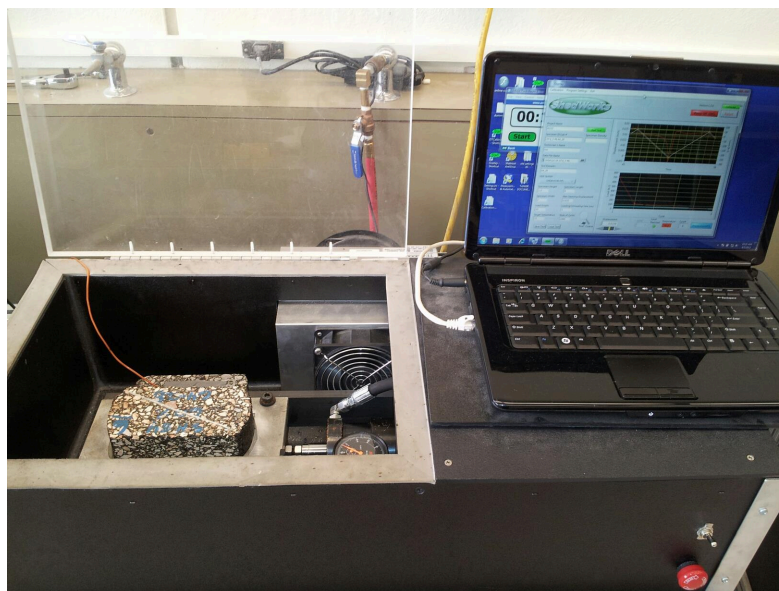


Figure D-2. The OT Machine during Testing.

The simplicity of the test led to its use as an index test for fatigue because in both reflection cracking and fatigue, the active mechanism is crack growth. The OT was selected to be used together with the Hamburg Wheel Tracking Test (HWTT) to establish a balanced asphalt mix design procedure to account for both fatigue and rutting distresses (Zhou et al., 2007). This test was expected to be a good surrogate for the expensive and time-consuming beam fatigue tests (Kallas and Puzinauskas, 1971, Ramsamooj, 1991, Zhu et al., 2009).

The current OT analysis method relies on counting the load cycles to the failure and the failure criterion is satisfied when the initial maximum load is reduced by 93 percent. The resulting count on companion samples has proven to give a large variability. Especially, this method does not work well with coarse graded mixes and the COV is over 30 percent (Walubita et al., 2009).

The test method modifications and sample preparation techniques that TTI researchers conducted have reduced the variability of the results. This variability has several causes, all of which will be explained at the conclusion of this study. The study reported in this research was undertaken to determine the cause of the high degree of variability and to develop methods of using OT data that are more consistent and precise. This has been accomplished through the application of fracture mechanics.

This study uses a novel method to analyze the OT output to achieve accurate crack growth prediction using the principles of viscoelastic fracture mechanics and finite element (FE) simulation (Schapery, 1975). The FE simulation of the test has been developed and it was a key to understanding the energy release pattern as the crack grows.

Research has been conducted recently at TTI in order to find Paris's law constants. In this research, the crack length in each load cycle is measured with a Digital Correlation System (DIC). The results of this work indicated that the crack grows rapidly during the first few load cycles and after that the rate of growth decreases substantially with time (Jacobs, 1995, T. O. Medani and Molenaar, 2000, Zhou et al., 2007, Zhou and Scullion, 2006).

In this research, the pseudo strain energy concept and Paris's law were tailored according to the OT test conditions to obtain fracture and healing properties of the asphalt mixes in the same test. By applying this methodology, the OT can be used not only to obtain the number of load cycles to reach a standard crack length, but also the fracture and healing properties of the asphalt mixes for different quality assurance and performance prediction purposes.

This procedure has been extended for use with the field-aged specimens with a stiffness gradient rather than uniform modulus with depth. The field layers can be tested for both top-down and bottom-up fatigue cracking by placing the specimen in upright or inverted positions. However, testing aged asphalt layers requires specific analytical and test procedures due to the stiffness gradient and the high brittleness of the specimens. For instance, the opening size should be reduced in field-aged specimens because the field-aged layers are very brittle.

This study will describe a testing protocol that includes the extraction of the field cores, Direct Tension (DT) test, and OT test to calculate the viscoelastic properties of the field-aged asphalt concrete mixtures. The aged asphalt concrete layer can be categorized as a Functionally Graded Material (FGM) due to its stiffness gradient profile. The response of these materials to different loading and temperature scenarios have been studied in various research projects (Fang et al., 2007, Huang et al., 2005, Mukherjee and Paulino, 2003, Wu and Luo, 2011). A user-defined material subroutine (UMAT) in the finite element software ABAQUS was developed to simulate the response of the aged asphalt layers as functionally graded materials under repeated loadings. The FE program output is used in a constitutive model to predict the crack growth in a field asphalt layer under repeated loading. The FE model together with constitutive fracture mechanics-based model is able to estimate the crack growth rate, fracture properties, and healing properties of the field-aged asphalt mixtures.

METHODOLOGY

The methodology will be described in this research will include three main modules:

- Finite Element Model to find the strain profiles above the crack tip.
- The crack growth analysis module.
- The fracture and healing characterization module.

Figure D-3 illustrates the three main modules of the methodology. There is also some modification in the test procedure. E_1 and m_1 are the undamaged tensile mixture properties that regression analysis determines.

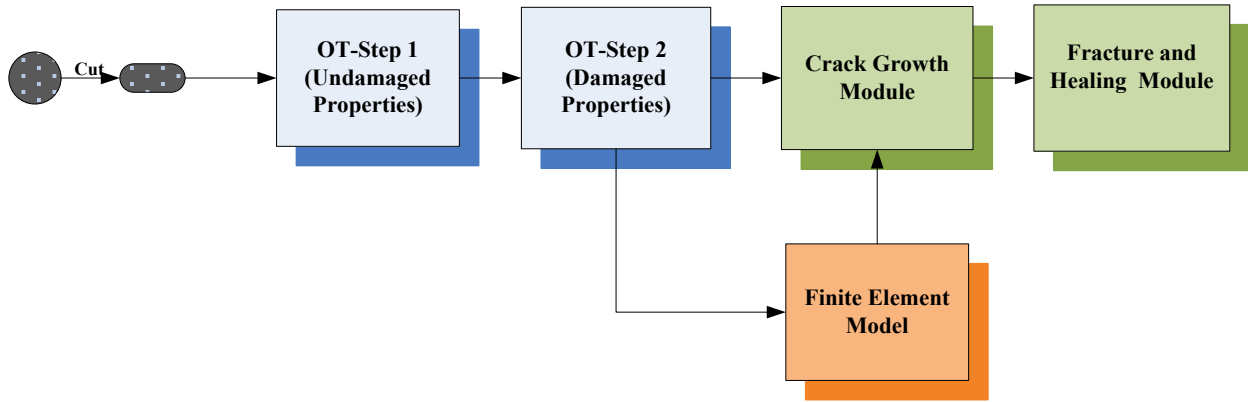


Figure D- 3. The Analysis of the Laboratory Compacted Specimen via OT Test.

Finite Element Duplication of the Test Boundary Conditions

As part of this task, the test procedure was simulated using ABAQUS. The test is modeled in a 2D format for an elastic material. It was assumed that Poisson’s ratio is 0.3 for modeling purposes.

Figure D-4 shows the boundary conditions used in the FE model. As shown in Figure D-3, the left portion of the specimen is fixed and the right portion moves back and forth in the horizontal direction. The crack initiates from the bottom of the specimen above the opening and closing joint, and grows vertically to the top.

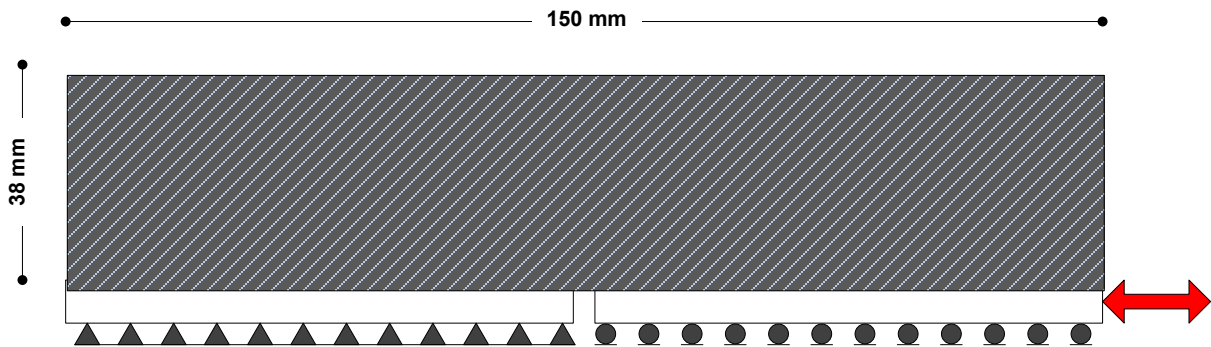


Figure D-4. The Boundary Conditions of the FE Model.

The crack with different lengths was modeled and the contour integral method was used to define the crack tip function. Figure D-5 shows the deformed specimen and the corresponding principal stress distribution in the specimen when the crack length is 15.875 mm and the opening is 0.635 mm.

Since the test is displacement controlled, the strain profiles above the tip of the crack remain the same, regardless of the magnitude of the elastic modulus. This information was used to predict the crack length in each cycle, as the strain profiles above the tip of the crack depend only on the maximum displacement magnitude.

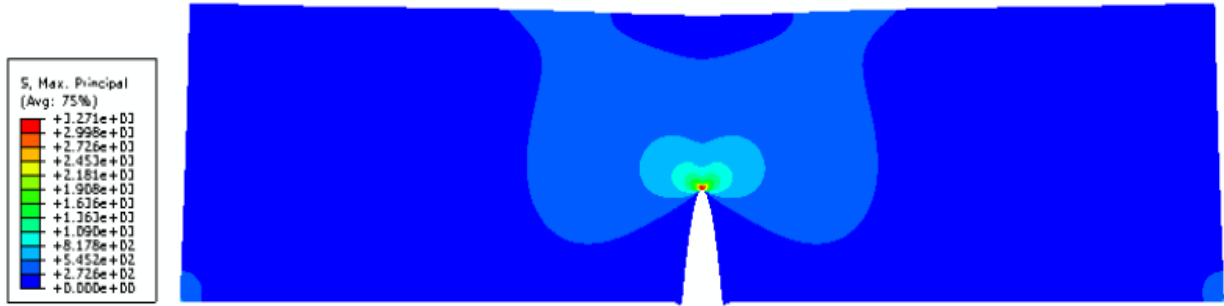


Figure D-5. The Deformed Specimen and the Corresponding Principal Stress Distribution.

The computed strain profiles for four different crack lengths are plotted against specimen depth in [Figure D-6](#). As seen in [Figure D-6](#), as the crack advances, the area under the strain profiles in the intact material decreases. In this study, the change of the area under the strain curve at different crack lengths was used to estimate the actual crack length in each load cycle. In specimens thicker than 40 mm, the strain in the upper 10 mm becomes compressive.

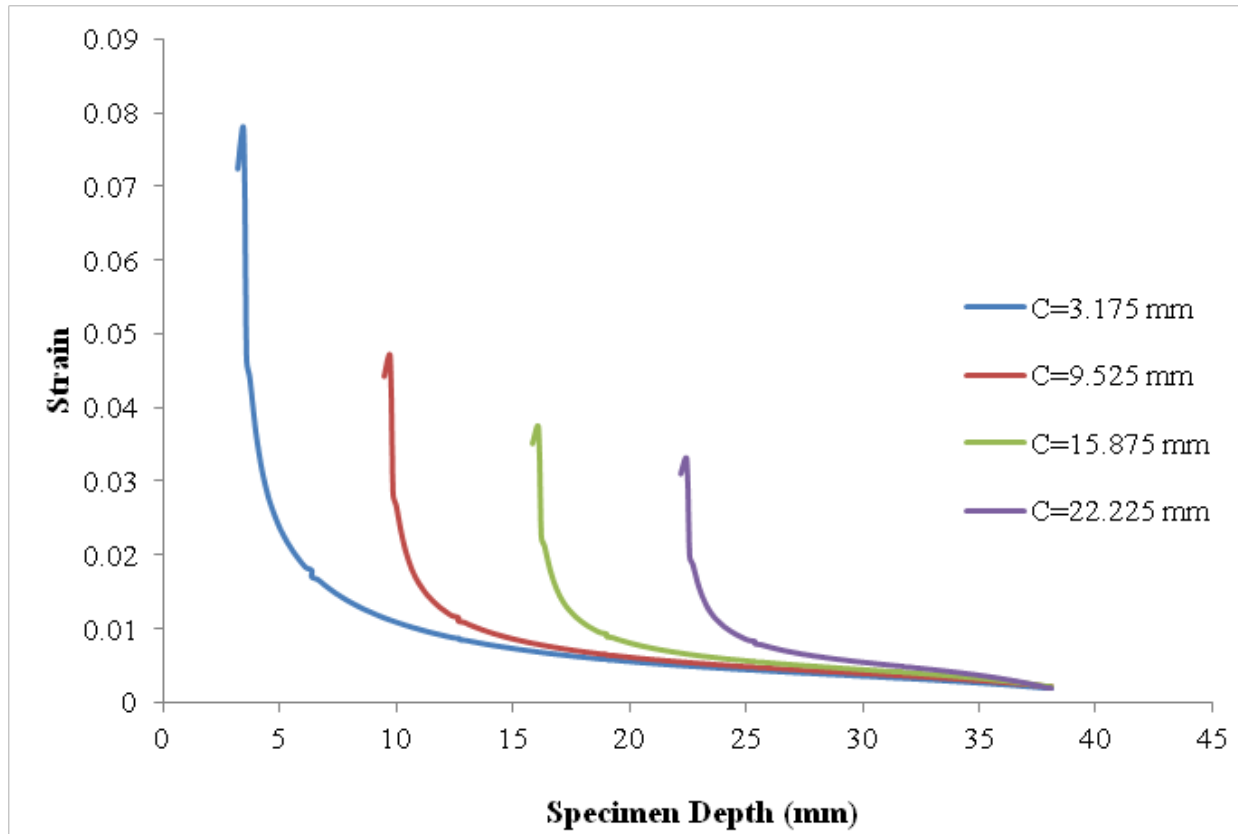


Figure D-6. The Strain Profiles above the Tip Of the Crack at Different Crack Lengths. (C = Crack Length)

The Effect of the Displacement (Opening) and the Thickness on the Test Results

The counting the number of the load cycles to failure has been used to compare the asphalt mixtures; however, users have reported substantial variability in this method. This may happen for different reasons. A sensitivity analysis was conducted to compare the strain profile contours above the crack. The results showed that in the specimens thicker than 38 mm (1.5 inches) the upper parts will be in the compression or very small tensile strains; therefore, as a crack enters these low tensile strain or compressive zones, the crack growth rate decreases significantly.

Figure D-7 shows the strain profiles above two specimens with the same crack length and different thicknesses. As shown in Figure D-7, the thicker specimen has a compressive zone at the top of the sample. This zone delays the crack growth. Unlike the method of counting cycles to failure, the methodology that is described in this research estimates the crack growth function

as it varies with the load cycles that, in turn, is already related to the strain profiles above the crack tip. Therefore, the problem of the high cycle count variability only occurs in the case in which the load cycles are counted to failure.

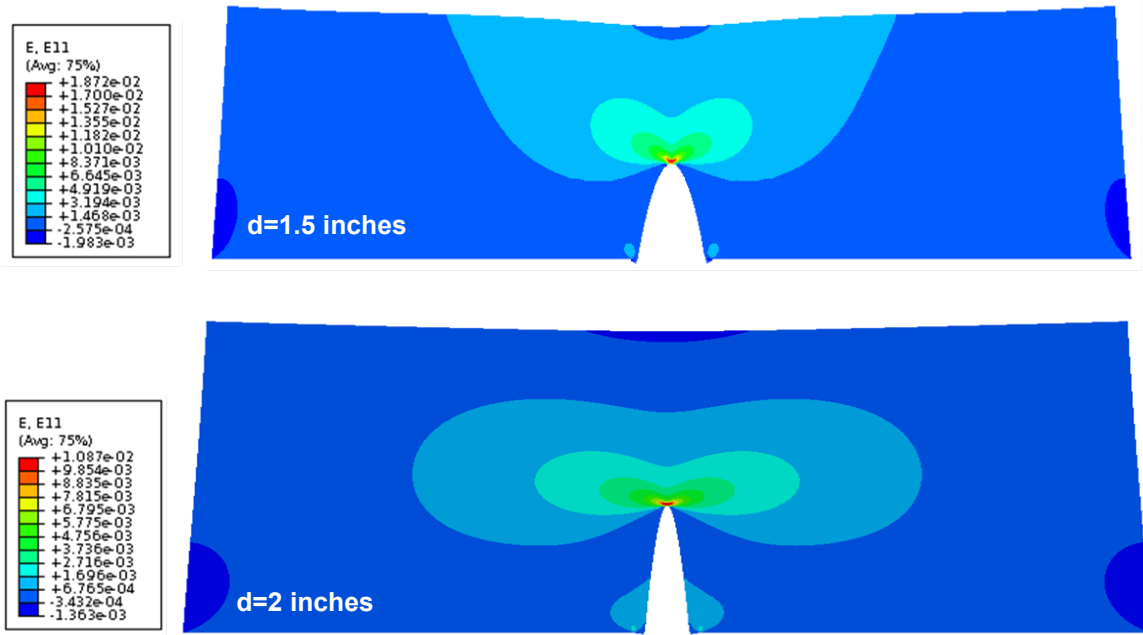
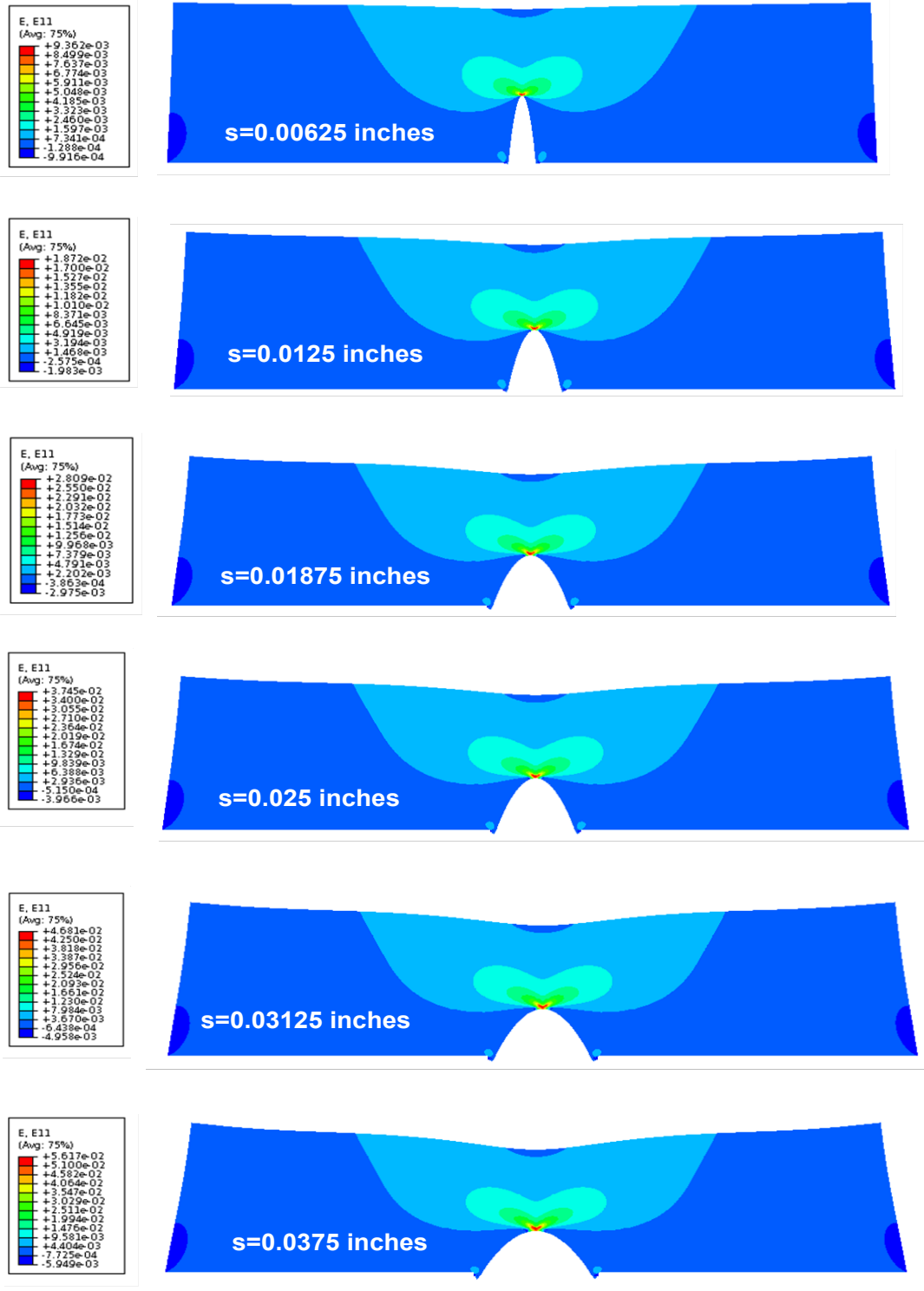


Figure D-7. The Effect of the Specimen Thickness on the Strain Contours above the Crack. (d = sample thickness)

Additionally, the effect of the destructive displacement opening is not very significant in changing the size of the compressive zone above the crack. As expected, the larger displacement results in a larger compressive and tensile strains; unlike the thickness, however, the shape of the strain contours above the crack remains the same. [Figure D-8](#) shows the strain profiles above the crack for different maximum openings.



**Figure D-8. The Effect of the Gap Opening on the Strain Contours above the Crack Tip.
(s = Gap Opening)**

The Stress Intensity Factor and the J-integral

The FE simulation results show that the energy release rate decreases as the crack grows. In order to understand the crack propagation process in the OT test, the stress intensity factor and J-integral were calculated with time as the crack grows. The FE simulation was used to obtain the changes in the stress intensity factor and J-integral against crack length. The crack in the OT test is a Mode I tensile crack. The size of the stress intensity factor, K_I controls the crack growth rate, which is defined in Equation D-1 as:

$$K_I = \sigma\sqrt{\pi C} \quad (D-1)$$

where σ is stress and C is the half crack length.

Figure D-9 shows that the stress intensity factor for Mode I reduces significantly as the crack grows.

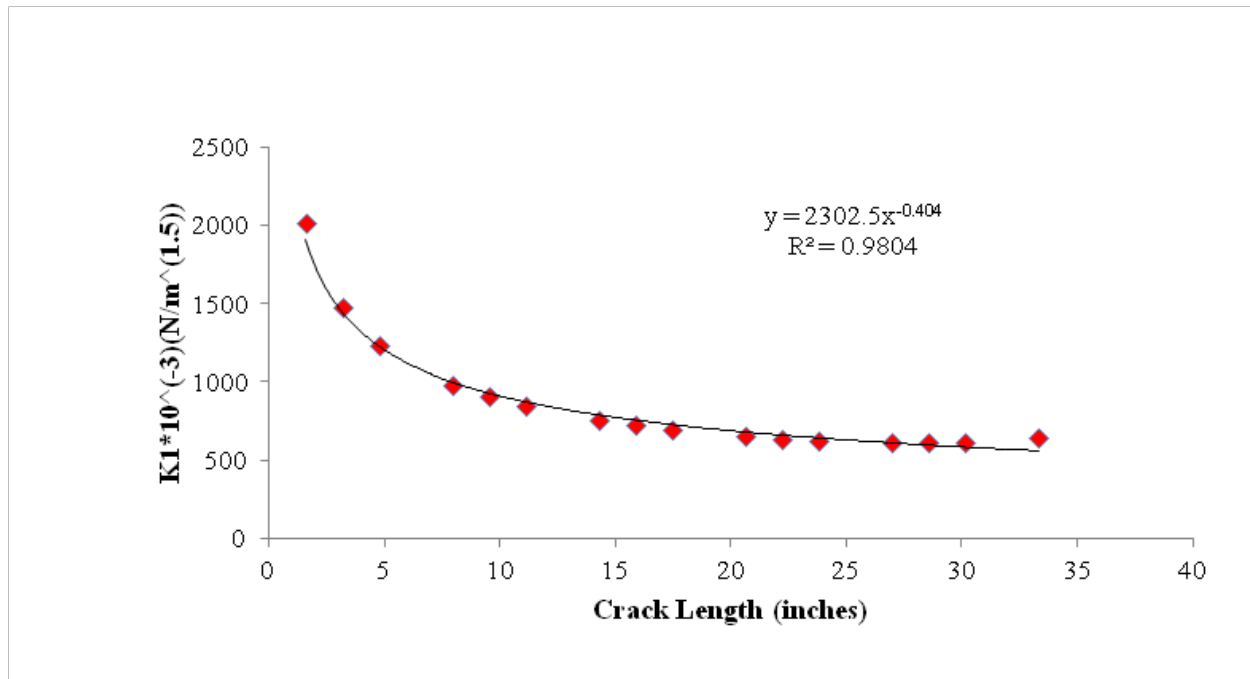


Figure D-9. The Stress Intensity Factor Versus Crack Length.

The same trend can be seen in Figure D-10 for the J-integral (strain energy release rate), which is related to fracture toughness under Mode I loading at the tip of the crack (Yoda, 1980).

$$J_I = K_I^2 \left(\frac{1-\nu^2}{E} \right) \quad (D-2)$$

where K_I , ν and E are the Stress Intensity Factor, Poisson's ratio, and Young's modulus, respectively.

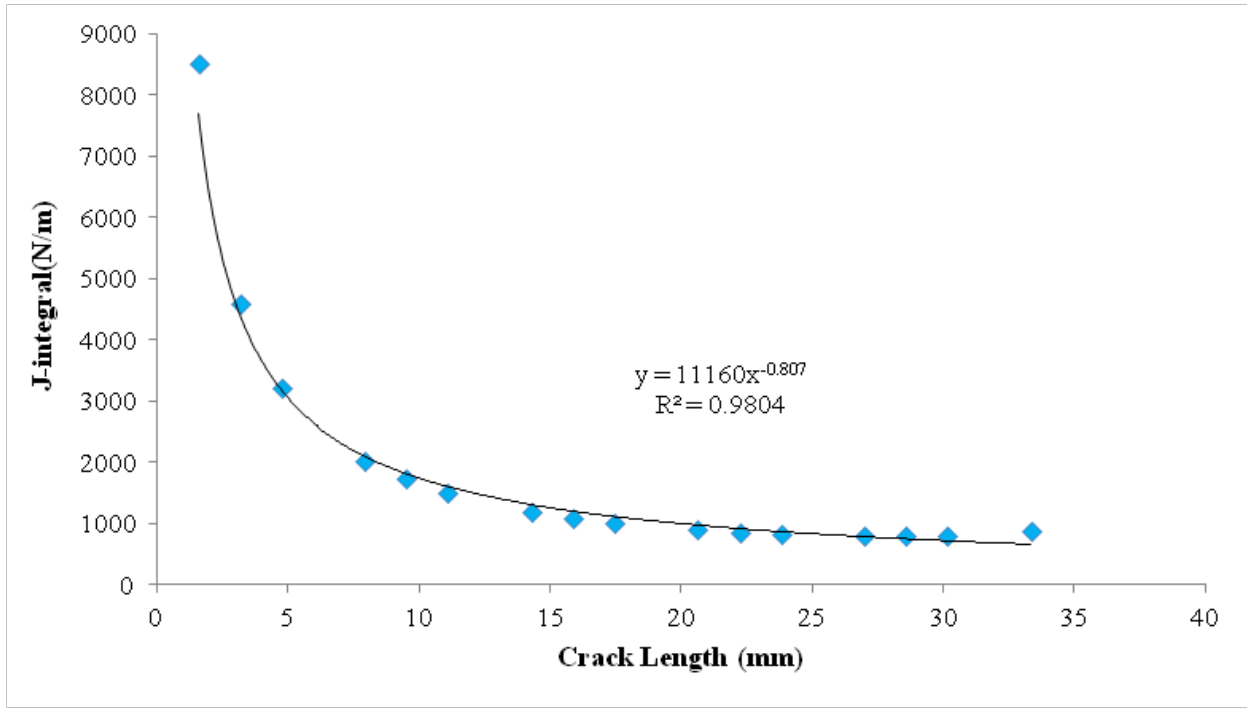


Figure D-10. The J-Integral versus Crack Length.

Development of the Crack Growth Estimation Model

As mentioned previously, one of the objectives of this research was to develop a method of predicting the crack growth rate with load cycles. The convolution integral was used to represent the time dependent properties of the asphalt.

The time-dependent stress in a linear viscoelastic material can be calculated using [Equation D-3](#):

$$\sigma(t) = \int_0^t E(t-\tau) \frac{d\varepsilon(\tau)}{d\tau} dt \quad (D-3)$$

where σ and ε are the Linear Visco Elastic (LVE) stress and strain, respectively; t designates a specific time; and τ is a time-integration variable.

As the outputs collected by the OT machine are load, displacement, and time, [Equation D-3](#) should be converted to a load-displacement equation. [Equation D-4](#) does this transformation.

$$\sigma(t) = \frac{P_{LVE}(t)}{A} \quad (D-4)$$

where $P_{LVE}(t)$ is the measured viscoelastic force and A is the intact area (the area above the crack tip).

The first part of the test is designed to obtain the undamaged properties of the asphalt mixes. The displacements in the nondestructive test are limited to ensure that there is no crack growth.

The relaxation modulus is given by the form shown in [Equation D-5](#).

$$E(t - \tau) = E_1 \cdot (t - \tau)^{m_1} \quad (D-5)$$

where E_1 and m_1 are the undamaged tensile mixture properties, which are determined by regression analysis. The loading pattern for this test is shown in [Figure D-11](#).

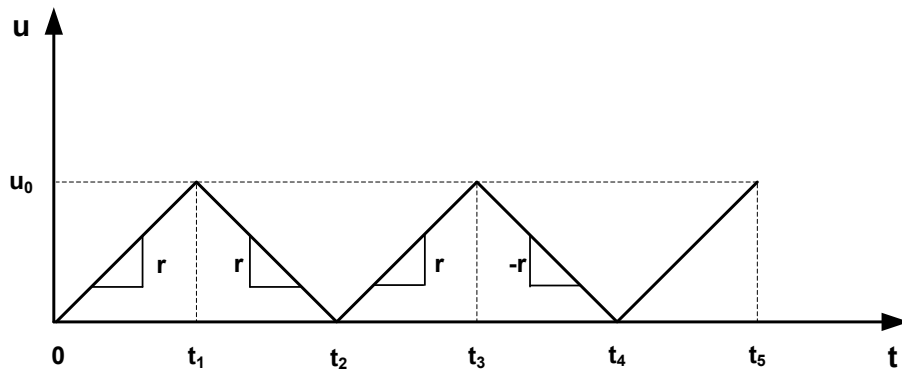


Figure D-11. The Loading Pattern in the OT Test.

The data from the first load cycle in the nondestructive test was used to obtain the undamaged properties. First the percentage of the maximum opening at the time $t < t_1$ is calculated using [Equation D-6](#):

$$\frac{u(t)}{u_0} = \frac{t}{t_1} \quad (D-6)$$

where $u(t)$ is the displacement at time t and u_0 is the maximum displacement.

The elastic strain at time $t < t_1$ and opening u for the no-crack condition are shown in [Equation D-7](#).

$$\varepsilon(c = 0, u(t), z) = \varepsilon(c = 0, u_0, z) \frac{t^2}{t_1^2} \quad (D-7)$$

where $\varepsilon(c=0, u(t), z)$ is elastic strain at time t and depth z ; and $\varepsilon(c=0, u_0, z)$ is the elastic strain at depth z at the maximum displacement. The viscoelastic force is calculated using [Equations 8-3 and 8-4](#). The time-dependent strain and the relaxation modulus values in the convolution integral are replaced by the corresponding values from [Equations D-7 and D-5](#), respectively. [Equation D-8](#) shows the final magnitude of the viscoelastic force. It should be noted the $s(c=0)$ in [Equation D-8](#) is the integration of the strain profile curve over the full depth of the specimen. This term is calculated with the FE model for the no-crack condition using the nondestructive phase's displacement.

$$P_{LVE}(t) = \frac{2bE_1}{t_1^2} s(c=0) \frac{t^{2-m_1}}{(2-m_1)(1-m_1)} \quad (D-8)$$

in which $P_{LVE}(t)$ is measured by the load cell as a function of time and $s(c=0)$ is calculated using the integrated strain profiles that were calculated with the FE model. The unknown parameters in [Equation D-8](#), E_1 and m_1 , are calculated using a linear regression method.

Subsequently, the viscoelastic force for the destructive cycles is calculated to find the actual crack length in each loading cycle.

[Equation D-9](#) applies to the destructive load cycles.

$$\varepsilon(z, t) = \frac{rt}{u_0} \varepsilon(z) \quad (D-9)$$

where t is a specific time and r is the slope of the applied displacement.

The convolution integral is solved for both loading and unloading intervals. The maximum tension (loading) and compression (unloading) viscoelastic forces are shown in [Equations D-10 and D-11](#), respectively.

$$\max .P_{LVE}(z=c) = \frac{E_1 b t^{1-m_1}}{(1-m_1)t_1} s(c) \quad 0 < t < t_1 \quad (D-10)$$

$$\max .P_{LVE}(z=c) = bs(c) \frac{E_1 t^{1-m_1}}{(1-m_1)t_1} - 2bs(c) \frac{E_1 (t-t_1)^{1-m_1}}{(1-m_1)t_1} \quad t_1 < t < 2t_1 \quad (D-11)$$

where $\max .P_{LVE}(z=c)$ is the measured maximum viscoelastic force within the specified time interval, b is the width of specimen, and $s(c)$ is the area under the strain profile above the tip of the crack length (c).

Figure D-12 shows the area under strain profiles above the tip of the crack for different crack lengths for the test displacement.

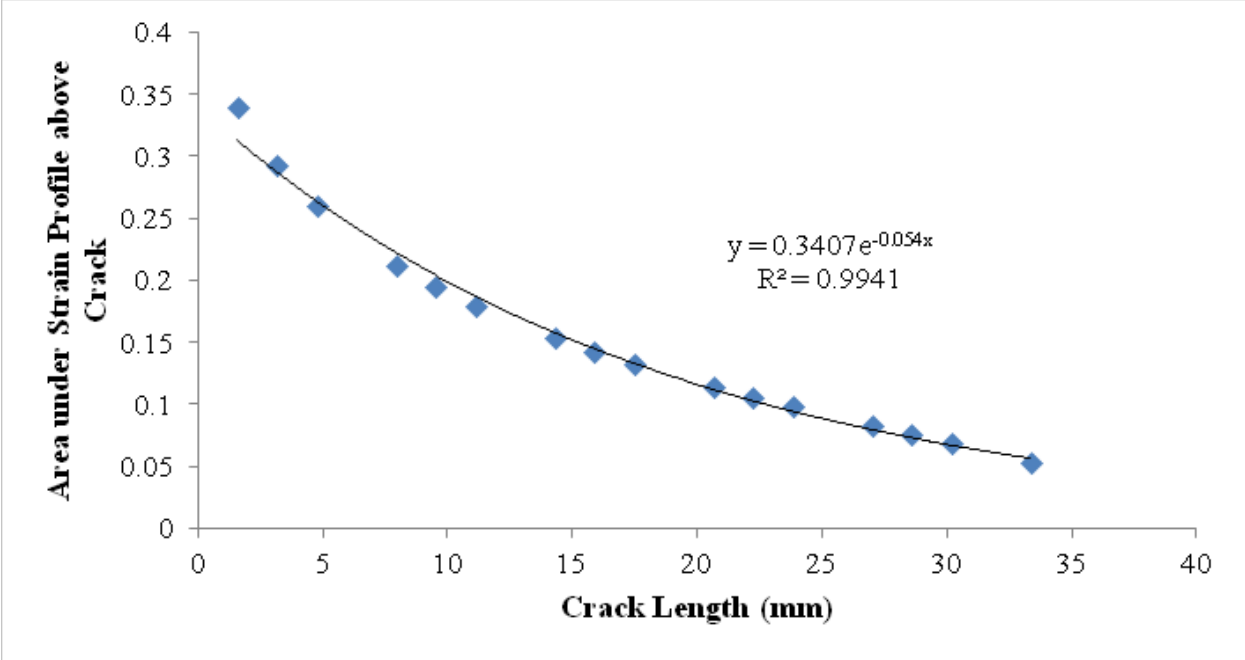


Figure D-12. Area under Strain Profiles above the Tip of the Crack.

To find the actual crack length in each cycle, the healing of the crack when the displacement is forced back to zero must be considered. The high magnitude of the compressive force in each cycle is responsible for the healing that occurs in a very short time. As seen in Figure D-12, the value of $s(c)$ decreases as the crack grows. Healing actually reduces the crack size, and as a result, the area under the strain profile above the tip of the crack increases. To include the healing effect, the areas under the strain profiles in tension and compression were calculated from Equations D-10 and D-11 and summed for each cycle. The resultant $s(c)$ was applied to the $s(c)$ versus crack length curve shown in Figure D-12 to find the corresponding crack length. Table D-1 shows the systematic procedure to find the actual crack length in each load cycle.

Table D-1. Systematic Procedure to Find the Actual Crack Length in OT Test.

Step#	Procedure
1	Calculate the area under strain profiles for no-crack condition using FE model
2	Calculate the area under strain profile for various crack lengths and estimate the function
3	Conduct the undamaging test, 10 cycles with maximum opening of 0.05mm
4	Conduct the damaging test, 150 cycles with opening of 0.635 mm
5	Use the load-time data, Step 3 and Step 1 output to find the E_1 and m_1 values in Equation 8
6	Find $(s_t(c))_i$ and $(s_c(c))_i$ for each cycle using outputs of Step 4, 5, and Equations 7-10 and 7-11
7	Find $(s(c)_{total})_i = (s_t(c))_i + (s_c(c))_{i-1}$ to consider the effect of healing occurs in each cycle
8	Use the $s(c)_{total}$ and step 2 output function to find the crack length in this cycle
9	Repeat steps 6 to 8 for all cycles to find the crack length in each cycle
10	Fit the power function of the crack length versus the load cycles

Fracture and Healing Properties Estimation

As discussed before, each loading cycle contains both fracture and healing phases and the test results show that a large amount of healing occurs during each displacement cycle. The fracture and healing properties can be determined from the OT test outputs using the dissipated pseudo work principle very efficiently. The pseudo displacement is calculated by [Equation D-12](#).

$$U_r(t) = \frac{P_{LVE}(t)}{k_r} \quad (D-12)$$

where $P_{LVE}(t)$ is the linear viscoelastic force and k_r is the reference stiffness, which is the value of the maximum load in the first load cycle divided by the maximum opening. [Figure 8-13](#) shows the pseudo displacement plotted against the measured load in a specific load cycle. The dissipated pseudo work area under the tensile loading part is related to the crack growth and the dissipated work area under the compressive loading part is related to the healing that occurs in each load cycle.

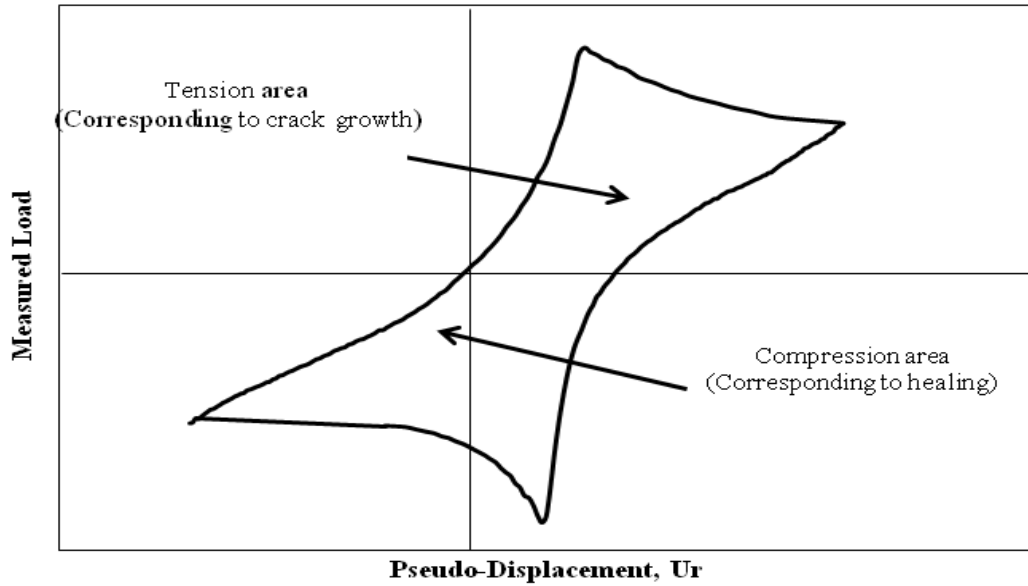


Figure D-13. Pseudo-Displacement versus the Measured Visco-Elastic Load.

By obtaining the crack length and dissipated pseudo work as functions of the displacement cycles, the pseudo J-integral is calculated using Equation D-13 for both healing and fracturing modes.

$$J_R = \frac{\frac{\partial W_{R1}(N)}{\partial N}}{\frac{\partial(c.s.a)}{\partial N}} \quad (D-13)$$

where the J_R is the pseudo J-integral, N is the number of load cycles, $\frac{\partial W_{R1}(N)}{\partial N}$ is the rate of change of dissipated pseudo work and $\frac{\partial(c.s.a)}{\partial N}$ is the rate of change of the crack surface area.

The conventional form of Paris's law (Paris and Erdogan, 1963) shown in Equation D-14, is commonly used to predict the crack growth response of different materials (Atzori et al., 2008, Bilir, 1990, Pugno et al., 2006).

$$\frac{dC(N)}{dN} = A(J_R)^n \quad (D-14)$$

where $C(N)$ is the crack length on the N^{th} load repetition.

The conventional version of Paris' law does not give realistic results because the energy release rate decreases as the crack grows in the OT test. Therefore, the format shown in [Equations 8-15 and 8-16](#) is used to determine the Paris's law's fracture and healing coefficients, respectively.

$$\frac{dC(N)}{d(N)} = A \left[\frac{WR_1(N)}{c.s.a} \right]^n \quad (\text{D-15})$$

$$\frac{dC(N)}{d(N)} = B \left[\frac{WR_1(N)}{c.s.a} \right]^m \quad (\text{D-16})$$

where:

$$c.s.a = 2bC(N) \quad (\text{D-17})$$

$$I = \frac{K_r}{K_n} \quad (\text{D-18})$$

For each cycle the areas under the tension and compression of pseudo work-load curves are calculated. Then the area is multiplied by the I factor, which is the ratio of the initial pseudo stiffness, K_r , divided by the damaged pseudo stiffness in the n^{th} load cycle. The corrected area is divided by the intact cross section to find the values of WR_t and WR_c in each cycle.

The power function is used to fit to the curves of WR_t and WR_c against load cycles. The resultant power functions together with the actual crack growth function are inserted into [Equations D-15 and D-16](#) to find the healing and fracture properties using regression analysis. [Equations D-19 and D-20](#) show the crack growth and the Pseudo-dissipated work functions, respectively. [Equations D-21 and D-22](#) are the results of the regression analysis for A and n . The same equations can be used to find the B and m values.

$$C = d \cdot N^e \quad (\text{D-19})$$

$$\frac{WR_1(N)}{2bC(N)} = a \cdot N^b \quad (\text{D-20})$$

$$n = \frac{e-1}{b} \quad (\text{D-21})$$

$$A = \frac{d \cdot e}{a^n} \quad (D-22)$$

Figures D-13 and D-14 show the change of WR_f and WR_c versus the load cycles. The area Pseudo-dissipated work decreases as the load cycles increase.

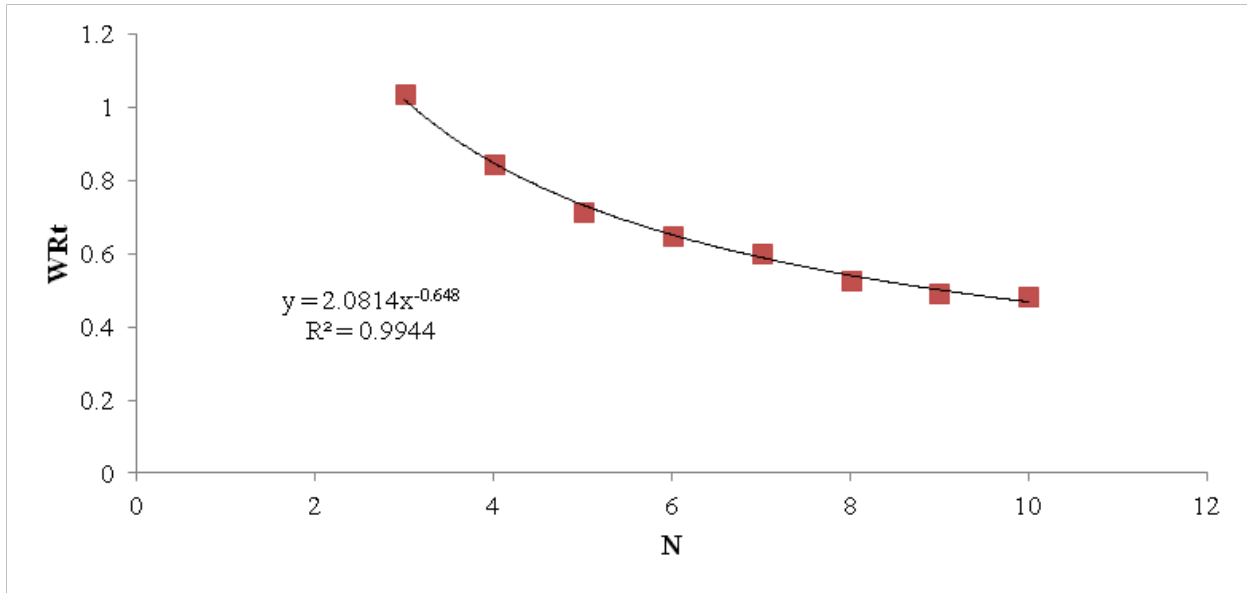


Figure D-14. The Fracture Pseudo Work Change against Load Cycles.

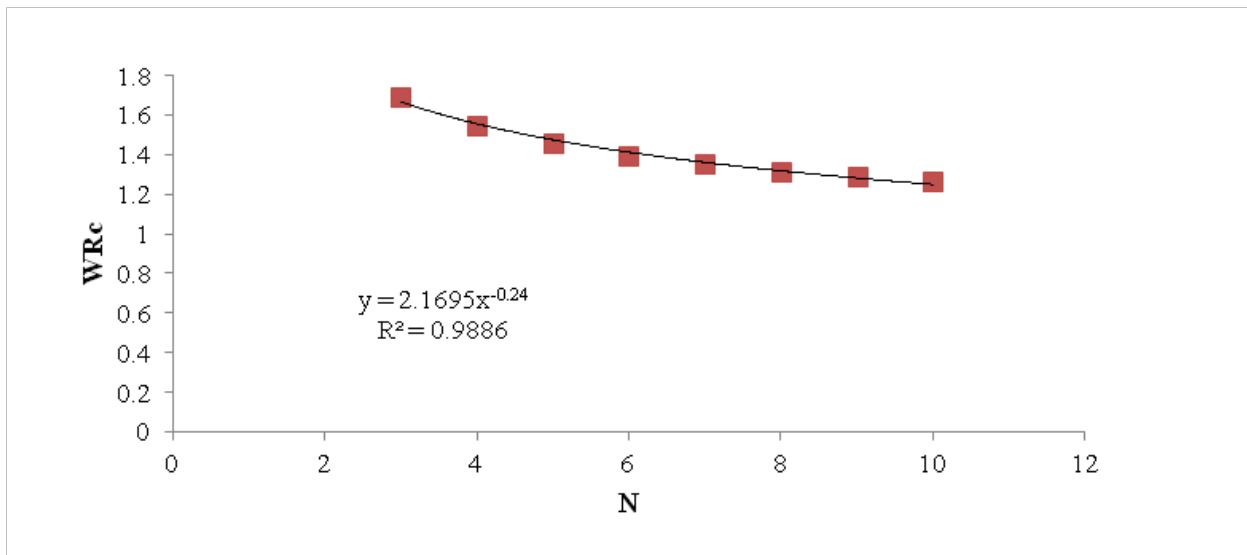


Figure D-15. The Healing Pseudo Work Change against Load Cycles.

Table D-2 illustrates the systematic procedure to determine the fracture and healing properties of the asphalt mix.

Table D-2. Systematic Procedure to Find Fracture and Healing Properties of the Asphalt Mix in OT Test.

Step#	Procedure
1	Calculate the viscoelastic force with time using the outputs of Table 1 procedure and Equations 10 and 11
2	Find the Pseudo displacement with time using step 1 and Equation 12
3	Sketch the Pseudo displacement against the measured load for each cycle
4	Calculate the areas under the compression and tension parts of each loop (Figure 9)
5	Correct the areas by multiplying the factor I from Equation 18
6	Divide the area by the area of the intact cross section to find WR_t and WR_c for each cycle
7	Repeat Steps 1 to 6 for all cycles
8	Sketch WR_t and WR_c against load cycles
9	Fit the power function to the WR_t and WR_c against load cycles' curves
10	Use Equations 15 and 16, the outputs of Step 9 and the actual crack growth curve to find fracture and healing coefficients using linear regression.

The Analysis Method for the Field Specimen

Part of the methodology described in this study is the result of the authors' previous research on measuring the stiffness gradient via DT test. The OT laboratory protocol has been tailored to be applied to the field samples. Figure D-16 shows the main modules of the methodology which are described in this paper. The procedure includes:

- Extraction of the three identical cores from the field.
- One core is used for X-ray CT (Computed Tomography)-scan, DSR (Dynamic Shear Rheometer), FTIR (Fourier Transform Infrared Spectroscopy) and binder extraction procedure, and the other two will go through DT and OT tests.
- The DT (Direct Tension) test outputs are analyzed using the stiffness gradient calculation module.

- The OT test and the stiffness gradient outcomes are plugged into the FGM (Functionally Graded Material) numerical module to calculate the crack growth pattern.
- The FGM output is used in another analytical module to calculate the healing and fracture properties of the AC.

The DT test is a nondestructive test; therefore, the test protocol can be completed with two replicates instead of three because the same sample can be used after the DT test for the binder extraction. The analytical and numerical models will be discussed in greater detail in the following sections.

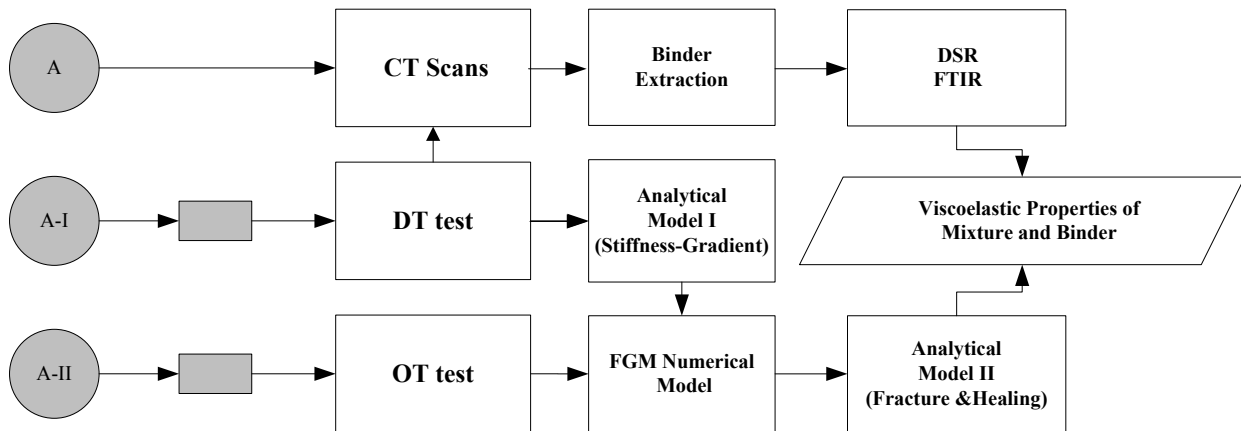


Figure D-16. General Procedure of the Test Protocol of the Field Samples.

Stiffness Gradient Calculation via Direct Tension Test

A rectangular specimen is cut from the field core used for the DT test, and steel end caps are glued to both ends of the rectangular specimen. Six Linear Variable Differential Transformers (LVDTs) are installed on each specimen, of which four LVDTs measure the strain at the surface, bottom, and the center of the asphalt layer; the other two record the horizontal strains at the surface and the bottom of the asphalt concrete layer. The rectangular field specimens oscillate under the monotonically increasing loads and these oscillations can be tracked in the strain outputs. The oscillations occur due to the effect of the feedback frequency and the stiffness gradient. The test is conducted at three different temperatures and each test

takes about three hours to complete, including the time required for the chamber to reach to the equilibrium temperature.

The analytical model assumes that the strain changes linearly with depth and the complex modulus of the asphalt layer changes from a higher modulus at the surface to a lower modulus at the bottom following a power function. Equations D-23 and D-24 show the stiffness gradient function and the relation between the modulus at the surface and the modulus at the bottom of the asphalt concrete layer in the field.

$$E(z) = E_d + (E_0 - E_d) \left(\frac{d-z}{d} \right)^n \quad (\text{D-23})$$

$$E_0 = k.E_d \quad (\text{D-24})$$

where $E(z)$ is the magnitude of the complex modulus at depth z ; E_0 and E_d are the magnitudes of the complex modulus at the surface and the bottom of the AC layer, respectively; n and k are model parameters; and d is the thickness of the specimen.

The analytical model uses a procedure that includes the signal processing to find the amplitude and frequency of the oscillations at the surface, center, and the bottom of the AC layer. Then, using an analytical method based on linear viscoelasticity and the correspondence principle, the complex modulus gradient function is calculated. For those who are not familiar with this approach, the detailed process has been described in a previously published paper (Koohi et al., 2011). This test and the corresponding analytical model estimates the stiffness gradient function with depth for the field specimen in the feedback frequency at three different temperatures.

Numerical Simulation of the Functionally Graded Material

- *The FGM model applications*

Asphalt layers in the field are usually stiffer at the surface because of more oxygen availability and more solar radiation at the surface. The stiffness gradient in the pavement layers usually is defined by dividing the pavement layer into smaller sublayers with each having a different modulus. This method increases the errors in the strain and stress calculations in the FE models (Dave et al., 2008).

A better approach would be the use of a FGM UMAT for which the user can define the gradient of the stiffness or any other properties as a continuous function. The accuracy of the gradient function can be defined by the user with the coarseness of the FE mesh because the UMAT is defined at the integration points in the mesh and the number of the integration points can be increased by using a finer mesh. A user-defined material subroutine (UMAT) in ABAQUS was developed to define the stiffness gradient with depth in the asphalt layer. The model has been developed for a general case, which includes three dimensional stress, plane stress, and plane strain cases. It can be used as a subroutine along with the various simulated field asphalt concrete models to define the aging, stiffness, and Poisson's ratio changes with the thickness of the asphalt concrete layer.

- *Strain profiles calculation above the crack tip using FE-FGM model*

As previously discussed, a power function was shown that fits well to the actual stiffness gradient profiles in the field-aged asphalt concrete layers. The developed FE simulation of the OT test for the laboratory compacted specimens was modified for the field specimens. The opening of the gap was decreased from 0.635 mm (0.025 inches) to 0.3175 mm (0.0125 inches) because aged field samples are more brittle than laboratory-made specimens, and therefore they break more easily under larger displacements.

The stiffness gradient function was plugged into the UMAT subroutine, and subsequently the OT simulation together with the subroutine was run via the Texas A&M supercomputer facility to find the strain profiles above the tip of the crack for different crack lengths. [Figure D-17](#) shows the strain profiles above the crack for a specimen with n value of 4.9 and k value of 1.42 where n is the power of the stiffness gradient function and k is the ratio between the surface and the bottom moduli. The magnitude of the stiffness modulus for this specimen is 6728 MPa and 4736 MPa at the surface and bottom of the layer, respectively. As shown in [Figure 8-17](#), some parts of the layer thickness are in compression, and when the crack enters this compressive zone, it will take more load cycles for the crack to grow through the thickness of the layer. This observation clearly explains the reason for the fact that counting the number of the load cycles to failure is not a reliable method to compare AC mixtures.

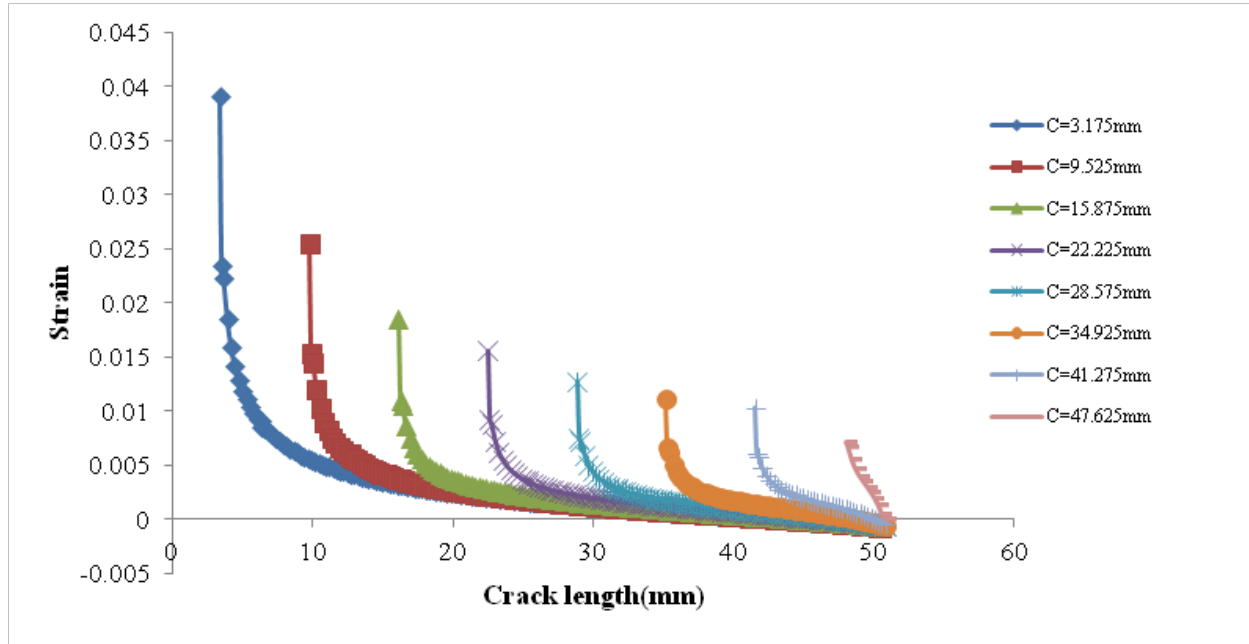


Figure D-17. Strain Profiles above the Crack Tip for Different Crack Lengths in the Field Specimen.

Sensitivity Analysis via FE-FGM Model

Additionally, a sensitivity analysis was conducted for a specific crack length in a field specimen to study the effect of the stiffness gradient function shape on different variables in the test. For this purpose, the model was run for a specimen with a crack length of 22.225 mm (0.875 inches) for different gradient curves by changing the n value but using a constant k value. The J-integral, stiffness profile, horizontal strain profile and the maximum principle stress contour are some of the outputs that were compared in this study.

Figure D-18 shows that as the n value increases, more of the specimen is in compression. An n value equal to zero represents a uniform stiffness profile or laboratory condition and the higher n values show greater stiffness gradient near the surface. The authors' experience with field specimens shows that the n value usually increases with age. This simulation confirms that a larger portion of the specimen will be under compression in highly aged specimens; therefore, even with very small openings during the OT test, the number of load cycles is not a reliable criterion to compare two specimens. Figure D-19 shows the change in the maximum principal stress contour for different stiffness profiles.

Figure D-20 shows that the J-integral at the tip of the crack decreases for the various stiffness profiles as the n value increases. The J-integral decreases as the stiffness gradient near

the surface of the AC layer increases. This means that the available energy for the crack to grow in the specimens with a sharper stiffness gradient near the surface is less than that for the less aged specimens.

As previously discussed, the results of the stiffness gradient model are plugged into the FGM numerical model to find the strain profiles above the crack for various crack lengths in the aged field specimen. After that, a replicate specimen is tested with the OT and the data are analyzed using the fracture and healing module along with the outputs from the FE program.

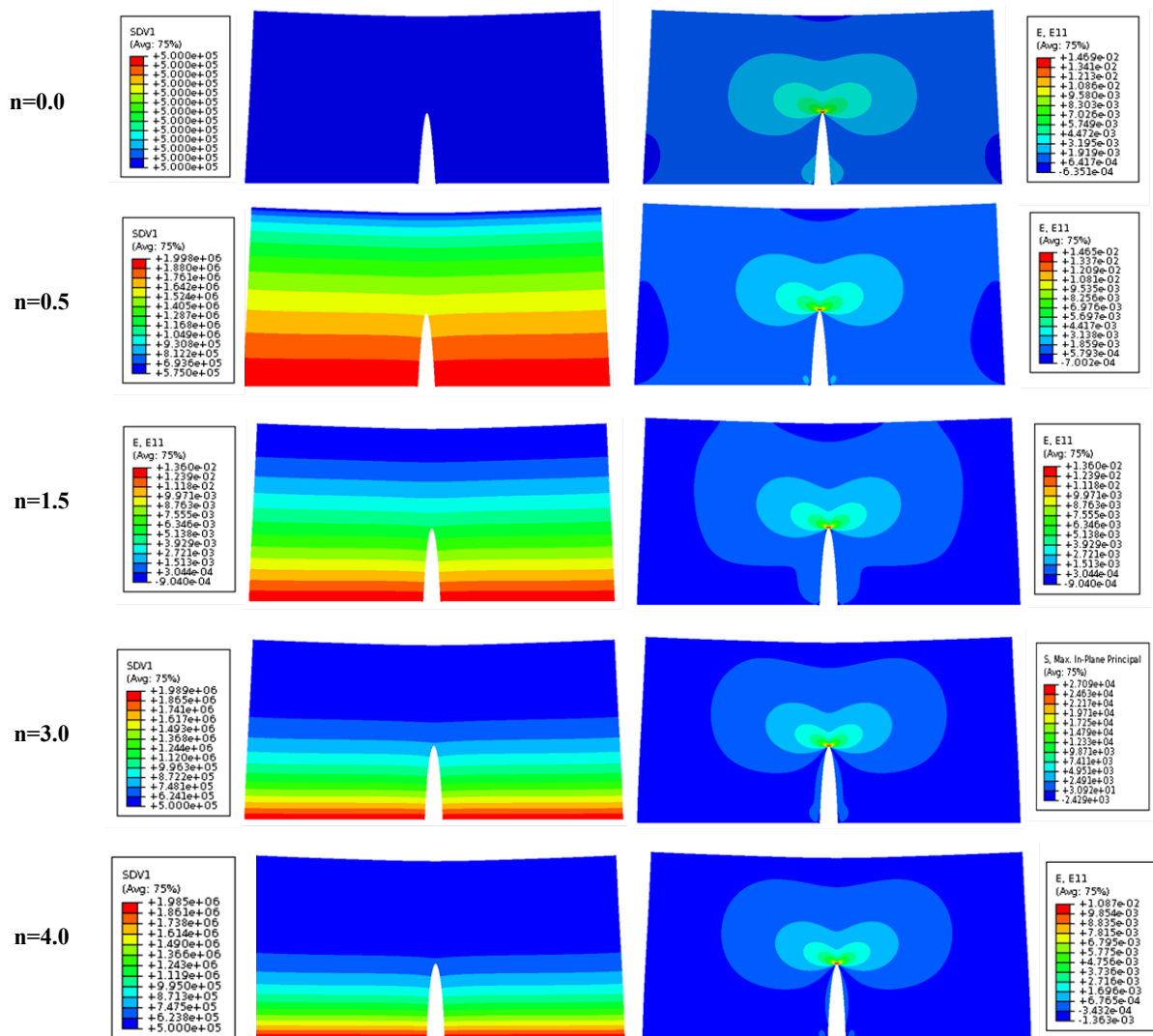


Figure D-18. Modulus and Horizontal Strain Contours for Different Stiffness Gradient Profiles.

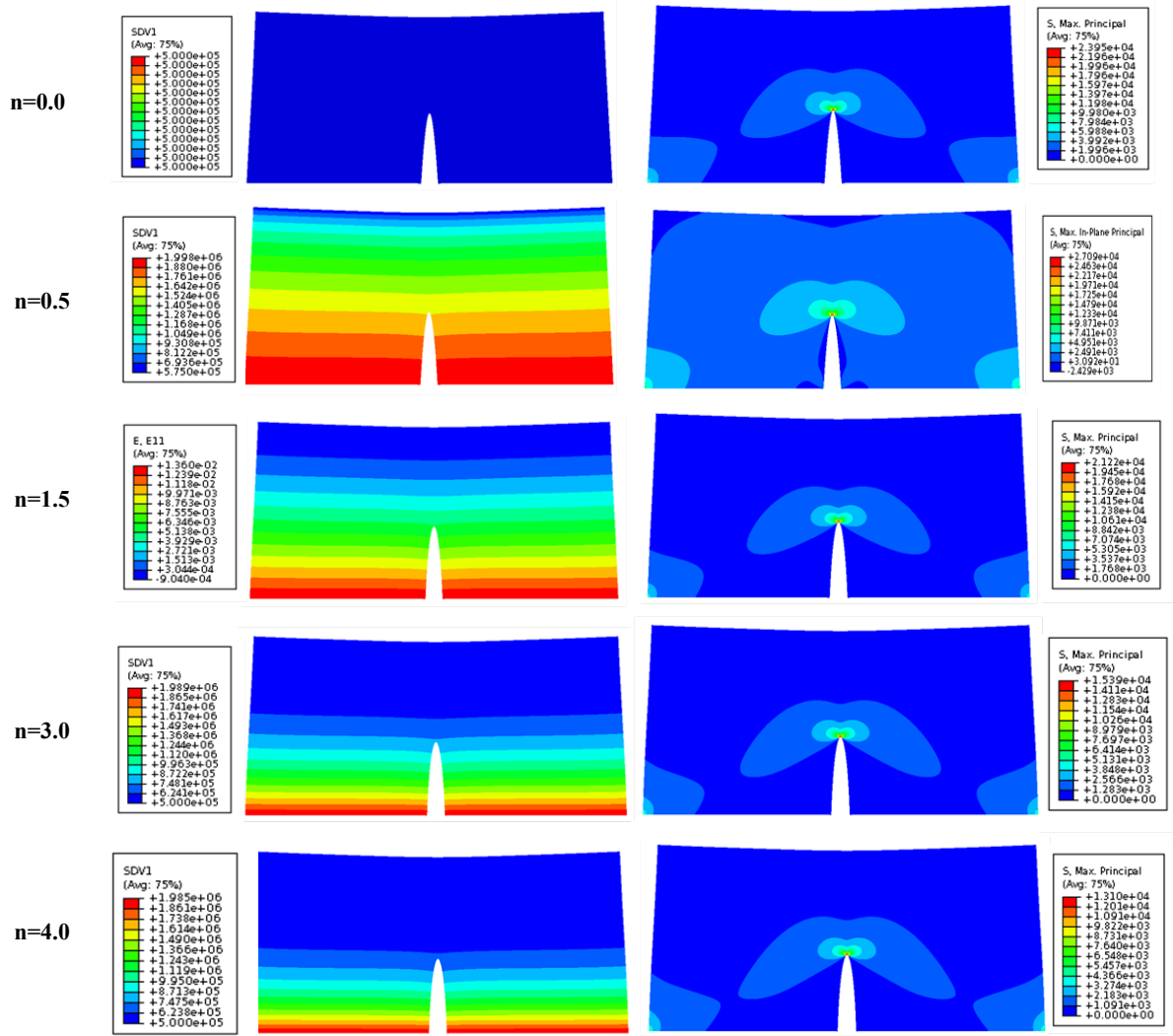
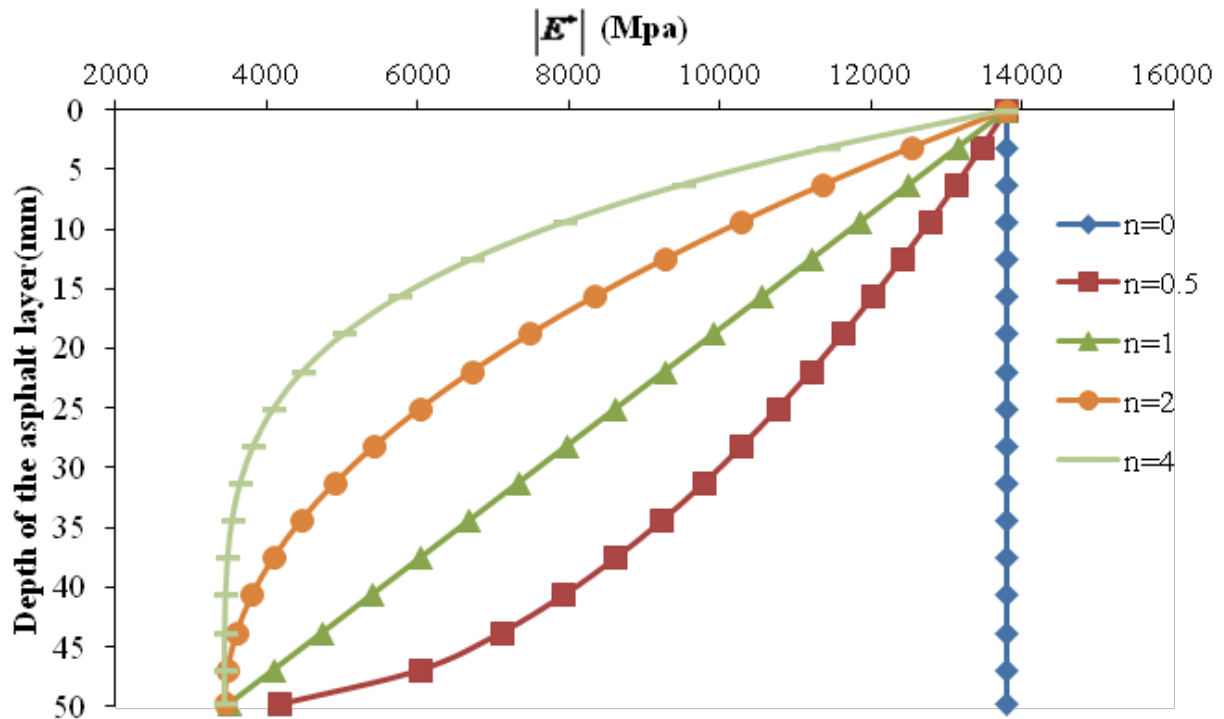
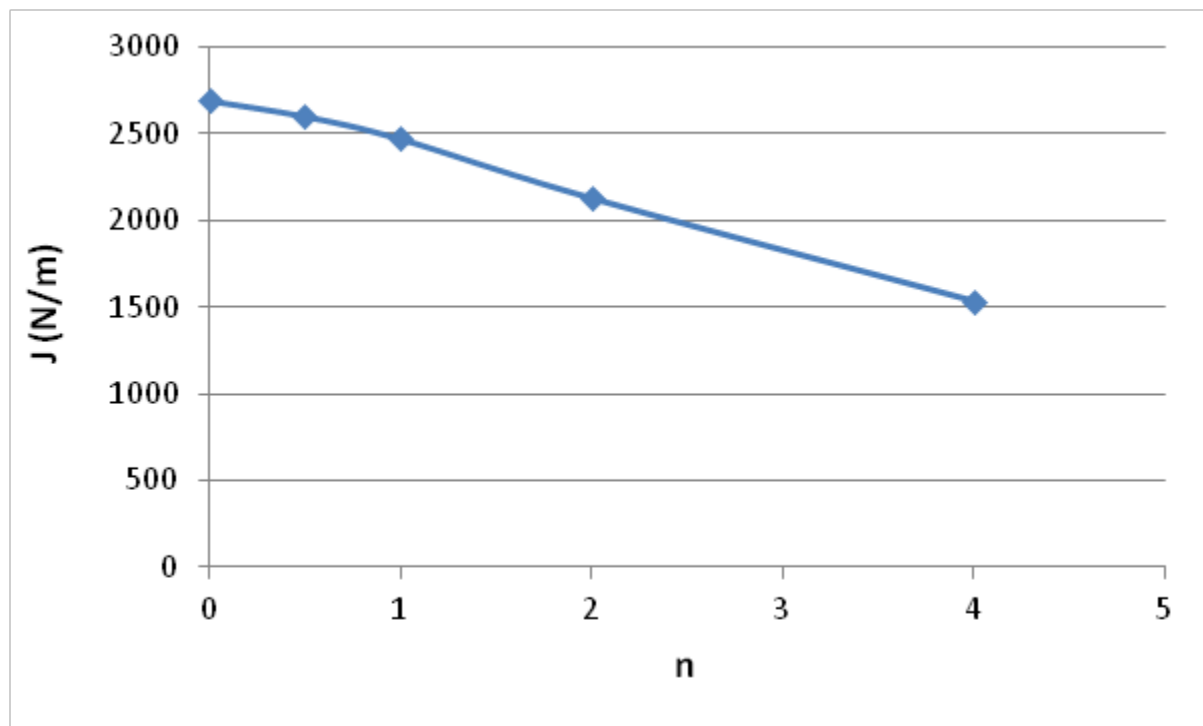


Figure D-19. Modulus and Maximum Principal Stress Contours for Different Stiffness Gradient Profiles.



(a) Stiffness profiles



(b) Relationship between J-integral and n value

Figure D-20. The Value of the J-Integral for the Different Stiffness Profiles.

The Analysis of the Fracture and Healing of the Field Specimens

The process to get the fracture and healing properties of the field specimen is the same as with the laboratory-compacted specimen. The strain profiles for the field aged asphalt concrete layers are estimated using the previously described FGM-FE model and a smaller displacement is applied to the field specimen because they are more brittle.

The output of the stiffness gradient model from the DT test gives the magnitude of the complex modulus at the feedback frequency, which is 20 Hz in the machine that was used in the test. However, the modulus obtained from the OT test is measured at a different frequency; therefore, the Equation D-25 is used to transfer the modulus to the desired frequency if it is needed in the calculations.

$$\left| E^*_{\left(\frac{1}{2t}\right)} \right| (OT) = \left| E^*_{(\omega)} \right| (DT) \cdot \left(\frac{1}{2t\omega} \right)^{m_1} \quad (D-25)$$

where $\left| E^*_{\left(\frac{1}{2t}\right)} \right|$ and $\left| E^*_{(\omega)} \right|$ are the magnitudes of the moduli in the OT test and DT test, respectively; m_1 is the undamaged parameter which is obtained from the nondestructive part of the OT test; t is the loading time in the OT test; and ω is the angular velocity of the DT machine.

MATERIALS AND EXPERIMENT

Materials

To illustrate the methodology with actual test results, a Texas Type D mix with a PG 64-22 grade binder was analyzed with the testing analysis method. The binder content of the mix was 5.2 percent. The specimens were molded at two different air void contents, 4 and 7 percent, to compare the effect of air void content on the crack growth, fracture, and healing properties of the mixes. Three replicates of each air void category were used to evaluate the consistency of the model. The laboratory compacted cores were cut to the standard specimen geometry and the specimens were glued on the aluminum plates.

Test Procedure

The test is conducted in two steps: the nondestructive test and the crack growth test. Figure D-21 shows the nondestructive and destructive loading patterns. The nondestructive phase

includes 10 load cycles with an opening of 0.05 mm and the destructive phase includes 150 load cycles with a maximum opening of 0.3175 mm. All tests are conducted at 25°C.

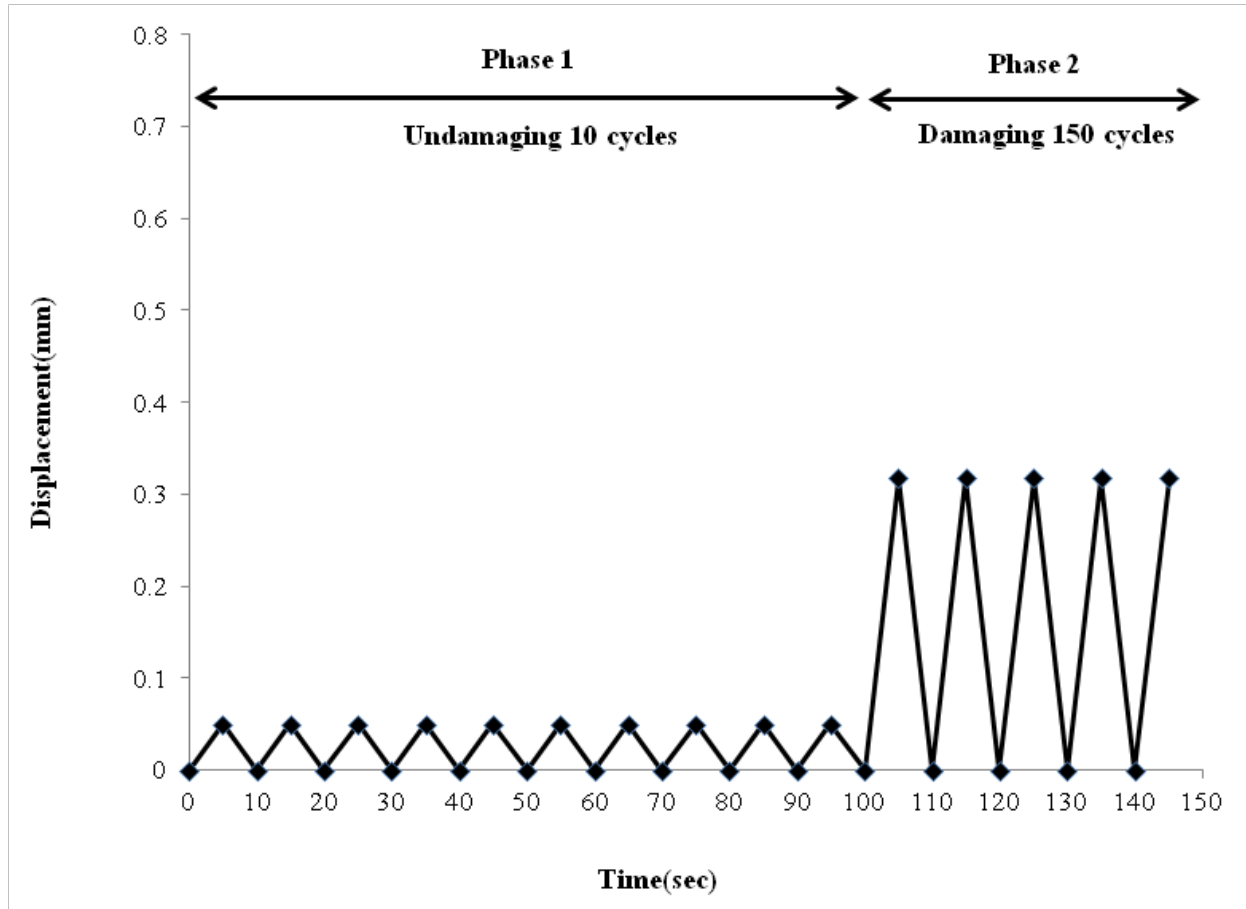


Figure D-21. The OT Test Loading Pattern for the Nondestructive and Destructive Tests.

RESULTS AND DISCUSSION

The test outputs were analyzed to obtain both damaged and undamaged properties.

Table D-3 and D-4 show the results for the undamaged, fracture and healing properties.

The numbers of cycles for the crack to grow to a length of 25 mm is counted for two reasons: (a) to reduce the length of time required for the test, and (b) because counting cycles after the crack enters the top 6 mm low strain zone in thin samples produces inconsistent results. In thicker samples, the top zone is in compression according to the FE analysis results and the crack growth rate decreases substantially in this zone. The coefficient of variation (COV) for the number of cycles corresponding to a crack length of 25 mm is calculated to demonstrate the

consistency of the methodology compared to previous methods. The COV values for the number of load cycles of mixes A and B are 19 and 16 percent, respectively.

Table D-3. The Damaged and Undamaged Properties of the Mix Type A Using OT Test.

HMA Mix Type D			Undamaged Properties		Damaged Properties			Healing Properties	
ID	AV (%)	AC (%)	E_1 (MPa)	m_1	N	A	n	B	m
A-1	4.2	5.2	253.805	0.42	56	0.046	1.720	0.019	3.430
A-2	4.4	5.2	257.432	0.41	44	0.035	1.190	0.021	2.320
A-3	4.2	5.2	246.451	0.4	65	0.038	1.374	0.023	2.461
μ	4.267	5.2	252.529	0.41	55	0.040	1.428	0.021	2.737
σ	0.115	0	5.649	0.01	10.536	0.006	0.269	0.002	0.604
COV	2.706	0	2.237	2.439	19.156	14.335	18.844	9.524	22.078

Table D-4. The Damaged and Undamaged Properties of the Mix Type B Using OT Test.

HMA Mix Type D			Undamaged Properties		Damaged Properties			Healing Properties	
ID	AV (%)	AC (%)	E_1 (MPa)	m_1	N	A	n	B	m
B-1	6.9	5.2	172.444	0.53	44	0.030	1.750	0.016	3.040
B-2	7.4	5.2	189.350	0.48	36	0.049	1.470	0.051	2.580
B-3	7.4	5.2	193.791	0.54	50	0.024	1.640	0.011	2.825
μ	7.233	5.2	185.195	0.52	43.33	0.034	1.620	0.026	2.815
σ	0.289	0	11.264	0.035	7.024	0.013	0.141	0.022	0.230
COV	3.991	0	6.082	6.744	16.209	38.013	8.708	83.825	8.176

In addition, the undamaged properties are very consistent. The COV values for the undamaged relaxation moduli of mixes A and B are 2.23 and 6.08 percent, respectively. According to [Table D-3](#), the fracture and healing COV parameters are below the 30 percent level, which was a characteristic of the previous method of using the overlay tester.

The average number of cycles corresponding to 25 mm crack growth is higher in mix A compared with mix B. This happens because of the lower air voids of mix A relative to mix B.

As mentioned previously, a large amount of healing occurs during each load cycle. The higher magnitude of the m values in both mixes also confirms this observation.

Previous methods of analyzing OT test data by counting the number of load cycles for the crack to reach the top of the sample have shown coefficients of variation much greater than 30 percent especially for coarse-graded mixes (Walubita et al., 2009).

Figure D-22 depicts the actual crack growth against loading cycles. As shown in this figure, the crack grows very quickly during the first few load cycles and the rate of crack growth decreases substantially after that.

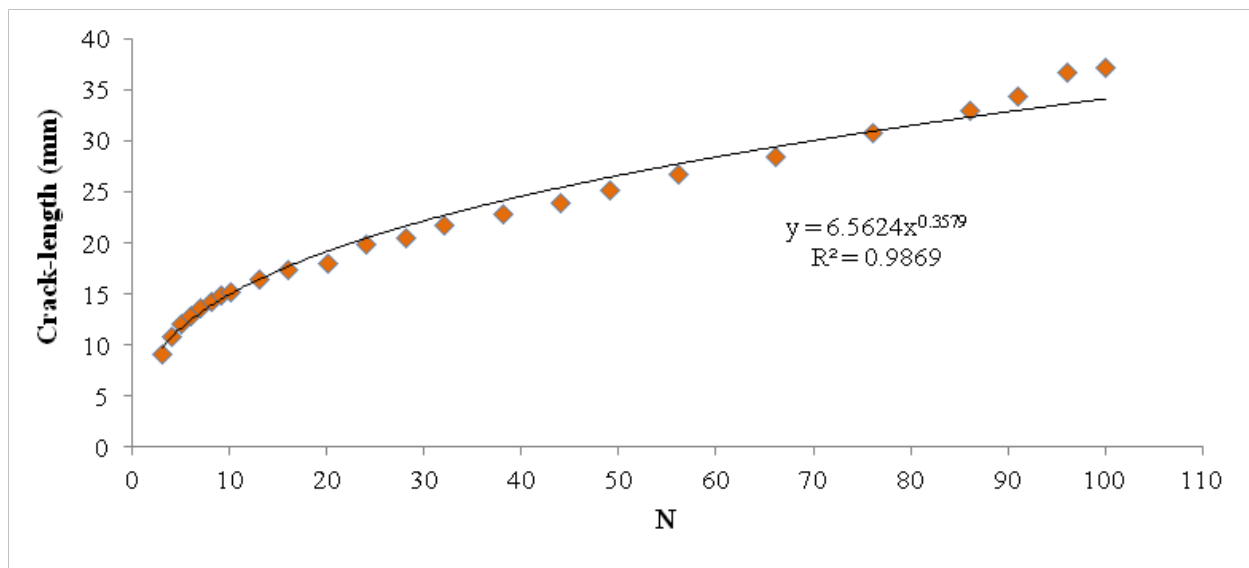


Figure D-22. The Actual Crack Growth for a Lab Mix with 4% Air Void.

SUMMARY

The results of this research show that the OT machine can be used as a quick and robust test for determining fracture and healing properties of asphalt mixes and a calculated number of load cycles for the crack to reach a standard length. The latter permits a direct comparison of the fracture resistance of different mixes. The accuracy and repeatability of this method has been demonstrated to be superior to previous methods of using the same test apparatus. The analyses that have been done in this study have shown the major reason for the high degree of variability of the number of load cycles to reach failure. Samples thicker than 38 mm will develop a small compressive zone at the top of the sample. When a crack growing upward enters this zone, it will

stall for an unpredictable number of load cycles. This makes the load-cycle count to failure an unreliable method comparing the fracture resistance of mixes, as has been observed. In contrast, the method of collecting and analyzing the OT data developed in this study has been automated and can be used to achieve more consistent data for comparing the fracture resistance of mixes. In addition, the analysis of the crack growth and Pseudo work dissipation produces both fracture and healing properties of mixes. The testing and analysis method presented here has been applied successfully to both lab-compacted samples and field cores.



APPENDIX E: THE DT AND R-DT TEST METHODS

In view of further perusing the development of surrogate HMA cracking test procedures, the direct-tension test was explored in repeated loading mode (R-DT) as well as the more traditional monotonic loading mode (DT). The testing setups and some results are presented in this appendix.

TEST SETUP

The key aspects of the two test methods are listed and compared in [Table E-1](#) and are discussed in further details in the subsequent sections.

Table E-1. IDT and R-IDT Test Parameters.

	DT	R-DT
Sample		
Dimensions	4"φ × 6" H	4"φ × 6" H
Loading mode	Monotonic tensile Displacement controlled	Repeated tensile Displacement controlled
Test parameters	Loading rate = 0.05"/min Temperature = 77°F	Frequency = 1 Hz (0.5 sec loading + 0.5 sec rest) Input strain = 35% of DT Tensile Strain Temperature = 77°F
Output data	Strength (σ_t), Strain (ϵ_t), Stiffness (E_t), FE (G_f), & FE Index	Number of load repetitions (cycles) to failure & peak load
Test time per specimen	≤ 10 minutes	≤ 180 minutes

Legend: H = height; φ = diameter

The Direct Tension (DT) Test

The DT test is one of the most straightforward tests and has the simplest analysis equation of all the test methods because the specimen is tested in direct-tension loading mode. The specimen is typically a cylinder of 6-inch in height and 4 inches in diameter ([Walubita,](#)

2006). This geometry is in part based on the specimen fabrication configuration using the Superpave gyratory compactor (SGC). The loading rate is typically 0.05 in/min (Walubita et al., 2006).

However, the specimen set-up process requires gluing end plates to the specimen ends that are in turn attached to the MTS hydraulic system. This is a very critical process for this test and it requires meticulous work to ensure reliable results. Gluing time can also be a hindrance to testing efficiency, as the process usually requires 24 hours for curing.

In addition, the failure of the specimen must be closely monitored as cracking near the ends can be an indicator that end effects may be introduced into the data and resulting analysis. In fact, proper gluing techniques must be ensured, otherwise the specimen may fail in the glued area. This also means that the HMA may not have failed before the test actually terminates and therefore, the calculated stresses and strains will be erroneous. As the LVDTs are generally attached to the specimen, HMA stiffness determination is thus possible with this test.

Like the all the crack tests discussed in the report, the DT test can be at any desired temperature, but room temperature (77°F) was utilized for consistency throughout this study. The data that are captured during DT testing include the load, vertical displacement, and time.

The Repeated Loading Direct Tension (R-DT) Test

Preliminary repeated DT loading tests were also conducted to investigate their R-DT suitability and practicality for characterizing the HMA mix cracking resistance potential. With the R-DT test method, the cracking resistance potential of a mix is characterized by the number of IDT load repetitions to crack failure. While the DT test has previously been conducted at TTI, its use as a repeated loading test is a novel approach. Therefore, no standard specification was found for this test method.

The same specimen dimension as the regular DT test (4 inch diameter × 6 inch tall) is used for its repeated R-DT counterpart. Different from the R-IDT and R-SCB, the test is a two point loading setup in a strain controlled mode. The repeated loading mode is established by loading the specimen at a frequency of 1 Hz with 0.5 seconds of loading followed by 0.5 seconds of rest. Thirty-five percent of the average DT tensile strain of all the HMA mixes was selected as the R-DT input strain for all the mixes. Consistency with other crack test methods evaluated, the R-DT was also conducted at room temperature (77°F).

TEST RESPONSE CURVES AND DATA ANALYSIS MODELS

The output data from the two tests and their subsequent data analysis models are discussed in this section.

The DT Data Analysis Models

Typically the result of interest from a DT test is the axial peak load which is analyzed using established models to calculate the HMA tensile strength. However, the full potential of the DT as a HMA cracking test is utilized when the complete loading history of a sample is taken into consideration by analyzing the full load-displacement response. A typical load-displacement response from the DT test is shown in Figure E-1. Several fracture parameters in addition to the HMA tensile strength are calculated from this output response curve.

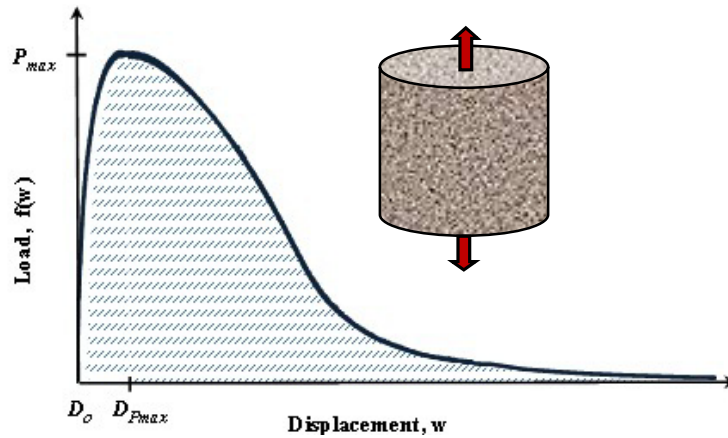


Figure E-1. Load-Displacement Response Curve: DT Testing.

The typical fracture parameters measured from the DT tests in this study included the HMA tensile strength (σ_t), HMA tensile strain at peak failure load or ductility potential (ϵ_t), HMA tensile modulus or stiffness in tension (E_t), and HMA fracture energy or FE (G_f). The model for calculating the tensile strength from a DT test data is as follows:

$$\sigma_t = \frac{4P_{\max}}{\pi D^2} \quad \text{E-1}$$

Where, D is the diameter of the specimen and P_{\max} is the axial peak load, as indicated in Figure 8-1. The tensile strain at peak load or the ductility potential is calculated as:

$$\varepsilon_t = \frac{\text{Disp. @ pick load}}{\text{Initial disp. @ zero load}} = \frac{D_{P_{\max}} - D_o}{D_o} \quad \text{E-2}$$

Where, $D_{P_{\max}}$ and D_o are the displacement at peak load and initial displacements respectively (Figure 8-1). The ratio of the tensile strength and the tensile strain is denoted as the tensile modulus or the stiffness in tension and is computed as follows:

$$E_t = \frac{\text{HMA tensile strength}}{\text{Tensile strain}} = \frac{\sigma_t}{\varepsilon_t} \quad \text{E-3}$$

The fracture energy is defined as the work required to produce a crack of unit surface area, measured in J/m^2 . The work required to fracture the sample is represented by the area under the load versus displacement curve, as shown in Figure E-1. Therefore, a general expression for fracture energy (G_f or FE) can be written as:

$$G_f = \frac{\text{Work}}{\text{Area of cracked section}} = \frac{1}{A} \int f(x) dx \quad \text{E-4}$$

Finally, the fracture energy index (FE Index), which is a new parameter derived in this study, is defined as a parametric ratio of the fracture energy to the HMA tensile strength and tensile strain at peak failure load per unit crack length. This FE Index was computed as follows:

$$\text{FE Index} = 1 \times 10^5 \frac{G_f}{l_{cr} \sigma_t} \varepsilon_t \quad \text{E-5}$$

where, l_{cr} is the length traversed by the crack which is equal to the diameter of the DT sample (D) in this case.

The R-DT Outputs and Data Interpretation

Compared to its monotonic DT counterpart, the data analysis for the R-DT is much simpler and the parameters of interest are the number of load cycles to failure and peak load. Both these parameters are automatically recorded on a computer connected to the MTS machine and can be extracted without performing any post-processing analysis. Details of both the DT and R-DT tests can be found in other publications by these authors (Walubita, 2006; Walubita et al., 2010).

LABORATORY TEST RESULTS

DT strength-strain response curves are also shown in Figure E-2. Some examples of the DT test results along with results from other test methods are comparatively shown in Table E-2.

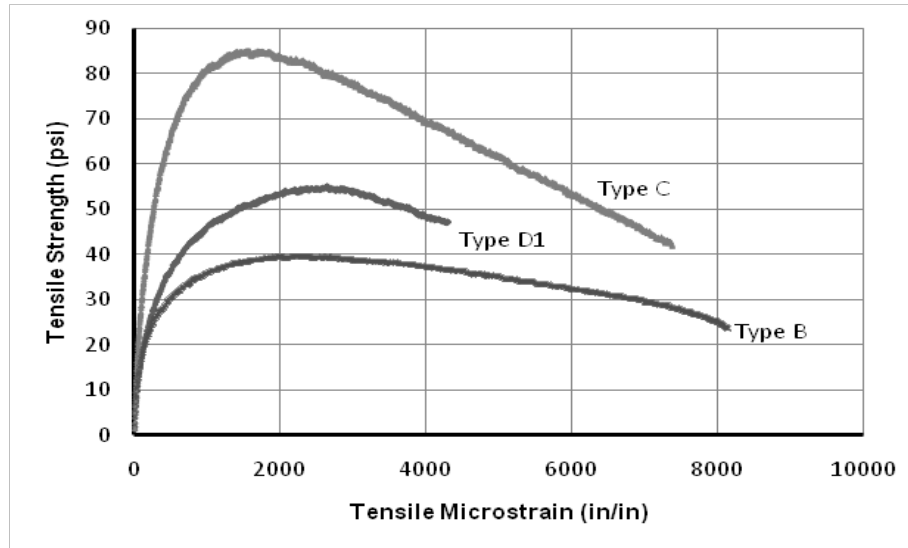


Figure E-2. Typical DT Stress-Strain Curves.

Table E-2. Example of Test Results for Type D, B, and C Mixes.

Test	Test Parameter	HMA Mixes			Discriminatory Ratio	
		Type D1 (Good)	Type B (Poor1)	Type C1 (Poor2)	Good/Poor1	Good/Poor2
OT	Peak load (lbf)	633 (8%)	773 (9%)	755 (6%)	0.8	0.8
	Cycles to failure	274 (17%)	47 (51%)	38 (18%)	5.8	7.2
DT	Tensile strength (psi)	55 (4%)	40 (8%)	86 (1%)	1.4	0.6
	Tensile strain ($\mu\epsilon$)	2 583 (13%)	2 500 (20%)	1 529 (16%)	1.0	1.7
IDT	Tensile strength (psi)	100 (5%)	84 (4%)	123 (5%)	1.2	0.7
	Horizontal tensile strain (in/in)	0.00281 (21%)	0.00271 (18%)	0.00154 (13%)	1.0	1.8
SCB	Tensile strength (psi)	126 (4%)	55 (25%)	166 (11%)	2.3	0.8
	Vertical strain (in/in)	0.03653 (22%)	0.02865 (18%)	0.02195 (7%)	1.3	1.7

COV = coefficient of variation (in parentheses)

While the results in [Table E-2](#) shows promise in terms of the variability, both the DT and R-DT were not evaluated further than the results shown in [Figure E-1](#) and [Table E-2](#) due to the following reasons:

- Sample fabrication (coring) and setup is comparatively complex, laborious, and very time-consuming.
- Cannot readily test field cores or slabs.
- The need for gluing and curing time adds complications.
- The need for experienced technicians/operators – this can be a source of negativity when it comes to industry applications.
- The need for attaching LVDT can be a source of errors particularly for industry setup.
- End failures or failing in the glue instead of the sample middle zone; see example in [Figure E-3](#).

To summarize, the DT and R-DT test methods, while they may be ideal for research-level testing, are not practical nor implementable for daily routine HMA mix-designs and screening. The sample preparation and setup alone are very laborious and time-consuming, which is not practical or cost-effective in a routine production lab or industry setting.

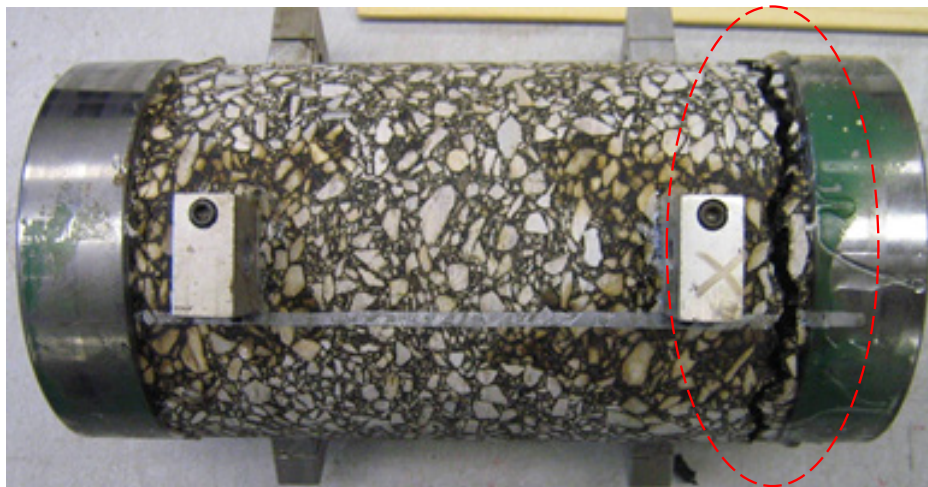


Figure E-3. Example of Common Undesired End Failures with the DT Test.